이학박사학위논문

인간 뇌의 구조적 커넥톰: 뇌의 구조적 네트워크 발달에 관한 분석 및 시뮬레이션

The human structural connectome: Analysis and simulation of brain network development

2015 년 8 월

서울대학교 대학원

자연과학대학 뇌인지과학 전공

임 솔

The human structural connectome: Analysis and simulation of brain network development

Sol Lim

August 2015

Department of Brain and Cognitive Sciences

College of Natural Sciences

Seoul National University

Abstract

Sol Lim

Department of Brain and Cognitive Sciences

College of Natural Sciences

Seoul National University

A brain can be represented as a graph (network) comprised of sets of nodes and edges called *connectome*, which is a natural representation of a brain;neurons form synapses with dendrites and axons to transfer neural signals and regions of grey matter are interconnected to each other through axon bundles in white matter. Moreover, by representing a brain as a network, we can study brains from other species in the same framework using this graph-theoretical approach. A brain, however, is also constrained by other factors such as its embedding space and metabolic cost. Therefore, spatial characteristics as well as topological traits are important. These topological and spatial characteristics of a brain change during development. In this work, I investigated how brain network develops over age in micro and macro scales to find organising and re-organising principles during development; microscopic scale refers to the synaptic connectivity between neurons and macroscopic scale refers to whole brain fibre tract connectivity between brain regions constructed from diffusion tensor imaging technique. Furthermore, I propose two-stage connectome maturation hypothesis by connecting both scales, which would elucidate principles of healthy and pathological brain development.

Keywords : Human connectome, Structural connectivity, Development, Net-

work analysis, Diffusion Tensor Imaging, Simulation

Student Number :2010-31299

Contents

List of Figures

List of Tables

Part I.

Introduction

0.1. Thesis structure

- Part I gives a brief introduction to network analysis and Diffusion Tensor Imaging (DTI).

- Part II presents synaptic level brain connectivity; how developmental time windows would affect topological and spatial characteristics in simulated neuronal networks.

- Part III examines how brain network develops over age based on DTI providing an organizing principle, in particular, regarding preferential detachment of specific types of connections.

- Part IV provides a new insight to look at normal and pathological brain network development by suggesting a two-stage connectome maturation hypothesis.

- Part V presents summary of the main findings, discusses possible improvement of the studies in methodological perspective and provides an outlook for future studies and applications.

In the following chapter, I provide methodological background used in later chapters. Network analysis (Section 1.1) is used throughout my studies and Diffusion Tensor Imaging (Section1.2) is used in chapter 3. More detailed information, however, can be found in references 5.3.

1. Methodological background

1.1. Network analysis

1.1.1. Topological properties

1.1.1.1. Graph theoretical approach

A *graph* $G = (N, E)$ consists of a pair of a set of *nodes* N(or vertices) and a set of *edges* E. Edges connect nodes, showing topological relationship among nodes. When E is an ordered set of nodes, we call the graph G a directed graph otherwise G is an undirected graph. A *loop* is an edge which connects a node to itself. Here we only consider *simple* undirected and directed graphs without loops. Two vertices are said to be *adjacent* if they are joined by an edge, thus we can summarise the graph with an n by n *adjacency* matrix $A_G = a_{ij}$ where $V = \{v_1, v_2, ...v_n\}$, w_{ij} is a weight of an edge between nodes v_i and v_j and the following adjacency matrices represent a binary graph and a weighted graph, respectively (See for example, Figure 2.13). For instance, nodes can be neurons when edges are the synapses between neurons or brain regions can be nodes and axon bundles connecting those regions can be represented as edges.

$$a_{ij} = \begin{cases} 1 & \text{if } \{v_i, v_j\} \in E \\ 0 & \text{otherwise} \end{cases} \qquad a_{ij} = \begin{cases} w_{ij} & \text{if } \{v_i, v_j\} \in E \\ 0 & \text{otherwise} \end{cases}$$

1.1.1.2. Edge density

The edge density represents the proportion of non-zero connections to the number of potential connections. Because our network is undirected, we used $d = 2E/N(N-1)$, where E is the number of edges and N is the number of nodes. Note that the weights of individual edges might change but edge density will remain the same as long as the total number of edges is unchanged.

1.1.1.3. Global and local efficiency

Global efficiency represents how well any two nodes of a network are connected, whereas local efficiency shows how well neighbours of a node are connected (Latora & Marchiori, 2001; Achard & Bullmore, 2007).

$$E_{global}(G) = \frac{1}{N(N-1)} \sum_{i \neq j} \frac{1}{l_{i,j}} \tag{1.1}$$

$$E_{local}(G) = \frac{1}{N} \sum_{i} E_{global}(G_i) \tag{1.2}$$

where $L_{i,j}$: the length of the shortest path between nodes i and j, N: the number of nodes, G: a graph, G_i: the subgraph that consists of neighbours of i without i itself.

Efficiency is greatly affected by the sparsity of the network (Kaiser, 2011); when there are fewer edges and also even fewer streamlines, efficiency decreases. Thus we normalized efficiency with values obtained by 100 randomly rewired networks where randomly selected edges were swapped while preserving both degree and strength of each node (Rubinov & Sporns, 2011). Whereas the

number of connected edges of a node forms its degree, the strength of a node is the sum of weights of all its edges (here: total number of streamlines of that node) (Barrat *et al.*, 2004). Such a network is called a *small-world network* (Watts & Strogatz, 1998; Latora & Marchiori, 2001) when the local efficiency is much higher than in a comparable random network, but the global efficiency remains about the same.

1.1.1.4. Modularity

We computed modularity Q, and estimated the modular membership, maximizing modularity (Newman, 2006), which may identify functional building blocks (Kaiser, 2011). Modularity measures the difference between the number of edges that lie within a community in the actual network (the first term) and a random network of the same degree sequence (the second term) for a certain membership assignment (Leicht & Newman, 2008):

$$Q = \frac{1}{m} \sum_{i,j} [a_{ij} - \frac{k_i^{in} k_j^{out}}{m}] \delta_{e_i,e_j} \tag{1.3}$$

where m: total number of streamlines in the network (note that bidirectional links are counted twice); a_{ij}: number of streamlines (weight) between node i and node j; k_i^{in}: sum of streamlines in incoming edges of node i; k_j^{out}: sum of streamlines in outgoing edges of node j; $\delta_{c_i c_j}$: Kronecker delta (only one if nodes i and j are in the same module and zero otherwise); c_n: label of module to which node n belongs to.

1.1.1.5. Within-module strength and Participation coefficient

We computed within-module strength and participation coefficient (Guimera & Amaral, 2005) to examine nodal changes in modular structure. The within-module strength represents how well the node is connected to the others in the same module; high within-module strength implies that the node is more connected in the module where it belongs than the average connectivity of the other nodes in the module.

$$z_i = \frac{\kappa_i - \overline{\kappa}_{c_i}}{\sigma_{c_i}} \tag{1.4}$$

where κ_i: within-module strength of node i, c_i: assigned modular membership, $\overline{\kappa}_{c_i}$ and σ_{c_i}: average and standard deviation of within module strength of nodes in module c_i.

Participation coefficient indicates how well the node is connected to all other modules. High participation coefficients index that the connections of a node are distributed to multiple modules. In the extreme case, when the participation coefficient of a node is one, the node is connected to all the modules uniformly; and when it is zero, the node is solely connected to the nodes in its own module.

$$P_i = 1 - \sum_{c=1}^{N_m} \left(\frac{\kappa_{ic}}{\kappa_i} \right)^2 \tag{1.5}$$

where κ_i: degree (strength) of node i, κ_{ic}: number (sum of weights) of edges from node i to module c, N_m is the number of modules.

For more extensive review of graph measures and graph theory see (Harary, 2008; Costa *et al.*, 2007; Kaiser, 2011; Rubinov & Sporns, 2010).

1.1.2. Spatial properties

Unlike a graph, a brain is embedded in 3-dimensional space, thus the distance between nodes matters. Minimising the total wiring length of a brain can be beneficial to an organism due to higher metabolic cost and a limited space. A brain network, however, does not minimise the connection lengths (Kaiser & Hilgetag, 2006), rather it seems to balance between minimising the total connection length and facilitation of global information transfer (Vértes *et al.*, 2012; Nicosia *et al.*, 2013). The distance between cortical areas can be estimated by calculating Euclidean distance between regions, which is not the actual length of an axon bundle but previous studies found that Euclidean distance could well-approximate the wiring length between brain regions (Kaiser & Hilgetag, 2006). Another way of measuring connection length is that using reconstructed fibres from tractography using diffusion MRI (see Section1.2).

1.2. Diffusion Magnetic Resonance Imaging (Diffusion MRI)

1.2.1. Diffusion Tensor Imaging(DTI)

Diffusion weighted imaging (DWI) (Le Bihan *et al.*, 1985; Merboldt *et al.*, 1985; Taylor & Bushell, 1985) is one of the MR techniques that uses diffusion rates of water molecules in the biological tissues. Diffusion can be thought of the phenomenon after introducing a drop of ink in a jar filled with water. Depending on the structure of the container and the medium, for instance whether it was olive oil instead of water in the jar, the displacement of molecules

given time and the shape of the *diffusion* of ink would be very different. Likewise, water molecules in the brain diffuse differently depending on the architecture and integrity of the tissue; they diffuse more easily parallel to the axon and relatively restricted perpendicular to the axon, resulting in *anisotropic* diffusion (Beaulieu & Allen, 1994); in contrast, water diffusion in the grey matter (GM) and cerebrospinal fluid (CSF) is relatively isotropic compared to white matter (WM). Diffusion tensor imaging (DTI) (Basser *et al.*, 1994) uses this anisotropic water diffusion to model macroscopic axonal organization in the WM by *tensors or eillipsoid* (Mori & Zhang, 2006; Soares *et al.*, 2013). Stejskal and Tanner (Stejskal & Tanner, 1965) introduced pulsed gradients into the basic spin echo sequence and the Stejskal-Tanner formula (Eq.(1.7)) providing a solution to the Bloch-Torrey partial differential equations (Torrey, 1956) for a symmetric pair of pulsed gradients (Hrabe *et al.*, 2007; Mori & Zhang, 2006; Kingsley, 2006b). The MR signal attenuation due to diffusion can be calculated as the following if we assume simple isotropic Gaussian diffusion. The assumption of monoexponential decay breaks down when b-value is higher than 1500 s/mm^2 (See Section 5.2.2.2).

$$S = PD(1 - e^{-TR/T_1})e^{-TE/T_2}e^{-bD} \tag{1.6}$$

where PD: proton density representing water concentration, T_1 and T_2: relaxation times, b: b-value or b-factor (s/mm^2) and D: (apparent) diffusion coefficient (ADC), which can be rewritten as

$$S = S_0 e^{-bD} \tag{1.7}$$

where $PD(1-e^{-TR/T_1})e^{-TE/T_2}$ was replaced by S_0 representing signal intensity without diffusion-sensitizing gradients

$$b = \gamma^2 G^2 \delta^2 \Big(\tau - \frac{1}{3}\delta\Big) \tag{1.8}$$

This can be simplified as the following when $\delta \ll \tau$.

$$b = \gamma^2 G^2 \delta^2 \tau \tag{1.9}$$

where γ: gyromagnetic ratio (Hz/T), G: diffusion-sensitizing gradients strength (mT/m), τ: time between the two pulses (ms) and δ: duration of the pulses (ms).

$$\begin{aligned} S_1 &= S_0 e^{-b_1 D} \\ S_2 &= S_0 e^{-b_2 D} \\ \frac{S_2}{S_1} &= e^{(-b_1 - b_2)D} \\ D &= \frac{ln(S_2/S_1)}{b_1 - b_2} \end{aligned} \tag{1.10}$$

where b_1, b_2 are the b-values, S_1 and S_2 are the attenuated intensity of the signals, from which we can calculate diffusion coefficient D, assuming that PD, TR (ms), TE (ms) are fixed.

Detailed derivation can be found here (Basser & Jones, 2002; Hrabe *et al.*, 2007). The above formula is for 1-dimensional (1D) case, which is a 1D diffusion along the diffusion gradient vector. Thus, we obtain a map of diffusion coefficients, called Apparent Diffusion Coefficient (ADC) map. However, in order to determine the principal direction precisely in each voxel to reconstruct

axonal bundles in the WM, we need *diffusion tensor* to describe diffusion because diffusion cannot be represented by a scalar coefficient in the presence of anisotropy; at least six independent 1D diffusion measurements are required to fully assess the six independent components of the 3 by 3 symmetric diffusion tensor $\mathbf{D}$ as the following equation.

$$S_i = S_0 e^{-b\mathbf{g_i}^T \mathbf{D} \mathbf{g_i}} \tag{1.11}$$

$$\mathbf{D} = \begin{pmatrix} D_{xx} & D_{xy} & D_{xz} \\ D_{xy} & D_{yy} & D_{yz} \\ D_{xz} & D_{yz} & D_{zz} \end{pmatrix} \tag{1.12}$$

where S_i is the attenuated signal, $\mathbf{g_i}$ is the unit vector along the gradient direction, or normalized wave vector (Seunarine & Alexander, 2009) and $\mathbf{D}$ is a 3 by 3 covariance matrix describing the covariance of diffusion displacements in 3D. This diffusion tensor can be thought of as an ellipsoid. The principal axes of the ellipsoid are the eigenvectors and the three eigenvalues correspond to the three diffusivities along the axons of the diffusion ellipsoid.

After estimating a tensor in each voxel (Jones, 2009), by using eigenvalues, we obtain mean diffusivity (MD), axial diffusivity (AD), radial diffusivity (RA) and fractional anisotropy (FA) as the following.

$$MD = \frac{\lambda_1 + \lambda_2 + \lambda_3}{3} \tag{1.13}$$

$$AD = \lambda_1 \tag{1.14}$$

$$RD = \lambda_2 + \lambda_3 \tag{1.15}$$

$$FA = \sqrt{\frac{1}{2}} \frac{\sqrt{(\lambda_1 - \lambda_2)^2 + (\lambda_2 - \lambda_3)^2 + (\lambda_3 - \lambda_1)^2}}{\sqrt{{\lambda_1}^2 + {\lambda_2}^2 + {\lambda_3}^2}} \tag{1.16}$$

where λ_1, λ_2 and λ_3 are eigenvalues and $\mathbf{v_1}$, $\mathbf{v_2}$ and $\mathbf{v_1}$ are eigenvectors.

Here, I covered the diffusion tensor model that assumes only a single dominant diffusion orientation in each voxel; however, more complex local description are necessary to account for crossing fibres in the brain see section 5.2.2 (Tournier *et al.*, 2011; Seunarine & Alexander, 2009). More complex local description models may need longer acquisition time and a larger number of diffusion directions.

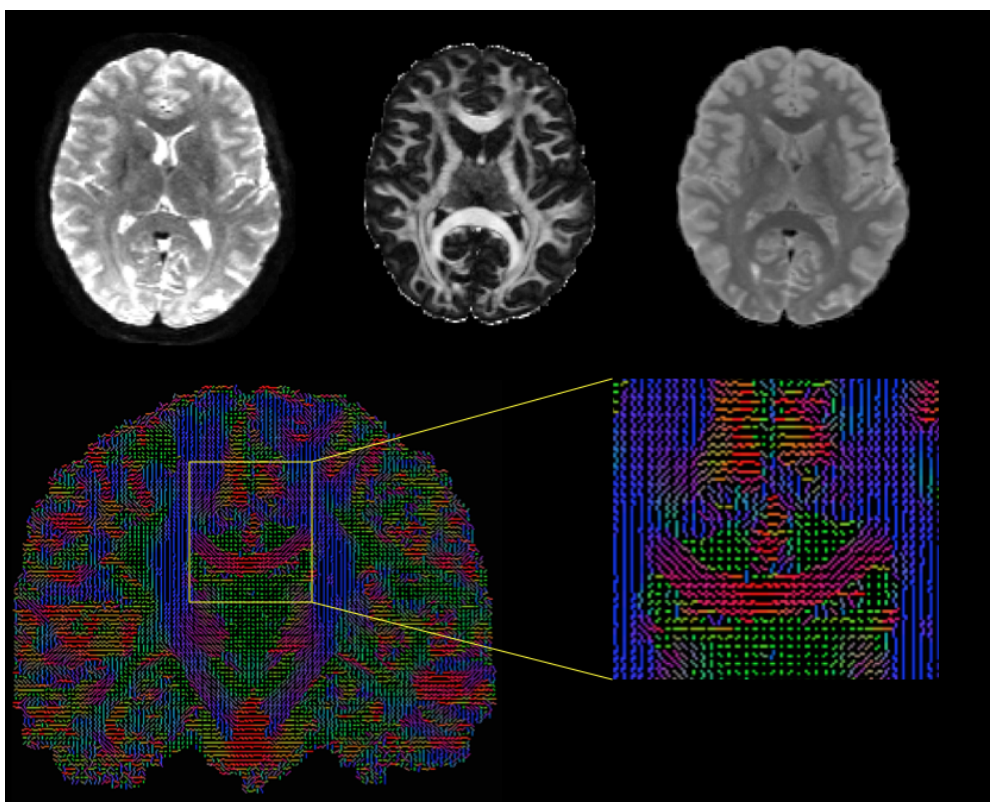

Figure 1.1.: First column: from left, B0 image, FA, MD; Second column, the principal direction map with color coding scheme (coronal view). Red: left-right(right-left); Blue:Superior-inferior(top-bottom); Green:anterior-posterior

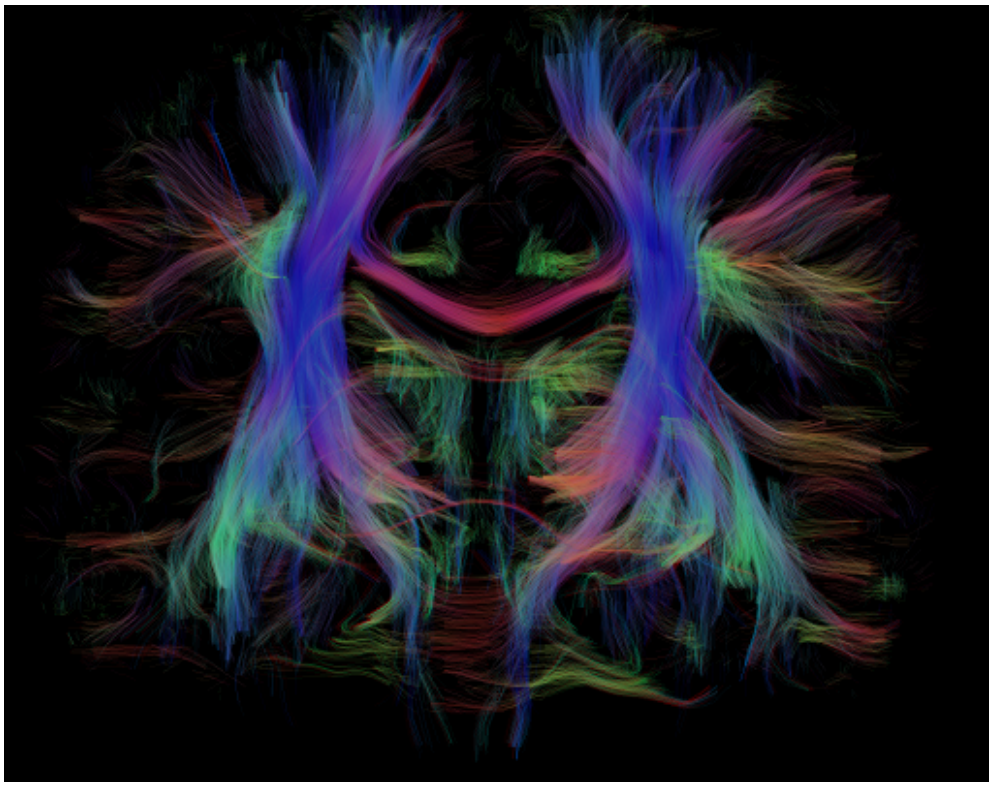

Figure 1.2.: *Coronal view* an example of the deterministic tractography from public DTI-database provided by the Nathan Kline Institute (NKI)(Nooner *et al.*, 2012) using TrackVis (Wang *et al.*, 2007). See Section 3.2.1 for more information .

1.2.2. White Matter Tractography

Above diffusivity measures have been used for clinical purposes detecting acute ischemia (Moseley *et al.*, 1990), multiple sclerosis, localising structural abnormalities in epileptic patients, classifying Alzheimer's dementia and non-Alzheimer forms of dementia and identifying subtypes of brain tumors (Bodini & Ciccarelliy, 2013). In addition to information from microstructural changes in WM, we can also reconstruct underlying wiring patterns in the WM to investigate which GM regions are inter-connected by using the technique called *Tractography* (Mori & van Zijl, 2002; Tournier *et al.*, 2011). When many axons

are align in the same direction preferably densely packed or with thick myelin sheath, water molecules diffusion would be much hindered perpendicular to the major direction of the axonal bundles or to the myelin sheath and they would diffuse much more along the axonal direction. Following the principal direction of each voxel, we can track pathways in the WM, which enables us to probe neuroanatomy noninvasively. Before tractography based on DTI was developed, researchers injected dyes into a brain region. The dye taken up by dendrites and cell bodies travels within a neuron either in an anterograde (from soma to synapse) or a retrograde (from synapse to soma) direction. After some time up to several weeks for the large human brain, the neural tissue can be sliced up and dyes can indicate the origin and target of cortical fibre tracts. Whereas this approach yields high-resolution information about structural connectivity it is an invasive technique usually unsuitable for human subjects except for *post-mortem* studies.

Tractography can be done globally or locally, deterministic or probabilistic, model-based or model free and model simple or complex representations of diffusion in WM (Seunarine & Alexander, 2009) for more information, see Section 5.2.2. The most common and intuitive tractography algorithm is **deterministic streamline tractography**. From a seed point or a mask, WM pathway can be reconstructed by using local fibre orientation information as streamlines. A streamline or fibre trajectory can be represented mathematically as a 3D space-curve by the following equation (Basser *et al.*, 2000; Behrens & Jbabdi, 2009). For alternative methods, see Section 5.2.2.

$$\frac{d\mathbf{r}(s)}{ds} = \epsilon_1(\mathbf{r}(s)) \tag{1.17}$$

where $\mathbf{r}(s)$ is the location that is distance s along the streamline and ϵ_1 is the first eigenvector of the diffusion tensor.

Although Eq.(1.17) is defined in continuous space, the measurements we obtain are from an imaging grid. Therefore, we need to interpolate the discrete measurements into continuous space. There are several integration approaches such as fibre assignment by continuous tracking (FACT) (Mori & Barker, 1999), Euler and Runge-Kutta etc.; some methods are better than others to reduce the propagation errors for tractography (Lazar & Alexander, 2003). Streamline tractography errors can be caused from imaging noise, modelling error and integration errors (Behrens & Jbabdi, 2009); larger errors are in cerebrospinal fluid (CSF), GM, fibres near cortex or at junctions where fibres cross, while major pathways have smaller errors. In general, heuristics such as FA threshold and a curvature threshold are used to stop streamline tractography where errors are likely.

1.2.3. Network construction

To represent a brain as a graph, we divide GM into smaller areas called region of interest (ROI) that would be our nodes in the graph, called *Parcellation* and registering tractography result with parcellation, we obtain a brain network. Parcellation depends on brain *atlases* such as Automated Anatomical Labeling (AAL), Harvard-Oxford atlas, Desikan-Killiany atlas etc. based on predefined structural information. On the other hand, connectivity-based parcellation is also used (Klein *et al.*, 2007; Jbabdi *et al.*, 2009; Cloutman & Lambon Ralph, 2012). Depending on the number of ROIs and brain atlases, reconstructed networks can be quite different, which inevitably introduces different results

on network measures (Zalesky *et al.*, 2010; Van Wijk *et al.*, 2010). Using tractography, edges can be defined when two regions are connected. Both binary and weighted networks can be used; binary networks concerns only whether two regions are connected or not, whereas weighted networks can represent different connection 'strengths' using weights. The definitions of weights in an adjacency matrix can be also diverse; the number of streamlines from deterministic tractography or probabilities from probabilistic tractography often accompanied by corrections for length of the trajectory, surface, or volume of ROIs, and sometimes multiplied by fractional anisotropy (Betzel *et al.*, 2014; Fornito *et al.*, 2012) can be used as weights. As studies use different definitions of weights for further topological analysis of brain networks, direct comparisons are often quite difficult (See Section 5.2).

1.2.4. Correction for artefacts of DW images

Diffusion MRI is very sensitive to motion and has low Signal-to-Noise ratio (SNR); moreover, it also suffers from possible artefacts inherited from acquisition methods (Tournier *et al.*, 2011; Jones, 2010; Jones *et al.*, 2013; Soares *et al.*, 2013). Therefore, before estimating diffusion tensors and tractography, we need to correct possible artefacts during the preprocessing step. The geometrical and intensity distortions from DWI data from spin-echo echo-planar images (EPI) are mainly caused by *field inhomogeneities* (Smith *et al.*, 2004; Holland *et al.*, 2010; Andersson & Skare, 2002; Andersson *et al.*, 2003). There are several approaches to correct these susceptibility-derived distortions (Holland *et al.*, 2010; Andersson *et al.*, 2003). *Eddy currents* also cause geometric and gradient distortions (Andersson & Skare, 2002) and *head motion* should also be corrected. Although we can correct motion-related movement, to use some

comfortable pads for the head is the best option to prevent distortions from head motion. Other artefacts can be caused by *Johnson RF Noise* and *Cardiac Pulsation* (Jones, 2009; Jones & Pierpaoli, 2005). Pulsation artefacts can be detected when using multiple b_0 images by taking standard deviations across b_0 images (Tournier *et al.*, 2011). Visual inspection of the raw data is also very important and examining the residuals of the tensor fitting even when one does not make use of tensor models to detect artefacts (Jones *et al.*, 2013; Tournier *et al.*, 2011; Jones & Leemans, 2011).

There are many freely available software packages to do the DWI data processing and there are studies comparing different software and methods see (Soares *et al.*, 2013). A typical pipeline of DTI involves (see Section 3.1), preprocessing of DWI to correct possible distortions, estimation of tensors, registration between structural (separate structural processing is necessary see Section 1.2) and diffusion spaces or also with standard space (e.g., MNI) and finally constructing a connectivity matrix by using tractography and one's choice of a brain atlas (for more information about brain templates and atlases see (Evans *et al.*, 2012)).

In this chapter, I provided methodological background essential to understand the following studies. In the next chapter, I will look at how microscopic neuronal network develops, in particular, how developmental time windows of axon growth affect topological (Section 1.1.1) and spatial properties (Section 1.1.2) in the neuronal network development.

Part II.

Microscopic neuronal network

2. Developmental time windows for axon growth influence neuronal network topology

Early brain connectivity development consists of multiple stages: birth of neurons, their migration and the subsequent growth of axons and dendrites. Each stage occurs within a certain period of time, or a *developmental time window*, depending on types of neurons and cortical layers. In this chapter, I show the influence of developmental time windows for axon growth on early neuronal network development. Forming synapses between neurons either by growing axons starting at similar times for all neurons (much-overlapped time windows) or at different time points (less-overlapped) may affect the topological and spatial properties of neuronal networks. Here, I explore the extreme cases of axon formation, particularly concerning short-distance connectivity during early development, either starting at the same time for all neurons (parallel, i.e., completely-overlapped time windows) or occurring for each neuron separately one neuron after another (serial, i.e., no overlaps in time windows). In addition, I tested simulated results with *Caenorhabditis elegans* connectivity data. This chapter is based on (Lim & Kaiser, 2015).

2.1. Introduction

The formation of synapses between neurons is influenced by genetic, activity-dependent, molecular and mechanical cues in combination and also in different temporal and spatial scales (Sperry, 1963; Yamamoto *et al.*, 2002; Yu *et al.*, 2012; Franze, 2013; Scheiffele *et al.*, 2000; Dickson, 2002). To avoid abnormal functionality, finding specific target neurons is important. Many guidance mechanisms ensure the correct specification between neurons to successfully establish appropriate synapses. One of the important mechanisms for global synaptic connectivity is chemotaxis. Diffusible and membrane-bound chemical cues guide axons to find their targets (van Ooyen, 2011; Dickson, 2002; Gotz *et al.*, 1992). Electrical activity also affects synaptogenesis and its reorganization (Butz *et al.*, 2014; Butz & van Ooyen, 2013). These guidance cues, however, cannot fully explain certain features of synaptic connectivity. In *C. elegans*, for example, around 40% of connection patterns cannot be accounted for by differences in gene expression patterns (Kaufman *et al.*, 2006; Baruch *et al.*, 2008). Activity-dependent mechanisms are crucial for the refinement of neuronal circuits (Van Ooyen *et al.*, 1995; Butz *et al.*, 2009), but activity seems to have a lower influence on the early connectivity in neural systems. For example, several patterns of connectivity are preserved in knockout studies with no neurotransmitter release (Verhage *et al.*, 2000). Short-range connectivity within less than 700 μm, or interneuron connectivity (Packer *et al.*, 2013; Packer & Yuste, 2011; Price *et al.*, 2011) is difficult to explain by chemical affinity guidance cues unlike long-range connectivity at s the global level (Kaiser *et al.*, 2009). Peters' rule (Braitenberg & Schüz, 1998) suggests that synapse formation in brain circuitry mainly depends on the overlap of geometrical locations of specific axons and dendrites in the absence of guidance cues (Binzegger *et al.*,

2004; van Pelt & van Ooyen, 2013; McAssey *et al.*, 2014; van Ooyen *et al.*, 2014). In particular, the specificity of early synapse formation to develop functional neural circuits was predicted by simple factors from the overlap of axons and dendrites in hatchling frog tadpole (Li *et al.*, 2007) and also in neocortical microcircuits (Hill *et al.*, 2012; Packer & Yuste, 2011).

Another crucial factor is the developmental time window of a neuron. Brain development occurs at different time periods depending on regions, cell types and types of development (Andersen, 2003; Rakic, 2002; Shaw *et al.*, 2008). Cells are born, migrate to certain regions of the brain, differentiate and form synaptic connections influenced by the aforementioned factors. Initial overproductions of neurons and synapses are reduced after 1 year from birth, suggesting particular time periods for neurogenesis, programmed apoptosis, early synaptic pruning and synaptogenesis (Rakic *et al.*, 1986; Purves & Lichtman, 1980; Kelsch *et al.*, 2010; Huttenlocher, 1984). Time windows of development for connections between brain regions influence the topology of cortical connectivity. Kaiser and Hilgetag (Kaiser *et al.*, 2007) and Nisbach and Kaiser (Nisbach & Kaiser, 2007) showed that overlapping time windows of development could generate clusters in brain networks by having more connections between neurons with overlapping time windows of network development. Whereas these time windows operate on the population level, Varier and Kaiser (Varier & Kaiser, 2011) found that neurons having similar birth times were more likely to be connected in *C.elegans*, indicating preferential synaptic connections between neurons with overlapping time windows for axon growth. Some studies have also reported preferential electrical coupling between neurons sharing genetic lineage that are likely to have similar developmental time windows in mice neocortex (Yu *et al.*, 2009; Yu *et al.*, 2012). Furthermore, non-overlapping time windows among neurons in CA3 resulted in selective synaptic connectivity forming sub-modules in the

hippocampus (Deguchi *et al.*, 2011; Druckmann *et al.*, 2014).

To investigate neuronal innervations, computational models (van Ooyen, 2003; van Ooyen, 2011) have been developed ranging from abstract models with few assumptions (Kaiser *et al.*, 2009; Willshaw & von der Malsburg, 1976; Perin *et al.*, 2013) to more complex models simulating neurogenesis and synaptogenesis with realistic neuronal morphologies forming layers and large-scale neuronal networks in the brain (Koene *et al.*, 2009; Godfrey *et al.*, 2009; Hennig *et al.*, 2009; Zubler & Douglas, 2009). In previous models, however, while time windows for neural migration and synapse formation were included it was not systematically studied how different time windows of axon growth would affect the characteristics of the brain network organization.

Here, we investigated how different time windows of axon growth would affect morphological, topological and spatial properties of short-range brain connectivity during early development. Whereas previous studies dealt with time windows that operate on the population level, our current study observes the effect of the timing of axon growth for individual neurons within a neural population. We compared two scenarios of non-overlapping (serial growth) and completely overlapping time windows (parallel growth). To study the role of time windows for axon growth in short-range connectivity, we used the approach of random axon outgrowth, randomly picking a direction, growing in a straight line and establishing a synapse when a target neuron is within certain proximity along the growth direction.

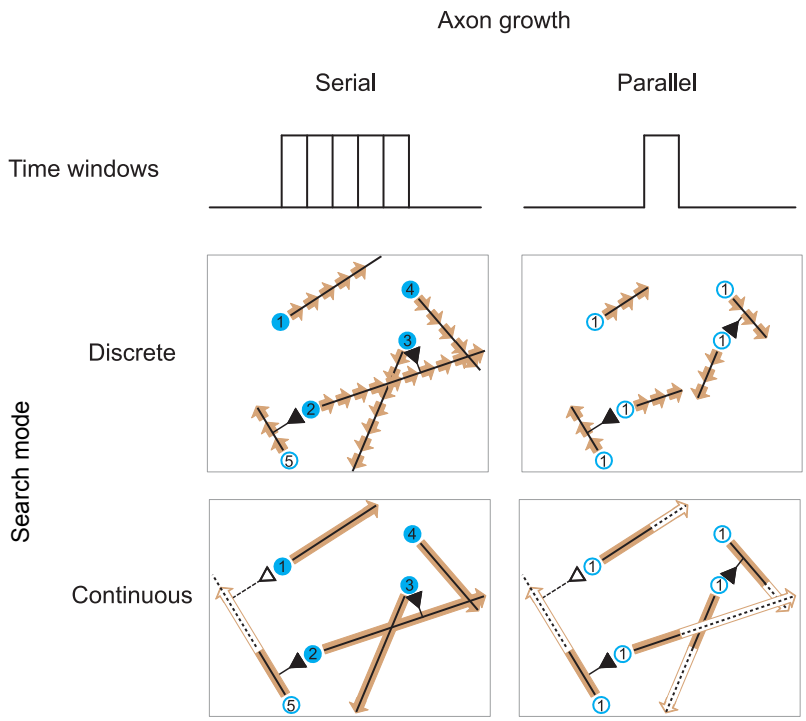

Figure 2.1.: Simulation setting: serial vs. parallel growth. Serial growth: neurons take turns to grow axons. Parallel growth: all neurons start to grow axons simultaneously. Continuous search mode: neurons examine all possible target neurons to establish synapses by finding whether the growth cone could find connectible neurons within a certain proximity, or whether the connectible space of growth cone intersects with the neuron sphere. Blue circles: solid circles denote neurons that finished axon growth and empty circles represent neurons that are active. Numbers in the circles represent the sequence of growth. Black triangles: synapses, Black solid line: axons, Black dashed lines: future axon growth path.

2.2. Methods and materials

2.2.1. Simulation

Most of the assumptions of the model were endowed from the previous study (Kaiser *et al.*, 2009).

Placement of neurons. Neurons were placed randomly in 3D space of 34 by 34 by 34 units except a neuron located at the centre, which was about 4 times as many as for 2D in order to have a comparable chance for establishing a cell position without cell overlap (Kaiser *et al.*, 2009)). The number of neurons varied in the given space: 1000, 1400 and 1800. The total volume of neurons occupied the embedding space from 1% to 14% depending on the cell size and the number of neurons in the simulation.

Sizes of neurons. A neuron was simplified as a sphere where the soma and dendrites were included. The radius of a neuron varied from 0.5 to 0.9 (0.500, 0.604, 0.735, 0.900) to make the volume of the sphere increase 1, 2, 4 and 8 times in each condition. There is an upper limit for the number of incoming connections for a neuron due to space around (Stepanyants *et al.*, 2002) or on the dendrite (Kaiser *et al.*, 2009) as well as due to other factors (van Ooyen, 2001; van Ooyen *et al.*, 2001) (See **Competition section** below). The maximum values of incoming connections were also varied 1, 2, 4 and 8 times according to volume of a neuron because the coverage of dendritic ramifications would expand as the size of our neuron sphere increased. The radius and the number of maximum incoming connections were fixed in each condition. The radius and the number of maximum incoming connection were fixed in each condition. We assumed that the dendrites of a neuron did not grow as the size of a neuron sphere was fixed during simulations. However, we could also

confirm that dendritic outgrowth, changing the size of our neurons (including soma and dendritic tree size) during development, did not affect our conclusions (Figure 2.9); dendrites were assumed to grow radially away from the soma based on the somatofugal growth of neurites (Samsonovich & Ascoli, 2003).

Growth direction. The direction of axonal outgrowth was randomly chosen uniformly in the 3D space, and an axon grew in a straight line toward the given direction as growth direction of axons has a propensity to grow in approximately straight lines unless axons encounter obstructions or guidance cues (Sperry, 1963; Easter *et al.*, 1985; Yamamoto *et al.*, 2002).

Proximity rule for establishing synapses. A synapse was established when the growing axon encountered another neuron within the connectible range (less than or equal to 1 unit length). The distance between a growth cone and a neuron was computed considering the radius of a neuron, or the shortest Euclidean distance between a growth cone and the surface of a neuron (the boundary of dendrites); thus, larger neurons increased their chances of establishing a synapse. We assumed that only the growth cone can establish a synapse.

Competition. Competition between neurons for synapse establishment was realized by limiting the number of incoming connections. A synapse was formed only when the neuron within vicinity could accommodate another synapse. All neurons keep growing their axons until they hit the border of the embedding space, as the maximum number of outgoing connections for a neuron was not limited assuming short-range connectivity within less than 700 μm.

Speed. Speed of outgrowth was fixed for all neurons; the axon lengthened by one unit for each time step.

Discrete and continuous growth. Discrete and continuous search mode were compared. For discrete search mode, the growth cone of a neuron proceeded

along its given direction by one unit Euclidean distance per each iteration time. For continuous search mode, neurons were assumed to have the same average speed as for discrete search mode (or one unit distance per unit time) but were allowed to establish synapses at real number distance, hence continuous search mode. Connectible neurons were found along a virtual direction of axon growth by computing the distance between neurons and the axonal growth line. In other words, check the whole axonal direction at once, to see if it ever comes close to dendrites, or encountering a neuron sphere.

Serial and parallel growth. For serial growth, each neuron takes turns to grow its axon, which represented no overlap in the time windows for axon growth; the first neuron grows out completely and forms all possible connections and finishes its growth, and only then the second neuron starts growing and makes synapses along the way.

Developmental time windows. Different areas in the brain have shown dissimilar growth trajectories over time having partially overlapping time windows (Rakic, 2002; Shaw *et al.*, 2008; Sur & Leamey, 2001). For instance, cortical neurons in Brodmann area (BA) 24 migrate to upper layers faster than neurons in BA11, BA46 and BA17; neurons in BA17 take the longest time to reach their final position in the macaque monkey (Rakic, 2002). Moreover, previous studies have shown that neurons are inclined to establish synapses with other neurons whose time windows of growth overlapped (Kaiser & Hilgetag, 2007; Nisbach & Kaiser, 2007; Deguchi *et al.*, 2011; Druckmann *et al.*, 2014; Yu *et al.*, 2009; Yu *et al.*, 2012). Therefore, by comparing network features between serial and parallel growth, we could observe the influence of time windows for neuronal network development. Additionally, we tested partially overlapping time windows with a small partial overlap and a large partial overlap; serial growth is the extreme case of small overlap, i.e., zero overlap and parallel

growth is the opposite end where time windows of axon growth are maximally overlapped (Section 2.3.4).

Data set. Positions of neurons and growth directions were generated constructing a total of 50 data sets to compare serial and parallel growth using equivalent positions of neurons and growth directions.

In summary, four growth scenarios with serial or parallel growth using discrete or continuous search mode (Figure 2.1) were compared with varying numbers of neurons (1000, 1400, 1800) and cell sizes (0.500, 0.604, 0.735, 0.900).

2.2.2. Comparison of growth scenarios

Serial growth and parallel growth were compared in terms of morphological, topological and spatial features. Morphological features included the number of established synapses, the number of potential synapses and the ratio between the two, or filling fraction (Stepanyants *et al.*, 2002). In biological neuronal networks, not all potential synaptic locations are realized due to competition between neurons (Kaiser *et al.*, 2009; van Ooyen, 2001; van Ooyen *et al.*, 2001), plasticity of connectivity, or limitations in volume (Stepanyants *et al.*, 2002). Next, topological properties such as out-degree, local efficiency, and the proportion of bidirectional connections were investigated (Newman, 2003; Brandes & Erlebach, 2005; Costa *et al.*, 2007). Out-degree of a neuron is the total number of outgoing connections from the neuron, or the total number of outgoing synapses. Out-degrees of neurons were averaged over 50 trials for each neuron and ordered according to the sequence of serial growth. Then, this distribution was fitted with exponential or polynomial curves to assess the difference in out-degree as a function of the sequence of start. This shows whether earlier starters would have an advantage over later starters in establishing outgoing

synapses. The maximum number of incoming connections was limited and increased according to the volume of a neuron. As a result, in-degree was constrained by the maximum number of incoming connections. Global efficiency is the inverse of the harmonic mean of the shortest path length between each pair of nodes Eq.(1.1) and local efficiency for a node is calculated in the same way as global efficiency in the subgraph of the node comprised of its immediate neighbours Eq.(1.2) (Latora & Marchiori, 2001; Latora & Marchiori, 2003).
Finally, we observed spatial properties of the grown neural connectivity. Connection probability between two neurons as a function of distance was calculated by dividing the number of connected edges by the number of possible connections given a distance between two neurons, where the distance between a pair of neurons was the Euclidean distance between the centers of the somata of neurons. Similarly, bidirectional connection probability as a function of distance was calculated by dividing the existing number of bidirectional connections by the number of all possible connections given a distance. The proportion of bidirectional connection was the ratio of bidirectional connections to all existing connections, and it was compared with that in the rewired networks to examine whether the proportion of bidirectional connections was higher in our random outgrowth model than that for random networks. We used rewired networks for benchmark random networks by randomizing or rewiring the original networks while preserving degree distributions (Maslov & Sneppen, 2002; Rubinov & Sporns, 2010). The connection length between two connected neurons was the Euclidean distance between the centers of neurons assuming that the distance between the growth cone and the target neuron was negligible. If a neuron made multiple synapses until it hit the boundary of the given space, the locations where the intermediate synapses were established were considered as synaptic boutons and consequently the axon length for the neuron was defined as the

distance between the neuron and the neuron where the last synapse was formed. Brain Connectivity Toolbox (Rubinov & Sporns, 2010) was used to calculate network measures: in and out-degree, local efficiency and the generation of random networks by rewiring our directed networks while preserving degree distributions.

2.2.3. Validation of our model prediction with *C. elegans* connectivity

We used data and information from previous studies based on the Worm Atlas (Chen *et al.*, 2006; Varshney *et al.*, 2011; Hall & Altun, 2008) as we could make use of birth times of neuron in *C.elegans* as a proxy for development al time windows (http://www.wormatlas.org/neuronalwiring.html#NeuronalconnectivityII). Unfortunately, there is no data from higher organisms since birth times or developmental time windows for axon growth and synaptogenesis are currently not available to the best of our knowledge. Chemical synapses were considered while electrical and neuromuscular junctions were excluded in the connectivity matrix. Spatial locations of neurons were obtained from a previous study (Choe *et al.*, 2004). Based on birth times of neurons, we grouped neurons into 3 groups using k-means clustering algorithm: neurons in group 1 and group 2 have similar birth times and were born early, whereas neurons in group 3 were born much later compared to group 1 and 2 (Figure 2.5A). As each time k-means clustering provides slightly different clusters, we perform 50 trials and classified neurons with the most stable or frequent grouping. We assumed all neurons start to grow axons and dendrites approximately similar latency period; birth time $+\alpha$ is the starting point of time window of axon outgrowth. Thus, birth time can be directly associated with

the start of the growth without losing generality since α is assumed to be about the same for all neurons. Groups are compared in terms of degrees, connection lengths and reciprocal connections. We tested the three most pronounced differences between serial and parallel growth: (1) whether earlier-born neurons acquired higher degrees than later-born neurons (group 1 vs. 2 and group 1 & 2 vs. 3), (2) whether earlier-born neurons established longer connections and (3) whether reciprocal connections are more numerous in neurons in group 1 and 2 than neurons in 1 and 3 or 2 and 3. Long-range connections were defined as connections where the length was at least one standard deviation above the mean of all connection lengths. Additionally, we examined local efficiency and connection probability as a function of distance (Section 2.6.3).

2.2.4. Statistical analysis

Topological and spatial properties between serial and parallel growth such as out-degree, local efficiency, connection probability and bidirectional connectivity were averaged over 50 trials for each neuron then fitted with exponential or polynomial curves. When curves followed close to a power-law (connection probability and bidirectional connectivity), double-logarithmic axes were used and fitted with linear models. Higher proportion of bidirectional connectivity for parallel growth than serial growth was tested by paired t-test and Wilcoxon signed rank test, two-tailed with an α level 0.05 and corrected by Bonferroni for multiple comparisons. To group neurons based on their birth times, we used k-means clustering using Euclidean distance. Degrees and long-range connection length were tested with Kruskal-Wallis test and *post-hoc* multiple comparisons were performed using Mann-Whitney test and corrected by Bonferroni. Calculations and statistical tests

were performed with Matlab R2012b (Mathworks Inc., Natick, MA). Algorithms are available online at http://www.dynamical-connectome.org/ and https://github.com/springdance/BICYcodes.

2.3. Results

2.3.1. Topological and spatial properties

Serial vs. parallel growth Serial and parallel growth scenarios assumed non-overlapping and completely overlapping time widows of axon growth, respectively. As there was no qualitative difference between the results using discrete and continuous search mode (for quantitative differences from a modelling perspective see Section 2.3.2.1), we show results with continuous search mode without losing generality.

2.3.1.1. Out-degree distribution

For serial growth, neurons that started growing their axons earlier took priority in establishing synapses over late starters, hence a decreasing trend of out-degrees as the indices of order in development increased. By contrast, for parallel growth where every neuron started growing their axons simultaneously out-degrees were independent of indices of neurons as the indices merely had nominal values in this case (Figure 2.2A). The contrasting distributions of out-degrees for serial and parallel growth applied to all conditions independent of the number of neurons and the maximum number of incoming connections.

However, the decreasing rate of out-degree for serial growth slowed down when allowing more incoming connections (less severe competition). Note that the less contrasting patterns between serial and parallel growth when larger numbers of incoming connections were allowed (e.g., the fourth column of Figure 2.14) should be attributed to milder competition among neurons rather than to higher neuronal density.

2.3.1.2. Local efficiency

Neurons that started axon growth early on were also characterized by higher local efficiency compared to neurons that developed later for serial growth whereas there was no difference among neurons for parallel growth. The effect was not as pronounced as the decreasing trend for the out-degree distribution for serial growth; the decrease in local efficiency was observed mostly in later starting neurons for serial growth. Similar to the out-degree distribution, the disparate distributions of local efficiency for serial and parallel growth applied to all conditions with different numbers of neurons and maximum numbers of incoming connections, thus we show a representative example (Figure 2.2B). The decreasing rate of local efficiency for serial growth slowed down when allowing more incoming connections (Figure 2.15).

2.3.1.3. Connection probability

Connection probability given a distance between two neurons decreased rapidly as the distance increased following power-law tail behaviour (Figure 2.3A). The rate of decreasing connection probability when competition was imposed was

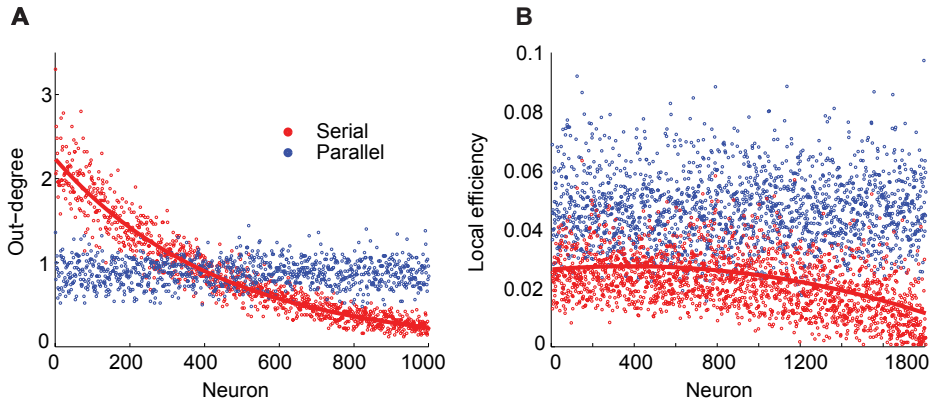

Figure 2.2.: Topological properties for Serial vs. Parallel growth. X-axis represents indices of neurons. For serial growth, the indices of neurons indicate the order of starting to grow axons, whereas for parallel growth the indices just represent nominal values. Red: serial growth, Blue: parallel growth (A) Out-degree (y-axis), (B) Local efficiency (y-axis). For a complete overview of all conditions see Figure 2.14 & 2.15.

almost similar to that without competition (Figure 2.3A inset). The connection probability decreased faster for parallel growth than for serial growth with distance between neurons, while the number of established synapses was the same between serial and parallel growth scenarios (Figure 2.3B). The discrepancy of slopes for serial and parallel growth in the doubly logarithmic plot became reduced as the maximum number of incoming connections increased (Figure 2.16).

Figure 2.4B shows a schematic view of the relationship between the distance between neurons and the connection probability of the two neurons. When neurons are located farther apart from each other, the connection probability decreases since the range of growth directions towards which it can successfully establish a synapse is more limited. In other words, the connection probability between a pair of neurons located a distance d apart is proportional to the range of growth angles a neuron can take, that is the connection probability given

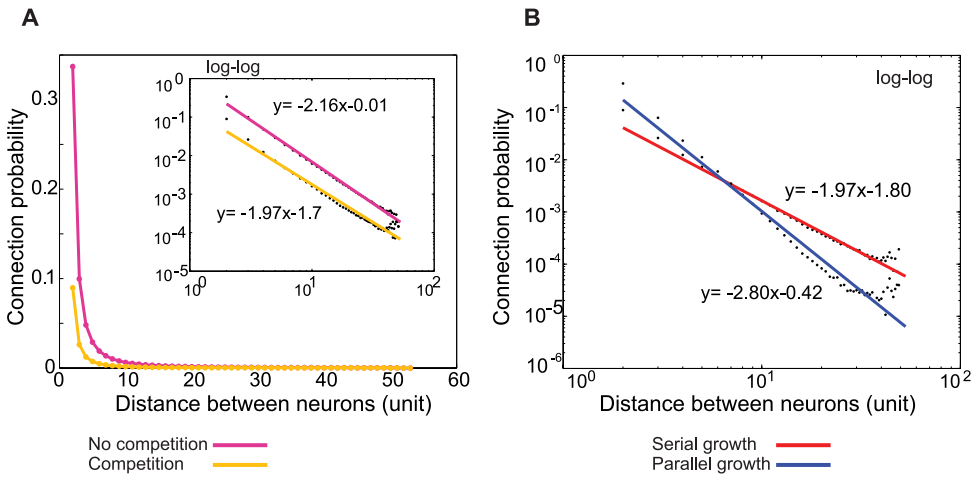

Figure 2.3.: Connection probability decreased with distance and decreased more rapidly for parallel growth than for serial growth. (A) Magenta: no competition, Yellow: competition. (Inset) Log-log plot of connection probability. (B) Log-log plot of connection probability for serial and parallel growth. Red: serial growth, Blue: parallel growth. For a complete overview of all conditions see Figure 2.16.

a distance d , $P(d) \propto \theta$. The growth angle θ from the straight line between the centres of neurons can be calculated using the inverse sine as from our assumptions a neuron grows onwards we can only consider $-\frac{\pi}{2} < \theta < \frac{\pi}{2}$,

$$P(d) \propto \arcsin \frac{1+r}{d} \tag{2.1}$$

$$\arcsin \frac{1+r}{d} \approx \frac{1+r}{d} \tag{2.2}$$

$$P(d) \approx \frac{1}{d} \tag{2.3}$$

where r represents the size or the radius of a neuron and d stands for the distance between the centres of neurons and inverse of sine can be approximated by its Maclaurin series when $1 + r < d$. Thus, Eq.(2.1) can be approximated as Eq.(2.2) taking only the first term of the series. The log-log plot of distance and angle also showed straight lines since the connection probability is inversely

proportional to the distance d (Eq.(2.3), Figure 2.4).

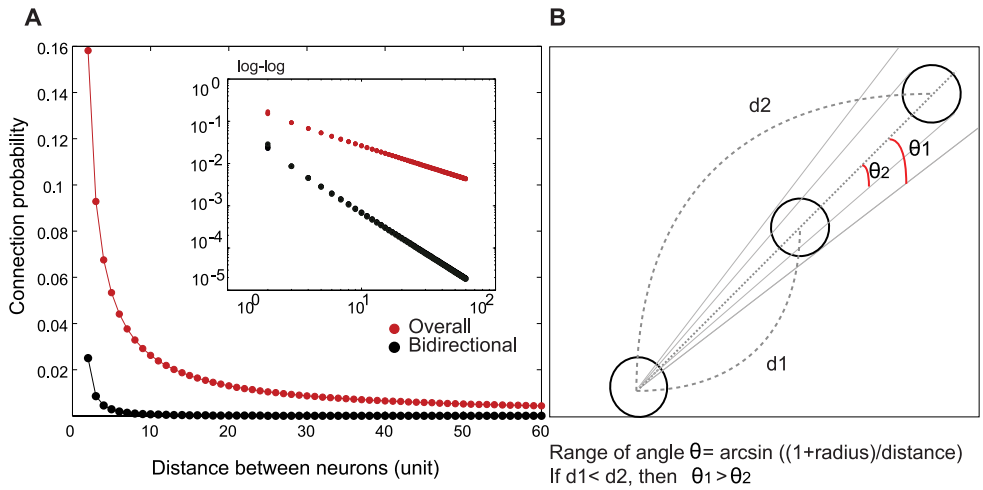

Figure 2.4.: Theoretically generated connection probability and the schematic relationship between the range of angle for a pre-synaptic neuron can take and the distance between two neurons. (A) Red: overall connection probability, black: bidirectional connection probability. Inset. Bidirectional connection probability decreased more rapidly with distance between neurons than overall connection probability. (B) Circles: neurons, d_1 and d_2: the distances between neurons, θ_1 and θ_2: the maximum direction angles a pre-synaptic neuron can have to establish synapses with a target neuron. As the distance becomes longer, the range of angles becomes narrower; if $d_1 < d_2$, then $\theta_1 > \theta_2$. Therefore, if a target neuron is far from the pre-synaptic neuron, it is less likely to form a connection, leading to lower connection probability.

2.3.1.4. Bidirectional connections

Two neurons located close to each other are more likely to form synapses (Figure 2.4) in general and consequently there would be more reciprocal connections between two neurons close to each other (Figure 2.4A). However, this higher connection probability for bidirectional connections for nearby neurons assumes that relevant neurons are available for incoming connections. Synapses would not be formed when the target neurons have reached its maximum incoming

limit even if neurons reside closely to each other and the growth directions are narrow enough to form synapses. For serial growth even if both of them are within proximity of the other neuron's growth direction, one of them is more likely to be occupied and no longer available for making another synapse. Since they started at different time points thus one neuron took much longer to reach the other neuron unlike for parallel growth. Therefore, bidirectional connections would be more numerous for parallel growth than for serial growth. As we expected, more frequent reciprocal connections were observed for parallel growth than for the serial growth scenario (Figure 2.5B). For example, 1000 neurons with one incoming connection per neuron allowed, neurons formed about six times as many bidirectional connections for parallel growth as for serial growth (Wilcoxon signed rank test, $p < 10^{-7}$ corrected by Bonferroni, Figure 2.5B). The difference between serial and parallel growth disappeared as neurons were allowed to have more incoming connections (Figure 2.17). The simulated bidirectional connection probability using inverse sine (Eq.(2.1)) was calculated by squaring the connection probability assuming independence among neurons for synapse establishment (Figure 2.4A, black).

We also investigated whether the bidirectional connectivity was higher than expected in random networks. Random networks were constructed by randomizing or rewiring the original networks while preserving degree distributions (Maslov & Sneppen, 2002; Rubinov & Sporns, 2010). For smaller neuron sizes such as radii 0.5 and 0.604 concomitant with 1 and 2 maximum incoming connections allowed, respectively, rewired networks did not have any bidirectional connectivity even when considering larger numbers of neurons up to 1800, or higher neuronal density. For larger neuron sizes, thus having a larger reach and more incoming connections allowed, originally generated networks with random outgrowth showed 10 to 17 times larger bidirectional connection pro-

portions for serial growth and from 11 to about 40 times larger proportions for parallel growth depending on conditions. In summary, both serial and parallel growth resulted in higher bidirectionality than that of the benchmark random network, indicating random outgrowth model with geometrical constraints can also reproduce higher synaptic clusters.

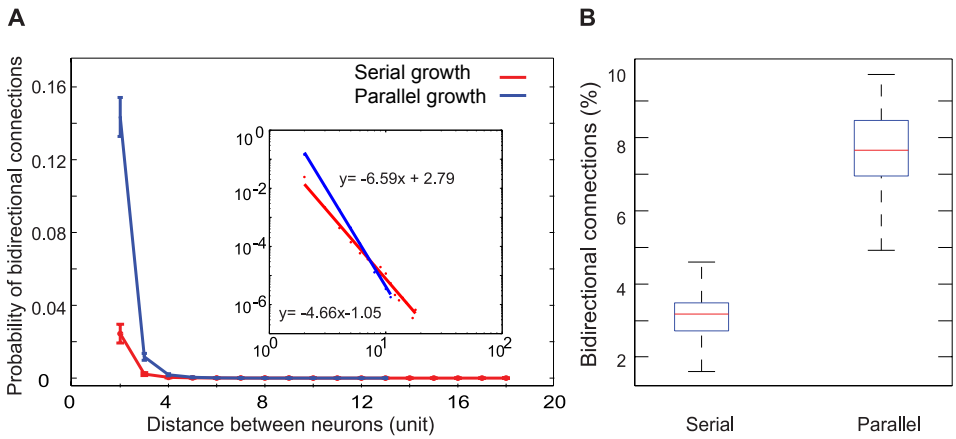

Figure 2.5.: Connection probability for bidirectional connections. (A) Connection probability of reciprocal connections for serial and parallel growth depending on the distance between neurons. (Inset) Log-log plot, more bidirectional connections and steeper of connection probability with distance for parallel growth, Red: serial growth, Blue: parallel growth. (B) The number of reciprocal connections for serial and parallel growth. For a complete overview of all conditions see Figure 2.17.

2.3.1.5. Connection length distribution and Axon length

Serial and parallel growth generated different connection length distributions where connection length was defined as the Euclidean distance between connected neurons. Note that the total number of connections (synapses) was the same both for serial and parallel growth scenarios. The connection length distribution for parallel growth was characterized by an exponential decrease

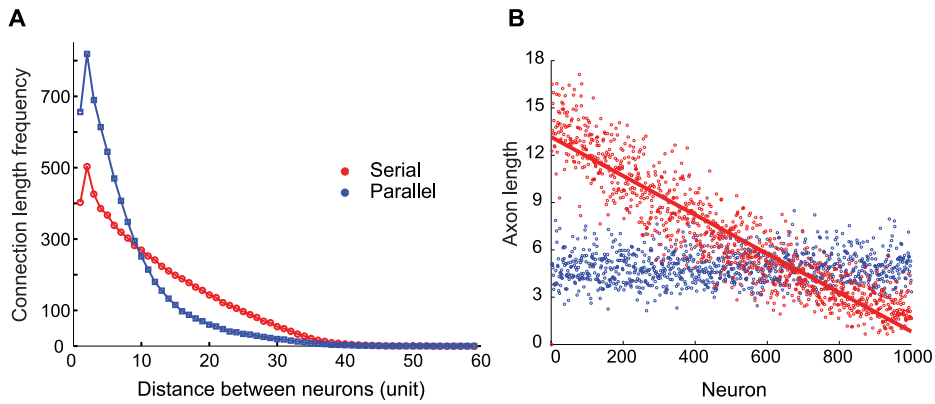

Figure 2.6.: Connection length frequency and axon length.(A) Connection length frequency. For parallel growth, Euclidean connection lengths between connected neurons were more concentrated around short lengths and decreased exponentially with distance while for serial growth the frequency decreased more linearly with distance and obtained longer connections in overall. (B) Axon length. Neurons that started axon growth earlier acquired longer axon lengths than later starters. X-axis for serial growth: the order of starting growth and x-axis for parallel growth: nominal indices of neurons, y-axis: axon length. For a complete overview of all conditions see Figure A2.18.

in the frequency, having a higher proportion of shorter connections while the connection length distribution for serial growth demonstrated almost linear and slower decrease in the frequency having a larger number of longer connections than for parallel growth (Figure 2.6A). The difference between serial and parallel growth became less obvious as more incoming connections were allowed for a neuron (Figure 2.18).

The axon length for the neuron was defined as the connection length between the neuron and the neuron to which the last synapse was formed assuming the intermediate synapses were synaptic boutons along the axon. Earlier starters demonstrated longer axon lengths than later starting neurons for serial growth whereas no difference was observed in axon length for parallel growth (Figure 2.6B).

2.3.1.6. Comparison of our model predictions with *C. elegans* connectivity

To validate our model predictions, we made use of *C. elegans* data (Chen *et al.*, 2006; Varshney *et al.*, 2011; Hall & Altun, 2008; Choe *et al.*, 2004). Using only chemical synapses, we tested our three major predictions from our model concerning degree, connection lengths and bidirectional connectivity. Group 1, 2 and 3 represent three groups of neurons clustered based on their birth times (Figure 2.7A). While birth times in groups 1 and 2 were, on average, 114.78 minutes apart, the time difference between groups 2 and 3 was more than 1255.70 minutes. As birth times of group 1 and group 2 do not differ much, we can assume that group 1 and group 2 represent large overlapping time windows case (or parallel growth), while group 1 and group 3 or group 2 and group3 indicate small overlapping time windows case (or serial growth).

Here birth time is used as an equivalent of the starting point of the time window for axon (and dendrite) outgrowth. Time windows for neurogenesis and synaptogenesis should be treated differently, however; here we assumed time windows for synaptogenesis in *C. elegans* started after equivalent time passes for all neurons for simplicity. We tested whether group 1 and 2, with neurons born early during development, achieved higher out-degrees than group 3. We found that neurons in group 1 and 2 indeed obtained larger numbers of connections (higher degrees) compared to neurons in group 3 (Kruskal-Wallis test, $p < 10^{-6}$ and *post-hoc* multiple comparison Mann-Whitney two-tailed: between group 1 and 3, $p < 10^{-4}$; between group 2 and 3, $p < 10^{-4}$, p-values are corrected by Bonferroni, Figure 2.7B). Neurons in group 1 and 2 established longer connections compared to neurons in group 3 (Kruskal-Wallis test, $p < 10^{-4}$; Mann-Whitney two-tailed: between group 1 and 3, $p < 0.0057$; between group 2

and 3, $p < 0.0002$, p-values are corrected by Bonferroni, Figure 2.7C) and larger number of bidirectional connections (Figure 2.7D). As expected for parallel growth case, group 1 vs. group 2 did not display significantly higher degree, long-range connection lengths or bidirectional connectivity differences. Local efficiency and connection probability, however, were not consistent with the model predictions indicating that there are factors excluded in the model which influence these features (See Discussion and 2.6.3).

2.3.2. Morphological properties

2.3.2.1. Potential synapses and established synapses

Neuron might miss a connectible neuron in discrete search mode because it establishes synapses only at discrete time steps along the direction (neglected space, Figure 2.8B). At the same time, it is also possible to find the same spot multiple times because the same neuron is likely to be within proximity again after one unit step away (multiple detection space Figure 2.8C). As we did not allow neurons to make multiple synapses with the same neuron in the simulated networks, the total number of potential synaptic places was always larger in continuous search mode than in discrete search mode (Table 2.1, Figure 2.8A), which also applied to the number of established synapses (Table 2.1). In contrast to the topological and spatial properties (Section 2.3.1), there was no difference in the number of potential synapses between serial and parallel growth since the placement of neurons and the growth directions were the same and they were independent of serial and parallel growth scenarios.

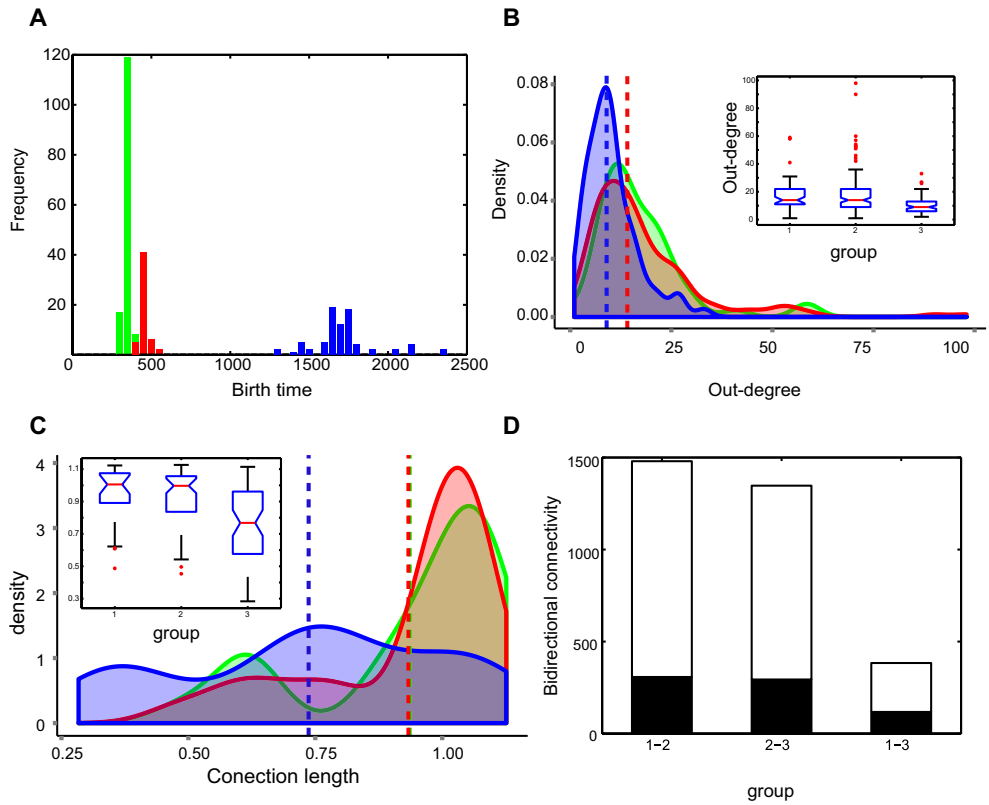

Figure 2.7.: Model predictions vs. neuronal connectivity in *C .elegans*. (A) Group 1, 2 and 3 using k-means clustering based on the birth times of neurons in *C .elegans*. Green: group 1, Red: group 2, Blue: group 3. X-axis: birth time (minutes), Y-axis: group membership. (B) Distributions of out-degree for group 1, 2 and 3 using kernel density estimation. X-axis: out-degree, Y-axis: density, vertical dashed lines: medians of distributions, (inset) Birth time and degree. Boxplot. X-axis: birth time group, Y-axis: degree of neurons. (C) Density plot of long-range connection lengths, x-axis: connection lengths, y-axis: density of distribution, vertical dashed lines: medians of connection lengths, (inset) Birth time and long-range connection lengths. Boxplot superimposed with data points. X-axis: birth time group, Y-axis: length, approximated by Euclidean distance between centres of connected neurons, of long-range connections (mm). (D) Birth time group and the number of bidirectional connections. X-axis: birth time groups Y-axis: the number of connections (black: bidirectional connections; white: the total number of connections between relevant groups).

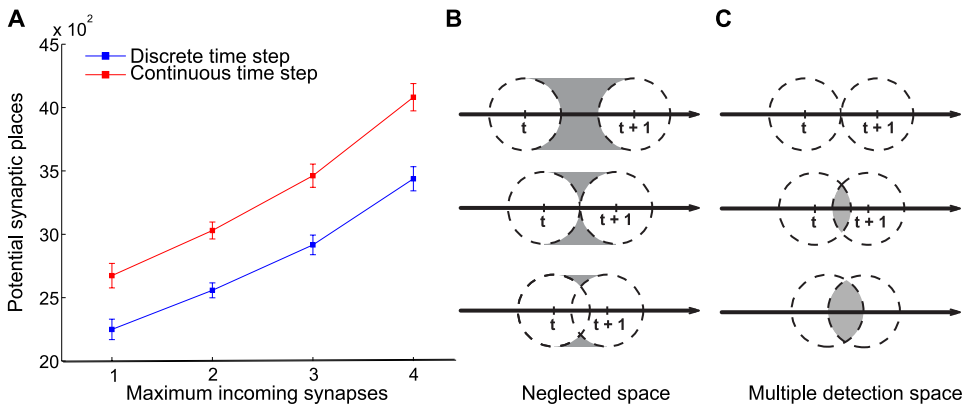

Figure 2.8.: Neglected space and multiple detection when using discrete time steps. (A) Neglected space using discrete time steps growing at times t and $t + 1$, thick black solid line: growing axon, dashed circles: if a neuron happens to be inside the dashed circle, a synapse can be formed with the neuron. The shaded areas represent neglected space due to discrete time steps. Depending on the ratio between the proximity criterion and the spatial distance covered in one time step, the neglected area can be enlarged and shrunk. (B) Multiple detection of the same neuron using a discrete time step. If a neuron happens to be inside the shaded area, the growth cone can detect the neuron multiple times. Again depending on the ratio between the proximity rule and the magnitude of a time step, the space can be expanded or narrowed.

2.3.3. Simulation results with dendritic development.

We have also explored the condition when neurons increase their sizes from a point to a sphere of radius 0.5 as a representative case to check the effect of outgrowing dendrites and its concomitant increase of the dendritic arborization area. Dendrites were assumed to grow radially away from the soma based on the somatofugal growth of neurites (Samsonovich & Ascoli, 2003). We could confirm that dendritic growth, changing the size of our neurons (including soma and dendritic tree size) during development, did not change our main results; neurons started earlier achieved higher out-degrees and longer axon lengths for serial growth, higher bidirectionality for parallel growth due to overlapping

Table 2.1.: Row (left) Column (right) where is among = , < and >. For example parallel continuous > serial discrete, which reads the number of potential synapses for parallel growth using continuous search mode is larger than that of serial growth using discrete time steps.

		Serial	
Parallel		Continuous	Discrete
	Continuous	=	>
	Discrete	<	=

time windows and connection probability decreases faster with distance for parallel growth than serial growth (Figure 2.9).

2.3.4. Partially overlapping time windows

We additionally examined partially overlapping time windows for axon growth with groups of neuron growing together. We tested a small partial overlap and a large partial overlap; neurons were grouped into 2, 3 and 4 groups and were assigned to start growing axons after neurons in earlier starting group have elongated five (larger overlap) and ten (smaller overlap) unit length, in other words, neurons in other groups wait for 5 or 10 unit time. For instance, we divide neurons into two groups randomly and after neurons in the group start growing axons for 5 unit length, neurons in the other group start developing their axons. Serial growth is the extreme case of small overlap i.e. zero overlap and parallel growth is the opposite end where time windows of axon growth for neurons are maximally overlapped. Likewise, if we divide neurons into many groups, say into the same number of neurons, we would expected the smooth decrease in degrees and connection lengths, which was observed in main figures (Figure 2.2A and Figure 2.6B, respectively) where single neuron is actively growing its axon rather than multiple neurons in our main results.

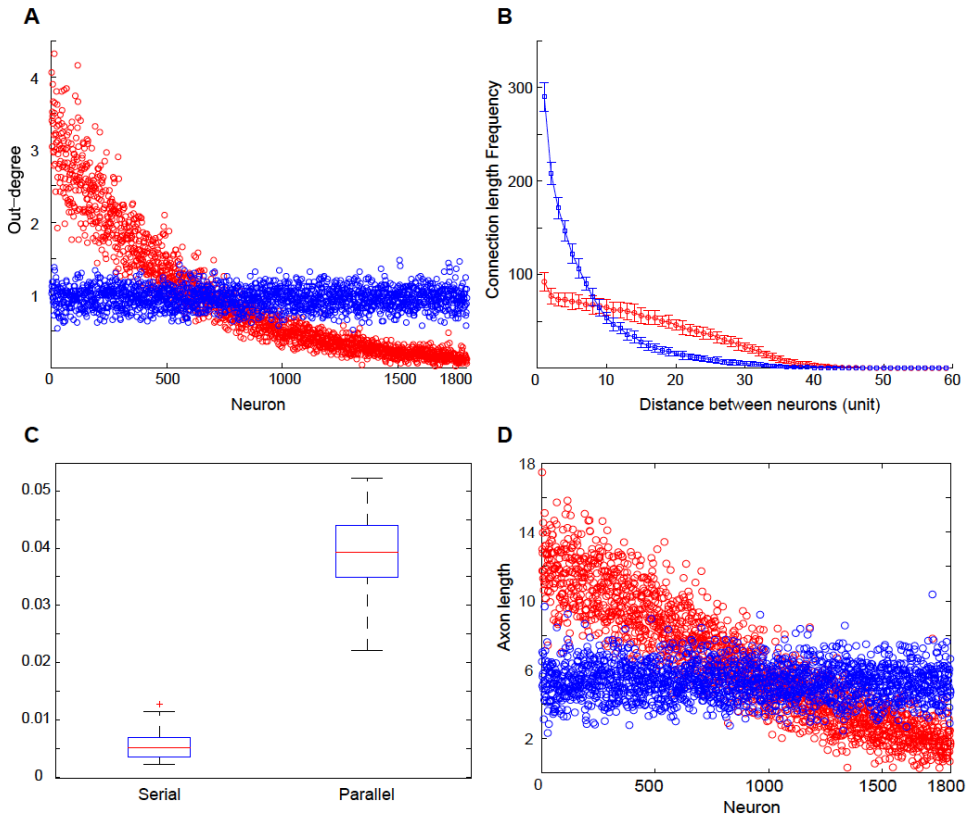

Figure 2.9.: Simulation results with dendritic development. A. Out-degree, red: serial growth, blue: parallel growth, x-axis: for serial growth- the order of growth, for parallel growth- indices of neurons. B. Connection length distribution with distance between neurons. Red: serial growth, blue: parallel growth, C. Bidirectional connection ratio. Left: serial growth, right: parallel growth. The results were consistent with our previous results. D. Axon length. red: serial growth, blue: parallel growth, x-axis: for serial growth the order of growth, for parallel growth- indices of neurons.

Earlier starting groups achieved higher out-degrees (Figure 2.10) indicating better chances of becoming hub nodes in the networks and also achieved longer axon lengths (Figure 2.11); larger overlap of time windows produced more reciprocal connections between neurons (Figure 2.12). In summary, the results were consistent with the previous findings.

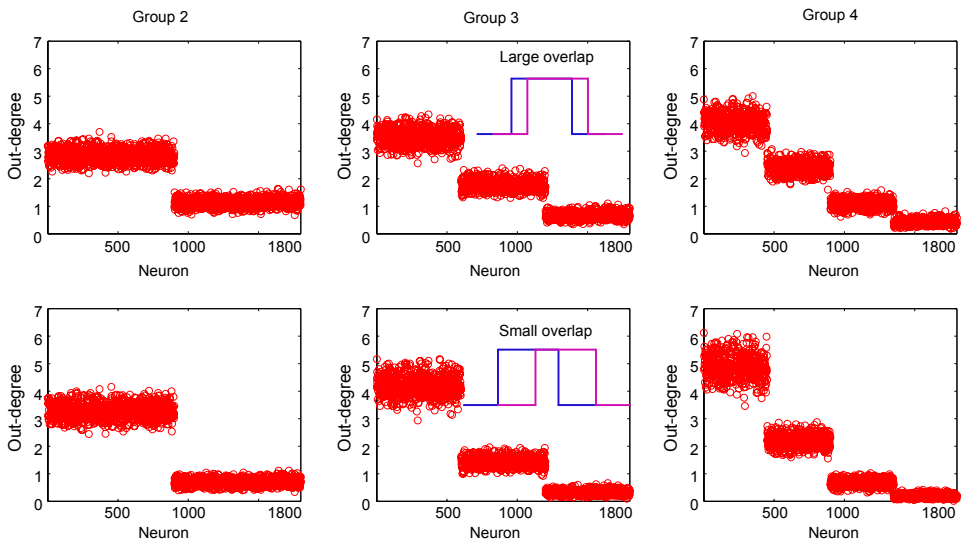

Figure 2.10.: 1^{st} row: a large overlap in time windows for axon growth; 2^{nd} row: a small overlap in time windows; column shows the number of groups in which neurons were divided. X-axis: neurons are orderly grouped according to their group time windows; Y-axis: out-degree. The discrepancy of out-degrees between groups is smaller with a large overlap than a small overlap case and earlier starting groups acquired higher out-degrees.

2.4. Discussion

In this study, we demonstrated that different time windows for axon growth could lead to distinct topological and spatial characteristics by exploring two extreme cases of time windows representing serial (heterogeneous) and parallel (homogeneous) growth. We also tested our model predictions with *C. elegans* connectivity data. Overlapping and non-overlapping time windows for axon growth resulted in different topological and spatial properties of neuronal networks, although morphological properties such as the number of potential synapses and established synapses were not different (Figure 2.13). For serial growth, neurons that started axon growth early on achieved higher out-degrees, higher local efficiency and longer axon lengths than later starting neurons, while no difference was observed for parallel growth. Bidirectional connections were

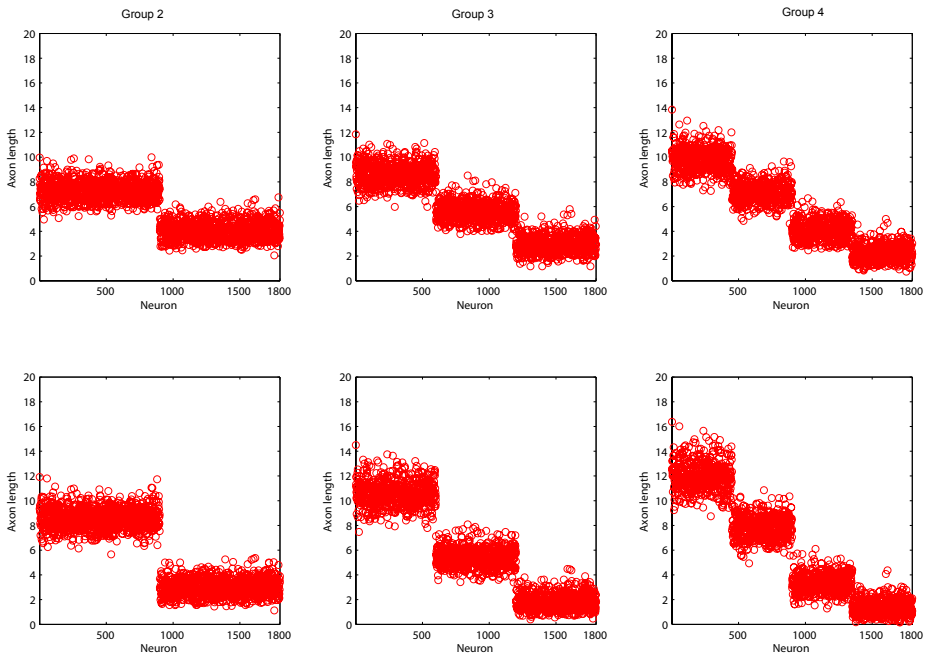

Figure 2.11.: 1^{st} row: a large overlap in time windows for axon growth; 2^{nd} row: a small overlap in time windows; column shows the number of groups in which neurons were divided. X-axis: neurons are orderly grouped according to their group time windows;Y-axis: Axon length. The discrepancy of axon length between groups is smaller with a large overlap than a small overlap case and earlier starting groups acquired longer axon lengths.

more numerous for parallel growth. Finally, axon lengths for serial growth were longer. Together, time windows for axon growth seem to have a major influence on network organization during neural development.

Non-overlapping vs. overlapping time windows for axon growth

Brain development shows region-specific time windows of growth that partially overlap (Rakic, 2002; Shaw *et al.*, 2008; Sur & Leamey, 2001). Previous computational studies (Kaiser & Hilgetag, 2007; Nisbach & Kaiser, 2007) as well as the analysis of the *C. elegans* cell lineage (Varier & Kaiser, 2011) strongly suggest that neurons are inclined to establish synapses with other neurons whose developmental time windows overlap (Varier & Kaiser, 2011; Deguchi *et al.*, 2011;

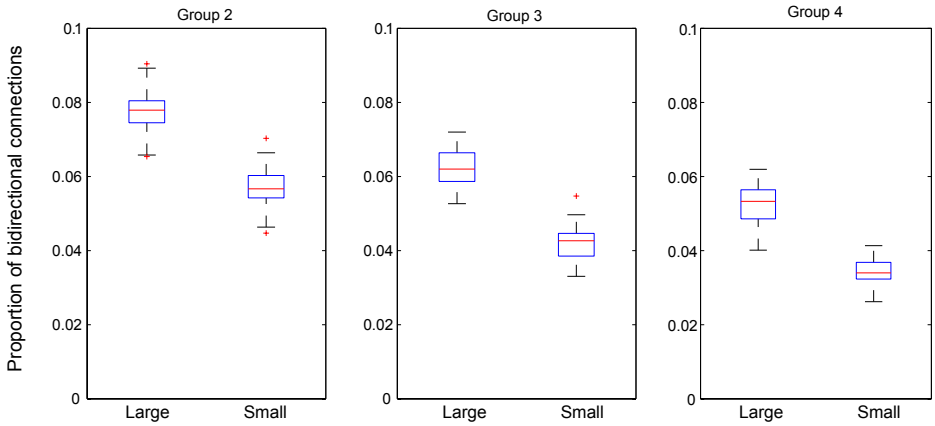

Figure 2.12.: X-axis: (left) a large overlap (right) a small overlap; Y-axis: the number of bidirectional connections. The bidirectional connections in neurons having large-overlapping time windows were more frequent than those of neurons with small-overlapping time windows; with more heterogeneous neurons i.e. larger number of groups, the number of bidirectional connection decreased (from left to right column).

Druckmann *et al.*, 2014). We investigated how developmental time windows for axon outgrowth affect network connectivity by analyzing non-overlapping (serial growth) and maximally overlapping (parallel growth) time windows for axon growth. For serial growth, a neuron is able to start growing its axon only after the previous neuron finishes developing its axon. Thus time windows of axonal growth do not overlap whereas for parallel growth, all neurons have the same time window onset, starting to grow axons simultaneously. Note, however, that the end point of the time window —the time when a neuron left the embedding space—could differ between neurons. Biologically, neurons with highly overlapping time windows of development can be interpreted as neurons whose birth times, lineage and cell types are homogeneous such as cortical neurons in the same layer or clone sister neurons sharing genetic resemblance, both of which were characterized with a higher propensity to establish synapses between them (Yu *et al.*, 2009; Deguchi *et al.*, 2011).

For serial growth, earlier development for axon growth facilitated more numerous synapse establishments resulting in higher out-degrees, higher local efficiency and longer axon lengths, suggesting a possible mechanism for network hub formation. These results are in line with experimental findings analysing the neuronal network of *C. elegans* (Varier & Kaiser, 2011) and even with findings for the network of fibre tracts between cortical regions in the macaque (Kaiser, 2011). As we expected, earlier born neurons in *C. elegans* established more connections than later born neurons. This might allow us to predict the history of neural development based on cell lineage and adult degree distribution. Local efficiency shows that how efficiently neighbour neurons of a neuron would communicate when the neuron is removed being linked to the fault tolerance of the network (Latora & Marchiori, 2001; Latora & Marchiori, 2003). Here, higher local efficiency of early starter neurons indicates that the local network comprised of the neuron's immediate neighbour neurons have more efficient communication among neighbour neurons and also more resilience against the removal of the early starter neuron. In line with these findings, an earlier study in *C. elegans* (Varier & Kaiser, 2011) found that most connected neurons were born at similar time points and that the majority of long-distance connections appeared early on. This suggests that overlapping developmental time windows could contribute to increase the connection probability and early establishment of long-distance connectivity, which could secure specifically targeted long-range connections. Starting early on is a mechanism for individual neurons to establish long-distance connections. However, serial growth also affected the neural population as a whole. In our simulations, the sequential serial growth generated significantly more long-distance connections than the more homogeneous parallel growth; neurons that started axon growth later often found that post-synaptic neurons were already occupied whereas earlier starters

successfully established synapses to the same target neurons even if they were distantly located.

The connection probability between a pair of neurons decreased as the distance between them increased in line with anatomical studies (Hellwig, 2000; Schüz *et al.*, 2006; Kaiser *et al.*, 2009). The rate of decrease was steeper for parallel growth indicating that neurons with the same time window of axonal growth tend to prefer short-distance connections rather than long-distance connections. In contrast, for serial growth, the distance was not the only factor to establish connections since late starter neurons may not be able to form certain synapses due to the limited number of incoming connections, thus having a slower decrease of connection probability with distance.

Bidirectional connections were more numerous for parallel growth than for serial growth, which we confirmed with *C. elegans* connectivity data; the discrepancy between neurons (or neuron groups) was negatively correlated to the degree of overlap in the developmental time windows. In other words, larger overlap of developmental time windows (group 1 and 2) reduced differences in degrees and connection length. More frequent reciprocal connections for parallel growth provide additional converging evidence that overlapping time windows during development would produce more reciprocal connections between neurons (Kaiser & Hilgetag, 2007; Nisbach & Kaiser, 2007; Varier & Kaiser, 2011). The bidirectional connection probability decreased more rapidly than the overall connection probability, which is consistent with previous studies using thick-tufted layer 5 pyramidal neurons in neonatal Wistar rats (Perin *et al.*, 2011; Perin *et al.*, 2013). Previous studies have shown over-represented reciprocal connections in the rat relative to random networks claiming that the synaptic connectivity is preferential rather than random (Kelsch *et al.*, 2010; Markram

et al., 1997). However, in this study we observed a higher proportion of bidirectional connections while still using a random outgrowth mechanism for both serial and parallel growth scenarios.

Earlier-born neurons in *C. elegans* acquired higher out-degree, longer axon lengths and higher reciprocal connectivity, which were consistent with the model predictions. However, local efficiency and connection probability as a function of distance between neurons showed discrepancy from what the model predicted (Section 2.6.3, Figure 2.19). We believe that the model predictions and the actual results from *C. elegans* were different because **i**) differences in local efficiency between serial and parallel growth were less apparent for all conditions and **ii**) connection probability in our model depends mainly on the geometrical arrangement of dendrites (neuron spheres) and axons, whereas the connectivity of *C. elegans* has additional constraints such as its elongated body shape and a higher prevalence of long-distance connections (Kaiser & Hilgetag, 2006).

Discrete vs. continuous search mode and neglected vs. multiple detection

While the previous results addressed the biological role of axon growth time windows, we also looked at the influence of the model used for computer simulations of axon growth. As modelling each growth step (numerical discrete simulation) is computationally expensive, using an analytical approach (continuous simulation) saves computational resources. Using continuous search mode increased the total number of potential synapses that neurons found and also increased the number of established synapses. This is due to the better coverage of the growth cone pathway: for discrete steps, neurons may miss possible synaptic places since they can only search for target neurons at specific

time steps. The volume of neglected space for discrete search mode depends on the ratio of unit time step to the length of proximity rule. If the proximity defining 'close enough to form a synapse' is smaller than the size of unit time step, the neglected space expands and if the vicinity covers larger space than the unit time step the neglected space shrinks (Figure 2.8B). On the other hand, if the proximity reaches farther than the half of the unit step, the overlapping space of proximity between previous time step and the next step increased the possibility of detecting the same neuron multiple times (Figure 2.8C). The length of time step is usually determined considering trade-off accuracy of the computation and processing time but here we also need to consider the ratio of time step to proximity criterion, or another trade-off between neglected space and multiple detection space. By adopting continuous search mode, we could reduce processing time, however, it can be only applied to piecewise straight lines when assuming that branching of axons or turning of growth direction does not occur often.

Limitations and future studies

This general study of axon growth uses simplifications both for axon growth and neuron morphology. The size of the neuron and the proximity rule can only be an estimate of the average behaviour of axons growing close to existing neurons. For models of specific tissue, the morphology of the dendritic tree and the number of spines would need to be taken into account. Such parameters, for many types of neurons and many different species are available in the NeuroMorpho database (Samsonovich & Ascoli, 2003; Ropireddy & Ascoli, 2011; Zawadzki *et al.*, 2012). Another simplification is the axon growth in a straight line. Even though growing in a straight line is the default behavior, axons can branch or their growth directions can be influenced by attractive or repulsive signalling cues in the external environment (Yamamoto *et al.*, 2002;

Krottje & Van Ooyen, 2007; Sakai & Kaprielian, 2012). Finally the embedding space of neurons for axon growth and synaptogenesis of our model was fixed during development, while internal volume changes through neurite growth and external mechanical factors could change the location of neurons and influence their synapse formation probabilities. For uniform expansion along all directions, this would increase connection lengths but differences between serial and parallel growth would remain (See Section 2.6.4 for detailed analysis and discussion).

2.5. Conclusion

In the current study, we showed that for serial growth of axons neurons with an early start of axonal growth acquired higher out-degrees, higher local efficiency and longer axon lengths while overlapping time windows for parallel growth contributed to higher reciprocal connection and faster decrease in overall connection probability and connection length distribution with an increased distance between neurons. These predictions were confirmed when comparing our findings with the organization and development of the neuronal network of *C. elegans*. In summary, we demonstrated that axon growth time windows —like time windows for synaptogenesis and neuronal migration—modulate the topological and spatial properties of neuronal networks. We hope that these findings elucidate the origins of normal and pathological network development. In next chapter, I examine the macroscopic brain network maturation using Diffusion Tensor Imaging (Section 1.2).

2.6. Appendix

2.6.1. Different connection patterns between serial and parallel growth

As the positions of neurons are fixed in the simulation, there are fixed number of possible synapses. Although, the topology of the connectivity among neurons is very different for serial growth and for parallel growth, neurons for serial growth can make as many synapses as neurons for parallel growth. I explained this in a very simple case with 4 neurons in the following Figure 2.13.

2.6.2. Results for all conditions

Out-degree, local efficiency, connection probability, percentage of bidirectional connections and connection length distribution for all conditions are shown below (Figure 2.14-2.18).

2.6.3. Comparisons of local efficiency and connection probability from *C. elegans* data with the model predictions.

We calculated local efficiency and connection probability for *C. elegans* data. Unlike out-degree, bidirectional connections and axon length results in the main text, showed discrepancy from what the model predicted In particular, local efficiency results showed the opposite pattern from the model prediction; later-born neurons showed higher local efficiency than earlier-born neurons (Kruskal-Wallis test and post-hoc multiple comparisons were performed using

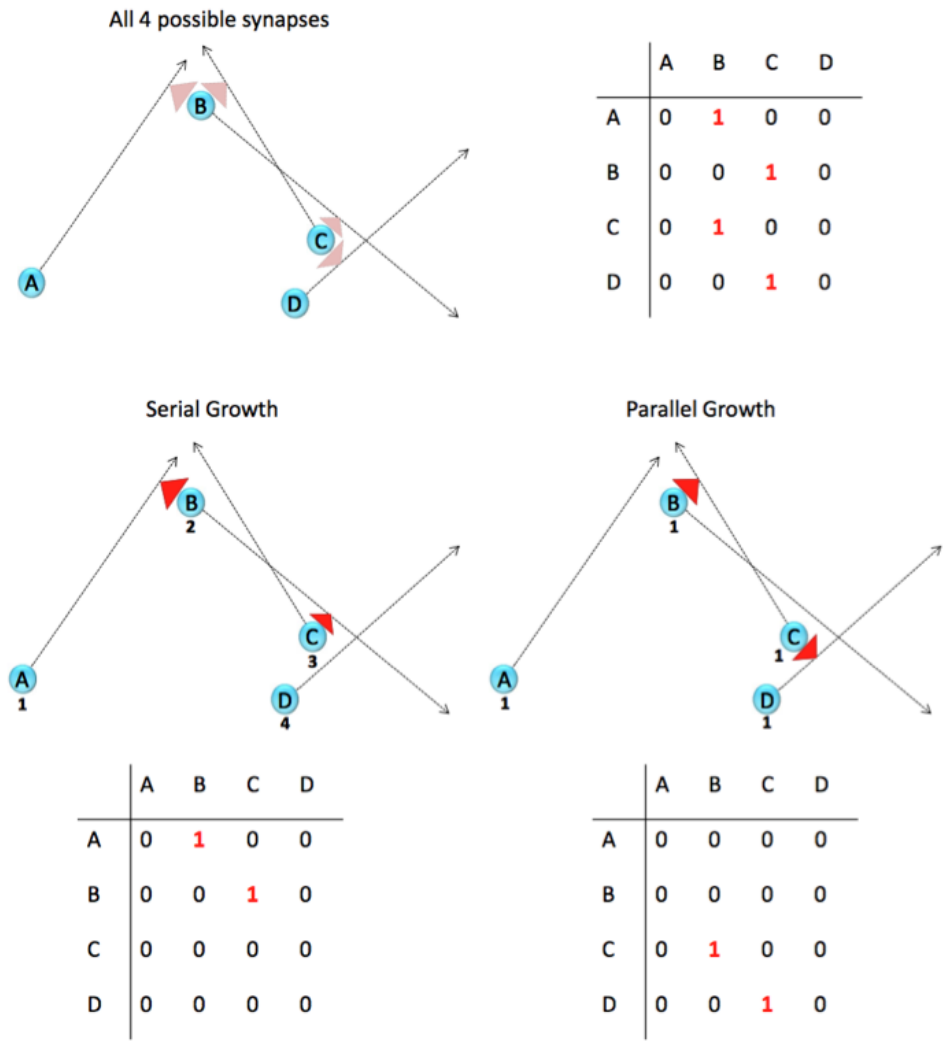

	A	B	C	D
A	0	1	0	0
B	0	0	1	0
C	0	1	0	0
D	0	0	1	0

	A	B	C	D
A	0	1	0	0
B	0	0	1	0
C	0	0	0	0
D	0	0	0	0

	A	B	C	D
A	0	0	0	0
B	0	0	0	0
C	0	1	0	0
D	0	0	1	0

Figure 2.13.: Solid circles are neurons A, B, C and D. Dashed lines with arrows at the end of the lines represent directions for axon growth. Light coloured triangles show potential synaptic spots between neurons and red triangles indicate established synapses. I: all 4 possible synapses, II: Serial growth and III: parallel growth. All were accompanied by their adjacency matrices. Numbers under the neurons in II and III represent the orders of growing axons; neuron A starts growing its axon first and then after neuron A finishes neuron B starts and neuron C and neuron D in order for serial growth and neuron A, B, C and D start axon growth simultaneously. Here, neurons are assumed to make only one synapse, which is an equivalent setting when the radius of a neuron is 0.5 in the main text.

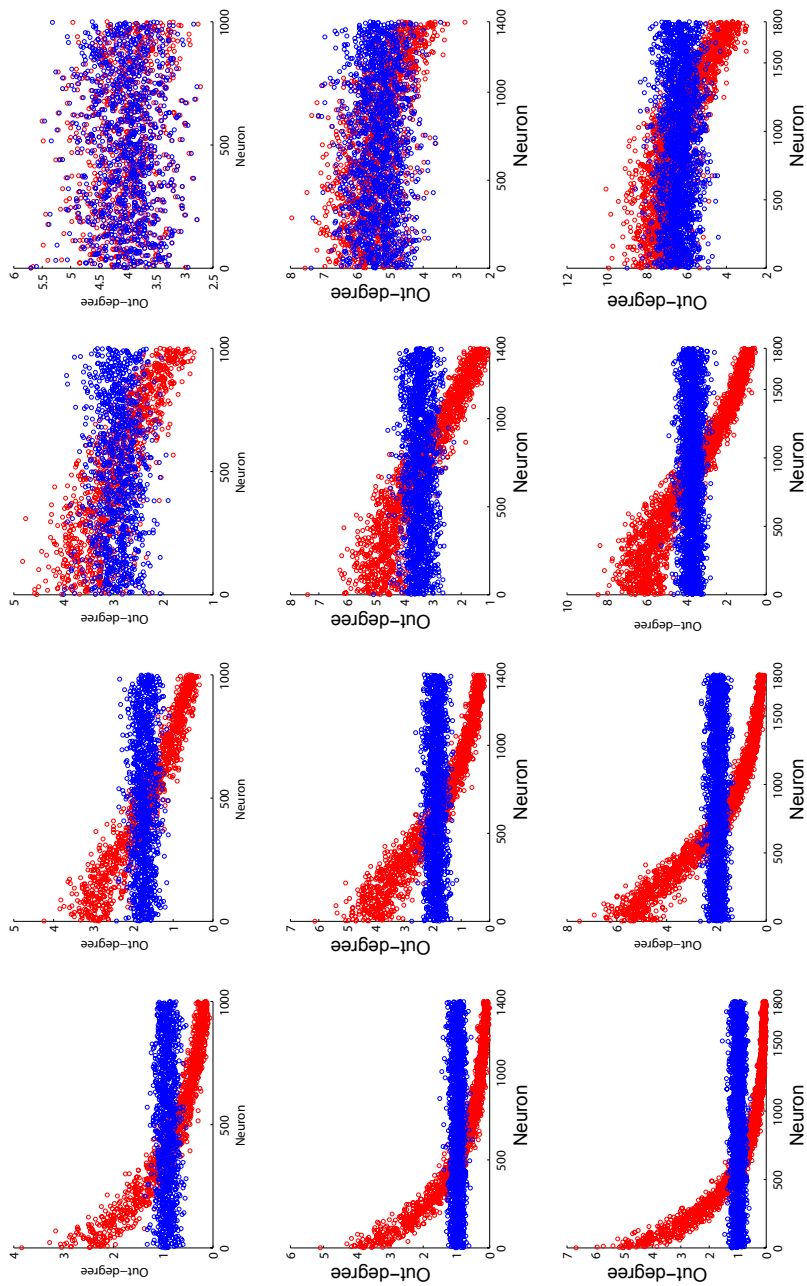

Figure A1. Out-degree Red: serial growth, Blue: parallel growth x-axis: the sequence (order) of neurons starting to grow axons, y-axis: out-degree From the left to the right, the size of neurons increases from 0.5 to 0.9 (0.500, 0.604, 0.735, 0.900) and also the maximum number of incoming connections increases. From top to bottom, the number of neurons increases from 1000 to 1800 by steps of 400. The discrepancy of out-degrees between serial and parallel growth became less obvious for bigger neurons with more incoming connections. For serial growth, neurons started growing axons early on were characterized by higher out-degrees than late starter neurons, whereas the order of growing axons did not influence out-degree distribution for parallel growth.

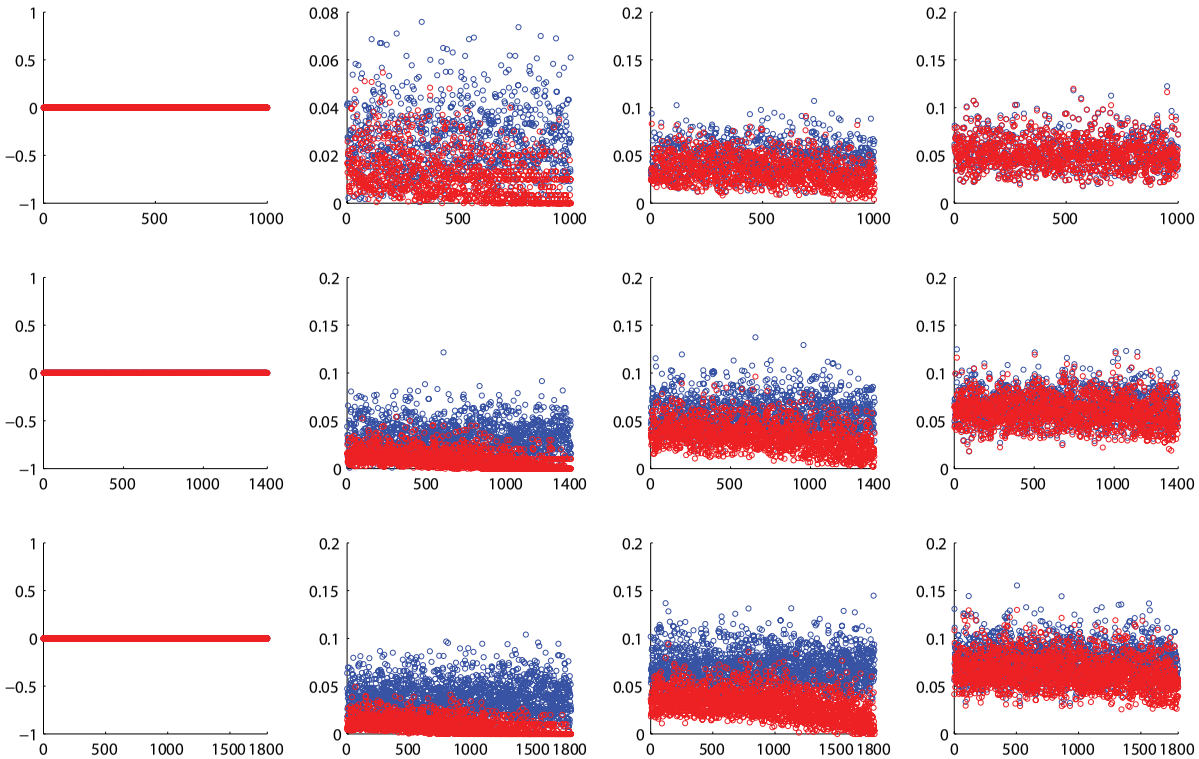

Figure A2. Local efficiency Red: serial growth, Blue: parallel growth,
x-axis: the sequence (order) of neurons starting to grow axons, y-axis: out-degree, from left to right, the size of neurons increases from 0.5 to 0.9 (0.500, 0.604, 0.735, 0.900) and also the maximum number of incoming connections increases. From top to bottom, the number of neurons increases from 1000 to 1800 by steps of 400. For serial growth, neurons started growing axons early on were characterized by slightly higher local efficiency than late starter neurons, whereas the order of starting did not influence local efficiency distribution for all neurons. The local efficiency for parallel growth was in general higher than the local efficiency for serial growth.The discrepancy of local efficiency between serial and parallel growth became less obvious for bigger neurons with more incoming connections. When neurons were allowed to accommodate only one incoming connections (1st column), all neurons had zero local efficiency, indicating all immediate neighbor neurons were disconnected.

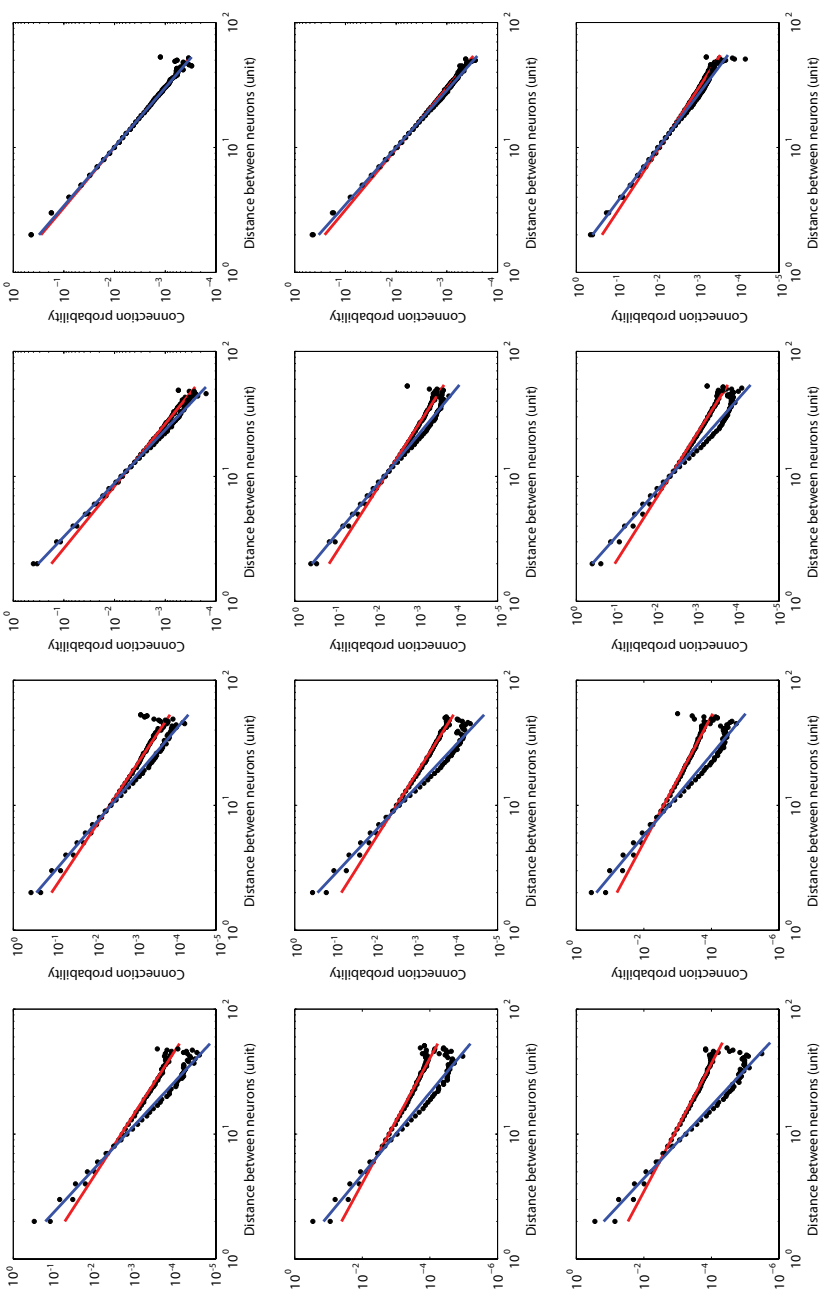

Figure A3. Connection probability: Serial vs. parallel growth. Doubly logarithmic plot (log-log plot), red: serial, blue: parallel, x-axis: distance between neurons (unit),y-axis: connection probability, From left to right: the size of neuron increased from 0,5 to 0,9 and from top to bottom: the number of neurons increases from 1000 to 1800 by steps of 400. Connection probability between two neurons at a given distance was inversely proportional to the distance between neurons. Connection probabiliy decreased more rapidly for parallel growth than for serial growth with distance; two neurons with a shorter distance are more likely to be connected for parallel growth. The discrepancy between serial and parallel growth became less obvious with the size of neuron and the number of incoming connections.

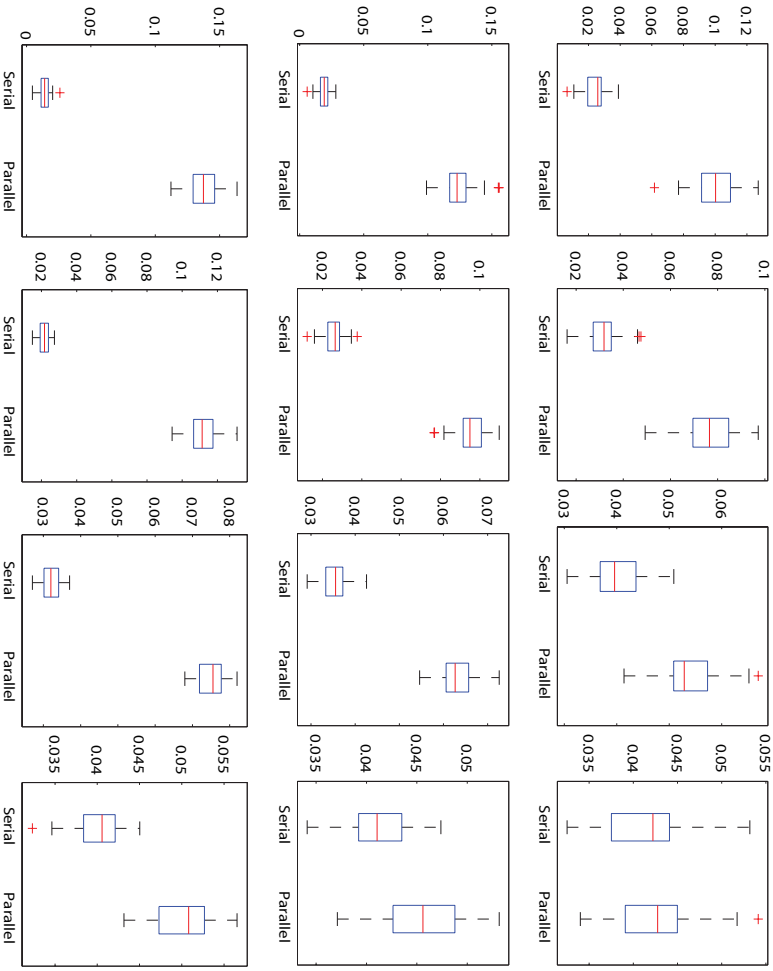

Figure A4 . Percentage of bidirectional connections with boxplot: Serial vs. parallel growth. x-axis: serial (left) and parallel (right), y-axis: the proportion of bidirectional connectivity. From left to right: the size of neuron increased from 0,5 to 0,9 and from top to bottom: the number of neuronsincreases from 1000 to 1800 by steps of 400. The bidirectional connections were more frequent for parallel growth than for serial growth. The discrepancy between serial and parallel growth became less obvious with the size of neuron and the number of incoming connections.

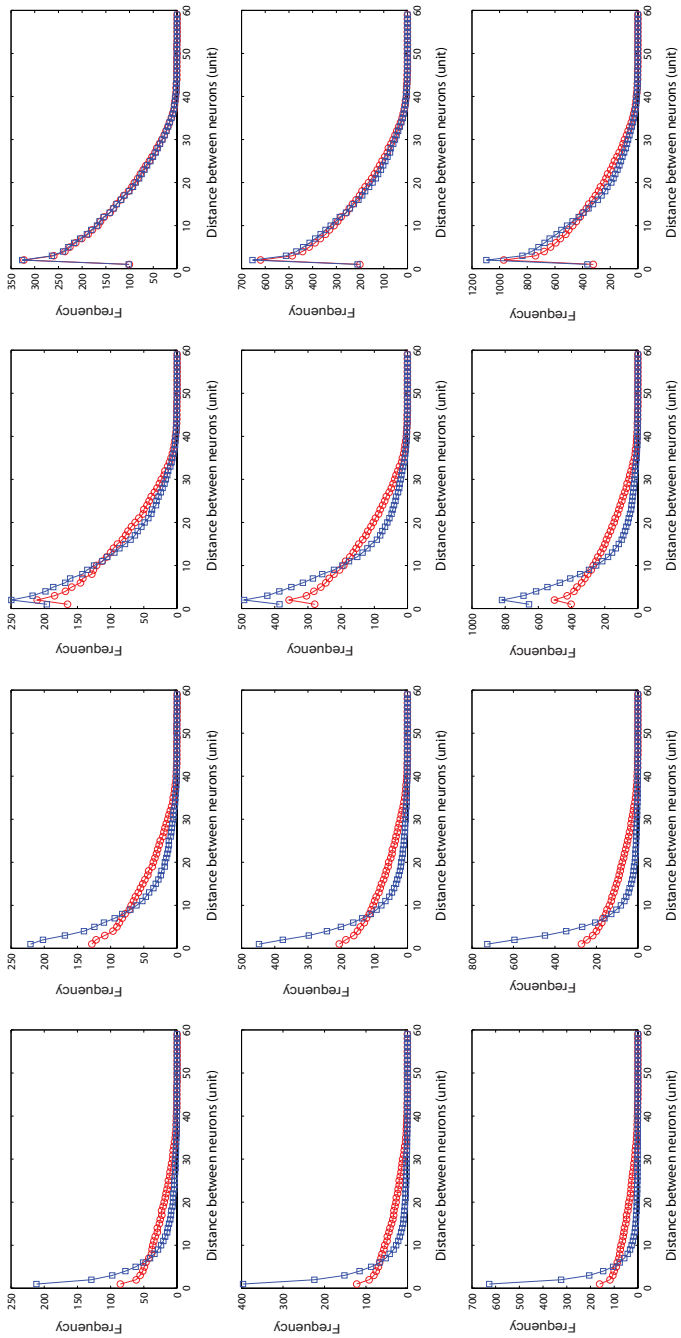

Figure A5. Connection length distribution. red: serial growth, blue: parallel growth x-axis: distance between neurons (unit), y-axis: connection probability, From left to right, the size of neuron increased from 0.5 to 0.9 From top to bottom, the number of neurons increases from 1000 to 1800 by steps of 400. For parallel growth, there were larger number of shorter connections whereas for serial growth there were less shorter connections and the proportion of longer connections was higher than for parallel growth. The discrepancy between serial and parallel growth in the connection length distribution became less obvious and almost no difference for larger size of neurons withi more incoming connection.

Mann-Whitney test and corrected by Bonferroni , see methods in the main text) and connection probability as a function of distance did not show a simple exponential decrease (Figure 2.19). We believe that the model predictions and the actual results from *C. elegans* were different because **i**) differences in local efficiency between serial and parallel growth were less apparent and consistent as other measures in all conditions Figure 2.15 and **ii**) connection probability in our model depends mainly on the geometrical arrangement of dendrites (neuron spheres) and axons, whereas the connectivity of *C. elegans* has additional constraints such as its elongated body shape and the higher prevalence for long-distance connections at the expense of having sub-optimal wiring cost to facilitate efficient information transfer in the network (Kaiser & Hilgetag, 2006). Additional analysis of participation coefficient and within-module degree (Guimera & Amaral, 2005) suggests that the higher local efficiency of late-born neurons were attributable to their lower within-module degrees and participation coefficients, which means late-born neurons were more connected within their modules resulting in higher local efficiency than earlier-born neurons (Figure 2.19C). Within-module degree and participation coefficient show nodal or local changes in modular organisation. Within-module degree indicates how well a node is connected to other nodes in the same module (Guimera & Amaral, 2005); high within-module degree implies that the node is more connected to nodes within the module in which it participates than the average connectivity of the other nodes in the module. The participation coefficient indicates how well the node is connected to all other modules with higher values if many connections of the node are distributed to other modules.

2.6.4. The effect on connection lengths when neurons change their position during development.

The embedding space of neurons for axon growth and synaptogenesis of our model was fixed during development, while internal volume changes through neurite growth and external mechanical factors could change the location of neurons and influence their synapse formation probabilities. To consider the effect on connection lengths when neurons change their positions during development, we need to consider the relative speed of axon and the movement (or migration) of neurons during development, what direction each neuron would choose to move or be forced to move during development due to the growth of the whole body for instance, whether neurons would still move their positions after they establish synapses with other neurons since it would affect the connection length between neurons, whether the growth direction of axons would change according to the position changes or not and so on. Thus, we start with the simplest condition for thought experiments and generalise to draw a conclusion.

For simplicity, let us assume that neurons can move their position in only one direction, e.g., x-axis of the reference frame and assume that the axon growth direction does not change. If the speed of axon growth is far faster than the movement of neurons, we do not need to worry about the effect on connection length because the changes of neurons' positions would be negligible. So the following scenarios assume that the speed of movement of neurons is not negligible compared to that of axon growth. Let neuron A grow its axons in the direction in the figure (Figure 2.20). Let the position of neuron A at time $t_1 : X(t_1) = (x_1, x_2, x_3)$, the position of neuron A at time $t_2 : X(t_2) = (x_1 + d_1 t, x_2, x_3)$, the position of neuron B at time $t_1 : Y(t_1) = (y_1, y_2, y_3)$ and

the position of neuron B at time $t_2 : Y(t_2) = (y_1 + d_2 t, y_2, y_3)$, where t is the time passed ($t = t_2 - t_1$) and d_1 and d_2 are the speeds in the x-axis direction of neuron A and B, respectively.

i) When $d_1 = d_2$, that is when all neurons have the same speed in the same direction (or the same velocity) to move their positions. As both of the neurons moved along the x-axis with the same amount of displacement, the changes of positions of neurons do not affect the synaptogenesis; if neuron A were to establish a synapse with neuron B due to the close proximity between the growth cone and the neuron B, then A would make a synapse with neuron B if neuron B is available. The connection length between neuron A and B that are connected is defined by the Euclidean distance between the centres of neurons (Methods 2.2). The connection length is the same as before because the distance between the two neurons is the square root of the sum of the position differences, which is equivalent with the connection length before they move to new positions. If those two neurons were not meant to be connected in the first place, which means that the axon growth cone would not find neuron B, then they would not be connected after both of them move their position in the same direction with the same amount of displacement for both neurons.

Connection length (distance between the two neurons' centres: $||X(t1) - Y(t1)|| = ||X(t2) - Y(t2)||$ when $d_1 = d_2$ and length are the same, therefore is the same before they change their position, which means that if the growth cone of A is meant to find neuron B it will find it after both of them move laterally if B is available to accommodate another synapse.

ii) When $d_1 < d_2$ (assuming neuron A and B moves in the same direction), If the growth cone could find neuron B in the vicinity (connectible range) in their

original positions, after moving their positions the growth cone of neuron A may not find neuron B because both the distance between neuron A and B (l) and the $sin\theta$ increased, it is more likely for neuron B to be away from the connectible range.

iii) when $d_1 < d_2$, both and $\sin\theta$ are decreased, if $l\sin\theta$ is less than the connectible range, neuron A can establish a synapse with neuron B when neuron B is available. Now if neuron B does not move toward the same direction as neuron A, everything depends on the neuron B; regardless of the trajectory of neuron B's movement, when the position of neuron B at time $t_2 : Y(t_2)$ falls within the connectible range of growth cone of neuron A, neuron A can make a synapse with neuron B, otherwise there will be no synapse from neuron A to neuron B.

In summary, depending on the position of the connectible neuron's position relative to the position of the axon growth cone, either neurons can establish synapses or cannot make synapses. It will definitely change the results of the simulation; however, it will not change the qualitative differences between serial and parallel scenarios. If we assume that the neurons move their positions further apart from each other, the average connection lengths would be longer than that for the condition not assuming the expansion, nonetheless, the intrinsic nature of the characteristics of serial and parallel growth scenarios would remain the same.

2.6.5. Simulation parameters

Four growth scenario (Figure 2.1) are implemented as in the following four files. All routines can be download from http://www.dynamical-connectome.org/

and other additional files including simulation dataset used in the paper (Lim & Kaiser, 2015) and codes for additional conditions such as considering dendritic growth of neurons and partially overlapping time windows for axon growth can be found here https://github.com/springdance/BICYcodes.

devolution3d_ng_ray_parallel.m

devolution3d_ng_ray_serial.m

devoluton3d_ng_discrete_parallel.m

devolution3d_ng_discrete_serial.m

2.6.5.1. Input parameters

n: the total number of neurons in the embedding space.

limit : the side length of the regular hexahedron.

flagtaken: when it is set to 1, the number of maximum incoming connections is limited. or competition among neurons is assumed.

cellradius: the radius of a neuron sphere.

flagsize: When set to 1, the radii of neurons are randomly assigned between 0 and the cellradius, otherwise all neurons have the same radius.

flagdistance: When set to 1, the distance between the growth cone and the connectible neuron is calculated considering the radius of the connectible neuron, otherwise the distance is calculated without considering the radius of the connectible neuron.

mplace: the maximum number of incoming connections.

range: the proximity criterion, a synapse is established when some neurons are within the range from the growing growth cone.

2.6.5.2. Output variables

matrix: the adjacency matrix

positions: the x,y,z coordinates of the centres of neurons

connectible: indices of connectible neurons

connection: indices of connected neurons

fc_abs: the total number of potential connectible synaptic places.

w: the lengths of connections

fc: filling fraction, which is the ratio of the number of established synapses to the total number of potential synaptic spots ((Stepanyants *et al.*, 2002)).

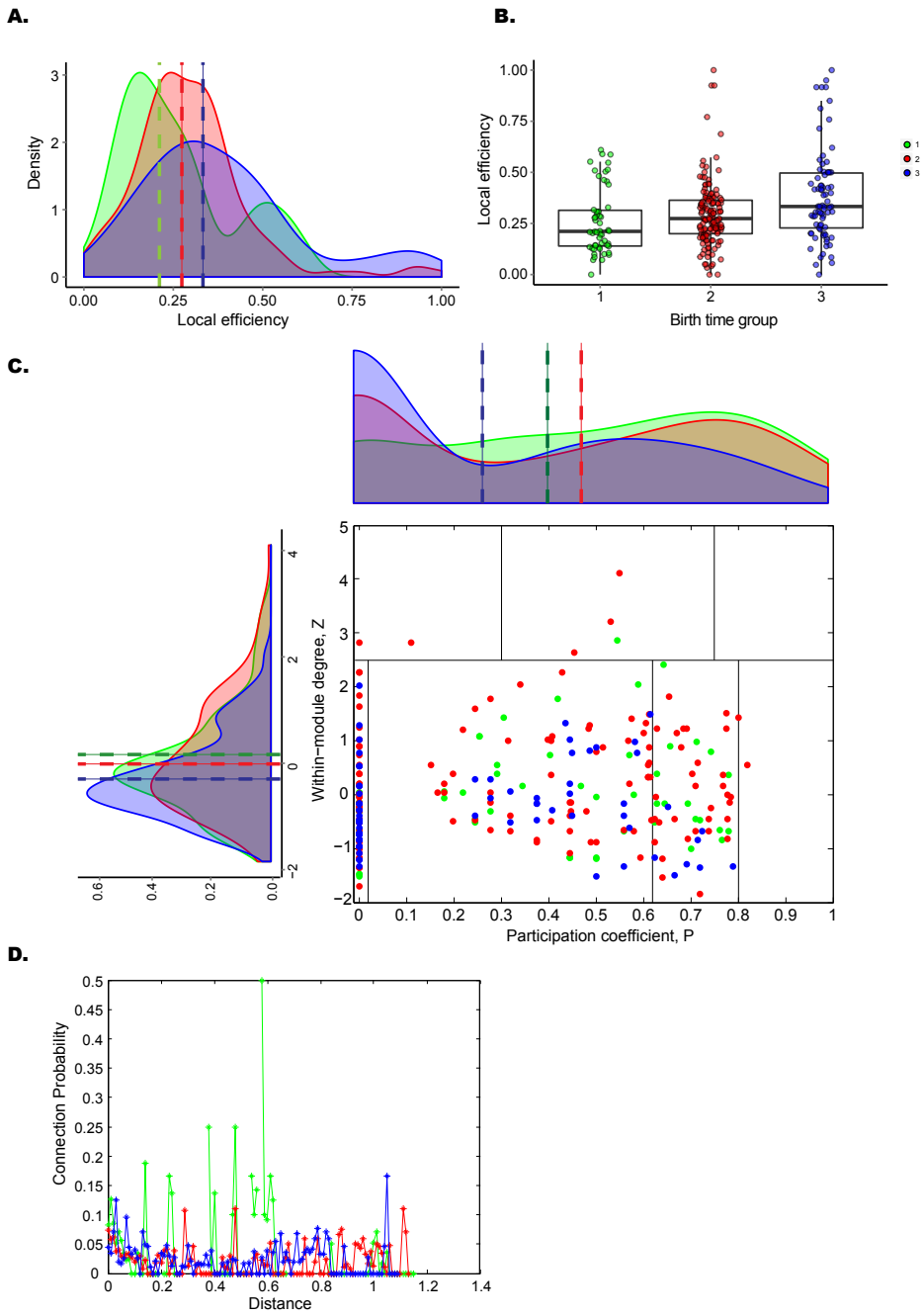

Figure 2.19.: A. Density distribution of local efficiency. Dashed line represents the median of the distribution, B. Boxplot of three birth time group and local efficiency, color scheme follows the main text. C. Participation coefficient and within-module degree Z, D. Connection probability as a function of distance.

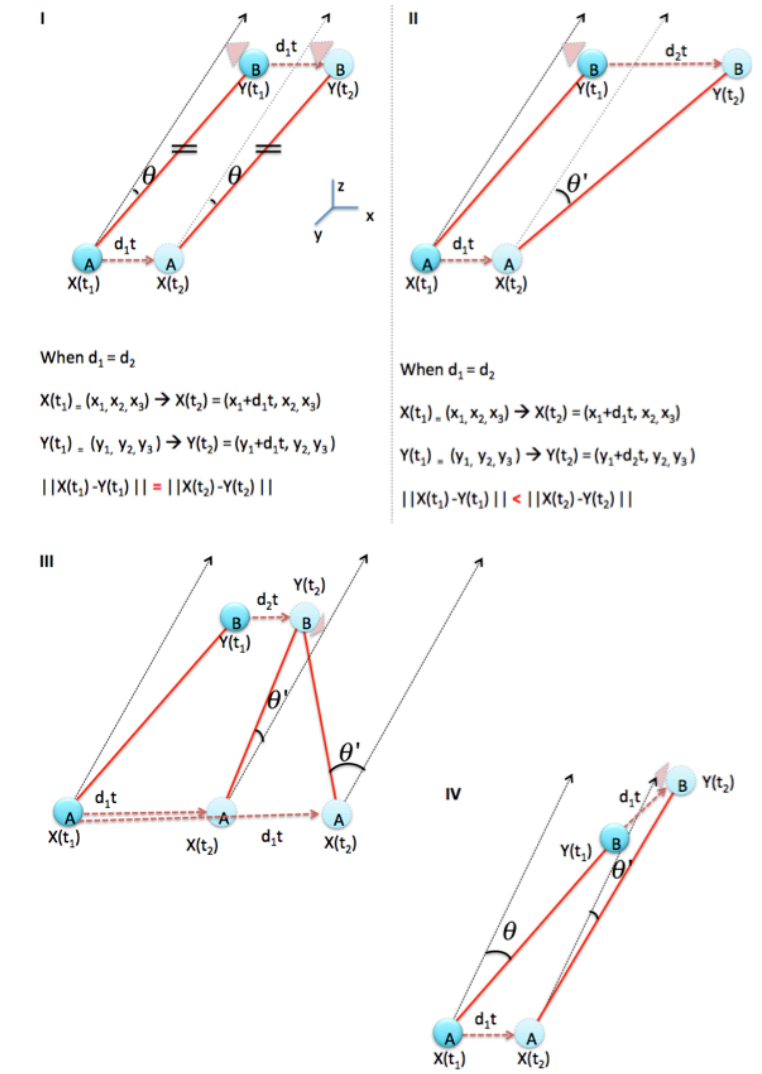

Figure 2.20.: Solid circles are neurons A, B, C and D. Dashed lines with arrows at the end of the lines represent directions for axon growth. Light coloured triangles show potential synaptic spots between neurons and red triangles indicate established synapses. I: all 4 possible synapses, II: Serial growth and III: parallel growth. All were accompanied by their adjacency matrices. Numbers under the neurons in II and III represent the orders of growing axons; neuron A starts growing its axon first and then after neuron A finishes neuron B starts and neuron C and neuron D in order for serial growth and neuron A, B, C and D start axon growth simultaneously. Here, neurons are assumed to make only one synapse, which is an equivalent setting when the radius of a neuron is 0.5 in the main text.

Part III.

Macroscopic brain network

3. Preferential detachment during human brain development: Age- and sex-specific structural connectivity in Diffusion Tensor Imaging (DTI)-data

In the previous chapter, I investigated the role of developmental time windows for axon growth on the neuronal network, which is a microscopic scale of the brain network. In this chapter, I examine the re-organising principles of the human brain network using DTI in the macroscopic perspective. Unlike the previous chapter, the brain connectivity in this chapter discuss how areas in the brain, not at a single neuron level, are interconnected by white matter axon bundles. As human brain maturation is characterised by the prolonged development that extends into adulthood, I focus mainly on which features change and which remain stable over time and what could be the possible underlying driving principle to achieve the patterns that I observe. Here, I examined structural connectivity based on DTI in 121 participants between 4 to 40 years of age. In summary, findings suggest that core properties of structural brain connectivity, such as the small-world and modular organisation, remain stable during brain maturation by focusing streamline loss to specific types of fibre tracts, which I call *preferential detachment*. This chapter is based on (Lim *et al.*, 2013).

3.1. Introduction

Human brain development is characterised by a protracted trajectory that extends into adulthood (Benes *et al.*, 1994; Sowell *et al.*, 1999; Lebel & Beaulieu, 2011). Evidence from magnetic resonance imaging (MRI) has indicated a reduction in grey matter (GM) volume and thickness across large areas of the cortex and changes in subcortical structures, which may be attributed to synaptic pruning and ingrowth of white matter (WM) into the peripheral neuropil (Sowell *et al.*, 1999; Sowell *et al.*, 2001; Sowell, 2004; Giedd, 2008; Giedd & Rapoport, 2010). In contrast, WM-volume increases with age (Giedd *et al.*, 1997; Giedd *et al.*, 1999b; Paus *et al.*, 1999; Bartzokis *et al.*, 2001; Sowell, 2004; Lenroot *et al.*, 2007) which could reflect increased myelination of axonal connections (Sowell *et al.*, 2001; Sowell, 2004).

In addition to volume changes, connectivity changes of axonal fibre bundles have been investigated using Diffusion Tensor Imaging (DTI). DTI allows the measurement of fibre integrity through estimates of fractional anisotropy (FA) and mean diffusivity (MD), which presumably relate to changes in axonal diameter, density and myelination (Jones, 2010; Jbabdi & Johansen-Berg, 2011). Several studies reported increased FA and decreased MD-values from childhood into adulthood in several major fibre tracts and brain regions (Faria *et al.*, 2010; Tamnes *et al.*, 2010; Westlye *et al.*, 2009; Lebel & Beaulieu, 2011).

Brain maturation is also accompanied by changes in the topology of structural and functional networks (Fair *et al.*, 2009; Gong *et al.*, 2009; Hagmann *et al.*, 2010; Yap *et al.*, 2011a; Dennis *et al.*, 2013). Topological features of neural networks that are now being linked to cognitive performance (Bullmore & Sporns, 2009) concern their small-world and modular organisation. For small-

world network with brain regions or ROIs as nodes and fibre tracts as edges, there are many connections between regions mostly located nearby. At the same time, it is also easy to reach other brain regions far apart in the network due to the existence of long-range connections or short-cuts (Watts & Strogatz, 1998). Therefore, small-world network shows high efficiency in facilitating information flow at both the local and the global scale (Latora & Marchiori, 2001; Latora & Marchiori, 2003). For example, functional connectivity with high global and local efficiency correlates with higher intelligence (Li *et al.*, 2009; van den Heuvel *et al.*, 2009), while disrupted small-world topology is associated with impaired cognition (Stam *et al.*, 2007; Nir *et al.*, 2012). For a modular organisation, large groups of brain regions can be considered as network modules (or clusters) if there are relatively more connections within that group than to the rest of the network (Hilgetag *et al.*, 2000; Meunier *et al.*, 2010). The higher connectivity within modules can segregate different types of neural information processing while fewer connections between modules allow for information integration. This community structure of the brain network incorporating and balancing both segregation and integration of neural processing has been shown to be disrupted in schizophrenic, autistic and Alzheimer's brains (Alexander-Bloch *et al.*, 2010; de Haan *et al.*, 2012; Shi *et al.*, 2013).

Small-world and modular organisation heavily rely on long-distance connectivity: long fibre tracts are more likely to provide short-cuts for reaching other nodes in the network and are also more likely to link different network modules (Kaiser & Hilgetag, 2006). For example, connections between hemispheres or between the visual and fronto-limbic network module are long-distance. By providing short-cuts, long-distance connections reduce transmission delays and errors, consequently enabling synchronous and more precise information processing. Conversely, a reduction in long-distance connectivity is well known

to impair cognitive ability by adversely affecting efficiency and modularity of a network (Kaiser & Hilgetag, 2004). For instance, patients with Alzheimer's diseases were shown to lose long-distance projections leading to an increase in functional path length (Stam *et al.*, 2007). In addition to long-distance connections, inter-module connections, or fibre tracts linking different modules are also important to keep the community structure of brain networks and these also provide short-cuts for communicating with other functional or structural modules. Reduced between-module connectivity was strongly associated with cognitive impairment in Alzheimer's patients (de Haan *et al.*, 2012).

Emerging data suggest that small-world topology and modular organisation in brain networks are already present during early development (Fan *et al.*, 2011; Yap *et al.*, 2011a). Despite of appreciable anatomical changes during brain maturation, these core topological features have shown to be spared (Bassett *et al.*, 2008; Fair *et al.*, 2009; Gong *et al.*, 2009; Supekar *et al.*, 2009; Hagmann *et al.*, 2010). Thus, we hypothesised that certain types of fibre tracts might have been preferentially affected during development to retain important topological features during development. These potentially spared fibre tract types are likely to include long-distance connections but also fibre tracts composed of fewer streamlines and inter-module fibre tracts. Fibre tracts of the latter two types are often, but not necessarily, also long-distance connections (Discussion 3.4 and Figure 3.10). Therefore we analysed all three types of fibre tracts in relation to topological changes.

To test our hypothesis, we obtained DTI-data from a large cohort of subjects between 4 to 40 years and constructed streamlines from deterministic tractography to identify fibre tracts in cortical and subcortical networks. Our results show that the number of streamlines overall decreased with age while small-

world and modular parameters did not change. Specifically, our results showed that streamline loss occurred mostly for fibre tracts composed of more than average number of streamlines, short and within-module/within-hemisphere fibre tracts. This focus on certain types of fibre tracts goes beyond what would be expected by a type's prevalence within network suggesting a preferential detachment of streamlines. In addition to modifications in cortical fibre tracts, pronounced changes were observed in subcortical structures in basal ganglia and in anterior cingulate cortex. Finally, streamline-reductions occurred at an earlier age in females than in males, suggesting sex-specific maturation of connectivity patterns during human brain maturation.

3.2. Methods and materials

3.2.1. DTI-Data

We made use of a public DTI-database (http://fcon_1000.projects.nitrc.org/indi/pro/nki.html) provided by the Nathan Kline Institute (NKI) (Nooner *et al.*, 2012). DTI-data were obtained with a 3 Tesla scanner (Siemens MAGNETOM TrioTim syngo, Erlangen, Germany). T1 weighted MRI data were obtained with 1 mm isovoxel, FoV = 256 mm, TR = 2500 ms, and TE = 3.5 ms. DTI data were recorded with 2 mm isovoxel, FoV = 256 mm, TR = 100000 ms, TE = 91 ms, and 64 diffusion directions with b-factor of 1000 s/mm^2 and 12 b_0 images. We included 121 participants between 4 and 40 years.

3.2.2. Data pre-processing and network construction

We used Freesurfer to obtain surface meshes of the boundary between GM and WM from T1 anatomical brain images (http://surfer.nmr.mgh.harvard.edu) (Figure 3.1). After registering surface meshes into the DTI space, we generated volume regions of interest (ROIs) based on GM-voxels. Freesurfer provides parcellation of 34 anatomical regions of cortices based on the Deskian atlas (Fischl *et al.*, 2004; Desikan *et al.*, 2006) and 7 subcortical regions (Nucleus accumbens, Amygdala, Caudate, Hippocampus, Pallidum, Putamen, and Thalamus) (Fischl *et al.*, 2002; Fischl *et al.*, 2004) for each hemisphere, thus leading to 82 ROIs in total (See Table 3.7 for full and abbreviated names of ROIs).

To obtain streamline tractography from eddy-current corrected diffusion tensor images (FSL, http://www.fmrib.ox.ac.uk/fsl/), we used the Fibre Assignment by Continuous Tracking (FACT) algorithm (Mori & Barker, 1999; Mori & van Zijl, 2002) with 35 degrees of angle threshold through Diffusion toolkit along with TrackVis (Wang *et al.*, 2007) (Figure 3.1). This program generated the tractography from the centre of all voxels (seed voxels) in GM/WM except ventricles; from each voxel's centre coordinates started a single streamline. Thus, the number of total streamlines never exceeds the number of seed voxels.

In addition, we performed tractography with the following parameters: 1) 45 degrees of angle threshold with a single seed point and 2) 10 random tracking per voxel for both and 35 and 45 degrees of angular thresholds, in total 3 more cases. These additional analyses were performed to assure that the results were consistent despite varied tracking parameters (Figure 3.12). For network reconstruction, we used the UCLA Multimodal Connectivity Package (UMCP,

http://ccn.ucla.edu/wiki/index.php) to obtain connectivity matrices from the defined and registered ROIs and tractography, counting the number of streamlines between all pairs of defined ROIs. The resulting matrix contains the streamline count between all pairs of ROIs as its weight. We also computed the average connection lengths between ROIs (if there is no connection between a pair, the length was set to zero). The connection length of a streamline was based on its three-dimensional trajectory.

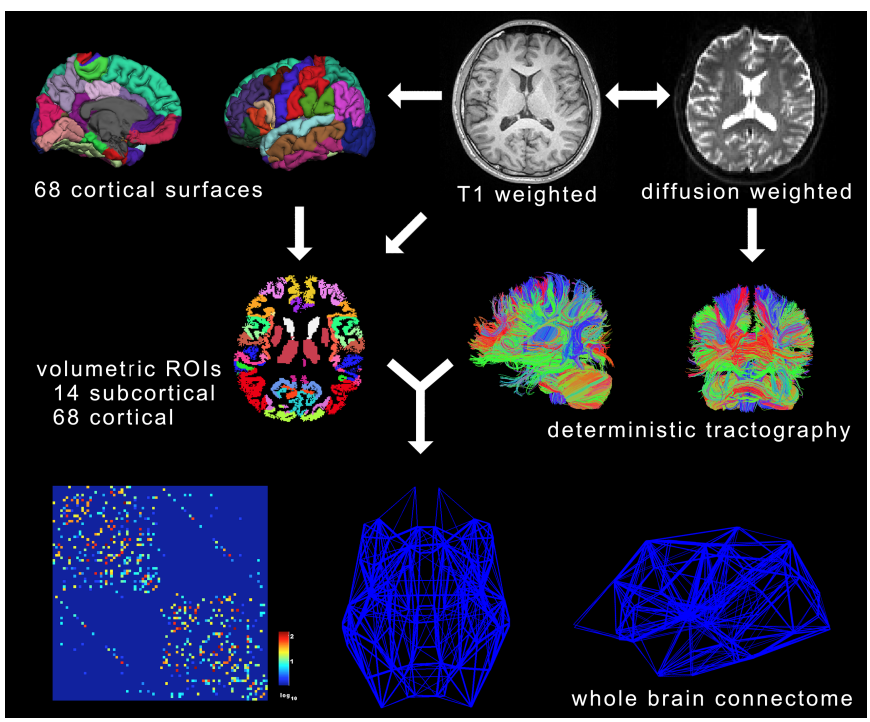

Figure 3.1.: From T1-weighted images, we generated 82 regions of interests (ROIs, 34 cortical areas and 7 subcortical areas per hemisphere, on the left). From diffusion tensor images (DTI), we reconstructed streamlines using deterministic tracking (on the right). Combining two pre-processing steps, we constructed weighted networks, where the number of streamlines between any pair of ROIs formed the weight of an edge (fibre tract).

3.2.3. Network analysis

Short explanations of network measures are provided here (for details, see Section 1.1). Edge density represents the proportion of existing connections out of the total number of potential connections (Kaiser, 2011). Note that the weights of individual edges (streamline count) might change but edge density will remain the same as long as the total number of edges (fibre tracts) is unchanged. Small-world topology can be characterised by high global and local efficiency (Latora & Marchiori, 2001; Latora & Marchiori, 2003). Global efficiency represents how efficiently neural activity or information is transferred between any brain regions on average and local efficiency indicates how well neighbours of a region, or nodes that are directly connected to that region, are interconnected. Efficiency is greatly affected by the sparsity of the network (Kaiser, 2011); when there are fewer edges and also even fewer streamlines, efficiency decreases. Thus, we normalised efficiency with values obtained by 100 randomly rewired networks where randomly selected edges were exchanged while preserving both degree and strength of each node (Rubinov & Sporns, 2011). Modularity Q represents how modular the network is; higher values of Q indicate that modules are more segregated with fewer connections between modules. In contrast, lower Q-values indicate more connections between modules and thus represent a more distributed connection distribution (Newman, 2006). We also compared the modular membership assignment using the normalized mutual information (NMI) (Alexander-Bloch *et al.*, 2012). Within-module strength and participation coefficient show nodal or local changes in modular organisation. Within-module strength indicates the degree to which a node is connected to others nodes in the same module (Guimera & Amaral, 2005); high within-module strength implies that the node is more connected to nodes

within the module in which it participates than the average connectivity of the other nodes in the module. The participation coefficient indicates how well the node is connected to all other modules with higher values if many connections of the node are distributed to other modules. We used Matlab routines from the Brain Connectivity Toolbox (Rubinov & Sporns, 2010).

3.2.3.1. Modular membership assignment

In addition to general linear model analysis across the entire age-range, we also grouped participants into five age-categories for modular membership analysis (Table 3.1). We tested the modular organization across age by matching module assignments of each participant to a representative participant whose average Normalized Mutual Information (NMI) is the closest to that of all other participants in an age group (Alexander-Bloch *et al.*, 2012). NMI quantifies how similar two modular structures are using information theory. We performed this procedure for each group and compared them by an omnibus test and also comparisons of consecutive groups.

$$NMI(A,B) = \frac{-2\sum_{i=1}^{C_A}\sum_{j=1}^{C_B} N_{ij}\log\left(\frac{N_{ij}N}{N_i N_j}\right)}{\sum_{i=1}^{C_A} N_i \log\left(\frac{N_i}{N}\right) + \sum_{j=1}^{C_B} N_j \log\left(\frac{N_j}{N}\right)} \tag{3.1}$$

where N is the number of nodes, C_A is the number of modules in structure A, C_B is the number of modules in structure B, N_i is the number of nodes in the i^{th} module of structure A, N_j is the number of nodes in the j^{th} modules of structure B, and N_{ij} is the number of nodes which are intersection of the i_{th} module of structure A and the j_{th} module of structure B.

We performed this procedure for each group (Table 3.1). Matching algo-

rithm maximized the overlap between modular structures. After matching the participants to the representative participants, we estimated most-frequently assignment for each node and compute the certainty as the ratio of the participants whose modular membership is the most-frequently-assignment to the number of total participants in the group.

In contrast to the previous methods (Duarte-Carvajalino *et al.*, 2011): averaging of connectivity matrices of individuals before estimating modular structure; (Fair *et al.*, 2009), averaging registered MRI scans before extracting networks), this method would 1) prevent the possibility that a spurious connectivity, which only exists in part of participants, may affect the modular structure and 2) provide how consistent modular membership were assigned to each node, showing inter-participant variability of modular membership assignment.

Alexander Bloch et al. (Alexander-Bloch *et al.*, 2012) also statistically tested regional differences in the modular membership between two groups, using the permutation test. For each node, they computed Pearson correlation coefficient of modular membership of the node between two participants, constructing similarity matrix of modular membership of the node. If there is a between-group

Table 3.1.: Subject statistics of five age groups. For the membership assignment comparison, we grouped our subjects into five age groups. The ratios between males and females were not significantly different between groups (χ^2 test, $\chi^2(df = 4) = 2.539, p = 0.638$).

Age range [years]	Number of subjects	Male/Female	Age Mean(SD)
4-11	13	6/7	8.31 (2.18)
12-15	20	13/7	13.60 (0.99)
16-19	14	7/7	17.43 (1.16)
20-28	48	30/18	23.19 (2.46)
29-40	26	13/13	34.19 (3.77)

difference, then the average within-group correlation would be higher than the between-group correlation. Using the permutation test (with 10,000 permutations), they sampled the distribution of average within-group correlations over permutations, and check where the true average within-group correlations was located to estimate p-value that the node's membership assignment differs between groups.

In this study, with the Pearson correlation coefficient for modular membership of each node, we followed Kropf et al. (Kropf *et al.*, 2004) to compare modular structure of multiple groups, because Alexander Bloch et al. (Alexander-Bloch *et al.*, 2012)'s permutation test only works for two groups. Instead of estimating the distribution of average within-group correlation, Kropf et al. (Kropf *et al.*, 2004) pursued the distribution of distances between average within-group correlation and average between-group correlation.

3.2.4. Edge group analysis

We grouped fibre tracts into categories in terms of (a) the number of streamlines (thin vs. thick), (b) the length of the streamline trajectory (short vs. long) and (c) whether they were within modules (intra-module) or between modules (inter-module) and counted the streamlines in each group. Then we examined with general linear model (GLM) if the number of streamlines in each category changed over age (see Section 3.2.6).

As the spatial (b) and topological (c) properties often overlap but do not always coincide (Figure 3.10), we investigated all three cases (Costa *et al.*, 2007; Meunier *et al.*, 2010). In general, more streamlines existed in 'thick' (by definition), short-length and intra-module edges. Therefore, larger changes in

those edges would occur for random selection. Accordingly, we used χ^2 tests to verify any preferential detachment that goes beyond the streamline loss that would be expected based on the number of fibre tracts of each type. We standardised weights and lengths for each individual and categorised edge into two groups by the mean of each participant to account for differences in brain volume and size. For instance, an edge or a fibre tract for a participant is classified as 'thin' when the weight of the fibre tract is less than the average weight of the participant. Likewise, a fibre tract is considered 'thick' when the weight is above the average of the participant. The same procedure was performed to differentiate short and long fibre tracts. Therefore, types of fibre tracts were distinguished using a subject-specific threshold.

3.2.5. Individual edge analysis

In addition to analysing types of fibre tracts differences, we also examined changes for individual edges that included the subset of total fibre tracts that all participants had in common (128 edges, approximately 32.3% of the total number of edges 396 $\pm$ 20). Note that the total number of edges was around 400, which is 12% of the total number (n = 3321) of possible connections. This proportion is consistent with previous evidence suggesting that the human brain has a sparse connectivity ranging between 10 to 15% (Kaiser, 2011). To analyse individual edges, each edge with significant age-related changes was mapped to the corresponding lobe according to Freesurfer Lobe Mapping (http://surfer.nmr.mgh.harvard.edu/fswiki/CorticalParcellation).

3.2.6. Statistical analysis

To assess how theoretical graph measures changed during development, we used linear model approach (see Eq.(3.2), Eq.(3.3), and Eq.(3.4)). Linear and quadratic effects of age and the interaction between age and gender were investigated. The quadratic term of age, gender factor and the interaction term between age and gender were dropped and refitted when the effects were not significant following an F test as all tested models were nested. AIC (Akaike Information Criterion) and BIC (Bayesian Information Criterion) were also used for model comparison and selecting variables when the Ftest alone did not provide a strong preference for a model. As AIC tends to prefer more complex models with a larger number of variables compared to BIC (Kadane & Lazar, 2004), AIC and the F test provided consistent results in general. When the results of the three tests conflicted, we chose the most conservative model with a smaller number of variables. Two-tailed tests were used for all analyses and tests were regarded as significant with an α level of 0.05. Quadratic age effect was found to be significant in a few fibre tracts but occurred less frequently than linear cases. We therefore chose to report age effects of the numbers of streamlines where decrease and increase could follow a linear or, less often, a non-linear pattern.

$$y = \beta_0 + \beta_1 \times \text{age} + \beta_2 \times \text{sex} + \epsilon \tag{3.2}$$

$$y = \beta_0 + \beta_1 \times \text{age} + \beta_2 \times \text{sex} + \beta_3 \times \text{age} \times \text{sex} + \epsilon \tag{3.3}$$

$$y = \beta_0 + \beta_1 \times \text{age} + \beta_2 \times \text{sex} + \epsilon \tag{3.4}$$

where y: measurement, β_0: intercept (bias), $\beta 1$: slope over age, β_2: coefficient for sex difference, β_3: coefficient for interaction effect of age (years) and sex

(binary) or quadratic age effect, ϵ: errors (noise), which are independent and identically distributed, having a Gaussian (i.e., normal) distribution with mean zero and variance σ^2.

Through the group analysis of edges (Section 3.2.4), we identified which types of edges were undergoing developmental changes. Using repeated measures GLM, we tested whether two groups had different slopes and χ^2 tests were used for verifying the slope difference of GLM considering the proportion of each group with each individual network. For individual edge analysis, χ^2 tests, and nodal properties such as within-module strength and participation coefficients, False Discovery Rate (FDR) procedure was used with a q level of 0.05, adjusting significance level and confidence intervals (Benjamini & Hochberg, 1995; Benjamini *et al.*, 2005; Jung *et al.*, 2011). All statistical tests were calculated in Matlab R2012b (Mathworks Inc., Natick, MA) and R (R Core Team, 2014) with R packages (Lemon, 2006; Bengtsson, 2007; Sarkar, 2008; Suter, 2011; Weisberg & Fox, 2011).

3.3. Results

We performed a combined analysis of fibre tracts with network parameters to examine on-going changes in fibre tracts in terms of small-world topology and modularity, which may account for a relationship between topological changes and modifications in fibre tracts. We compared developmental changes examining the following features: (1) overall connectedness: total number of streamlines, edge density, and thin vs. thick connectivity, (2) small-world organisation: efficiency and short vs. long-distance connectivity, (3) modular organisation: modularity and within vs. between module connectivity, and (4)

local organisation: individual edge analysis.

3.3.1. Age effect for both genders

3.3.1.1. Connectedness

3.3.1.1.1. Streamline count vs. Edge density

The total number of streamlines decreased ($\beta_1 = -68.87$, $t_{(118)} = -5.796$, $p < 0.001$, Figure 3.2A) with age; however, edge density remained stable ($t_{(118)} = 0.757$, $p = 0.451$, Figure 3.2B).

3.3.1.1.2. Thick vs. Thin

Edge density or the number of fibre tracts could be maintained either through new fibre tracts that make up for lost fibre tracts due to streamline reduction or through sparing thin edges and therefore retaining existing fibre tracts while changing only weights for fibre tracts. To test the latter hypothesis, we tested whether there were differences in developmental patterns of thick or thin edges (See Section 3.2.4).

Streamlines in both thick and thin edges decreased with age (thick edges: $\beta_1 = -60.184$, $t_{(118)} = -6.195$, $p < 0.001$, Figure 3.2C; thin edges: $\beta_1 = -8.685$, $t_{(118)} = -3.27$, $p = 0.001$). However, the slopes between thick and thin edges were significantly different (repeated measures GLM, $F_{(1,119)} = 40.196$, $p < 10^{-8}$, Figure 3.2C) with the slope of thick edges showing an approximately eight times steeper slope than thin edges. This preferential reduction of

streamlines within thick edges could not be explained by the frequencies of thin and thick fibre tracts (χ^2 test, $p < 10^{-20}$).

3.3.1.2. Small-world topology and long-distance connectivity

3.3.1.2.1. Efficiency and small-world topology

Global and local efficiency decreased during development (Global: $\beta_1 = -0.001$, $t_{(118)} = -2.496$, $p = 0.014$, Figure 3.2D, Local: $\beta_1 = -0.019$, $t_{(118)} = -4.435$, $p < 0.001$, Figure 3.2E). Although global and local efficiency may have been slightly compromised by the loss of streamlines, small-world features were maintained; global efficiency paralleled that of the rewired network (0.88 ± 0.036 approximately 0.9) while local efficiency was much higher (4.06 ± 0.446 approximately four-fold) than that of the random networks.

3.3.1.2.2. Short vs. long-distance connectivity

As topological and spatial organisations are often linked (Kaiser & Hilgetag, 2006; Costa *et al.*, 2007; Meunier *et al.*, 2010), we tested whether the pattern of changes in short- and long-distance connectivity corresponded to changes in efficiency. From the preserved small-world topology, we would expect long fibre tracts were likely to be conserved. Decreasing slopes of the streamline count between short and long edges were significantly different ($F_{(1,119)} = 44.965$, $p < 10^{-9}$) with short-distance connections showing a pronounced reduction (Short: $\beta_1 = -61.515$, $t_{(118)} = -6.773$, $p < 10^{-9}$, Figure 3.2 F), which was not solely explained by a higher proportion of short-distance edges (χ^2 test, $p < 10^{-6}$).

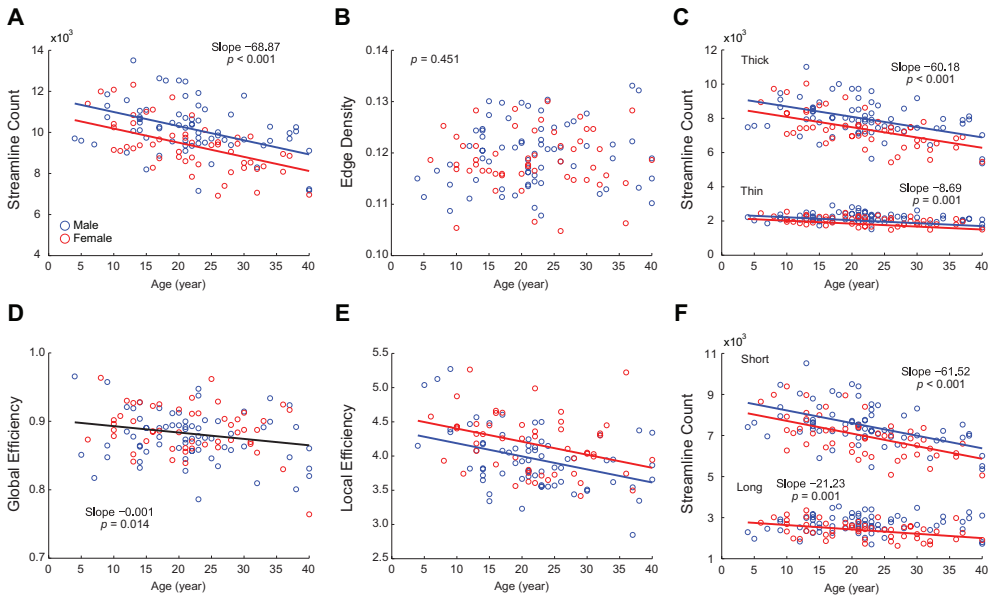

Figure 3.2.: Topological and spatial network properties. Fitted lines were drawn when there was a significant age effect (Red: female, Blue: male). When multiple lines were drawn, the lines are parallel unless otherwise noted. Black line represents significant age affect without a sex difference. A. Total number of streamlines B. Edge density C. Streamline count in thick vs. thin edges E. Global efficiency F. Local efficiency, and G. Streamline count in short vs. long streamlines

3.3.2. Modular organisation

3.3.2.1. Modularity and module membership assignment

Modularity did not change with age ($t_{(118)} = -1.335$, $p < 0.184$, Figure 3.4A) and community structure remained stable during development (Figure 3.3). Overall modular organisation based on the normalized mutual information (Eq.3.1) did not differ across age ($p = 0.355$) and there were no significant nodal changes in membership assignment after multiple comparison correction

using FDR with a q level of 0.05.

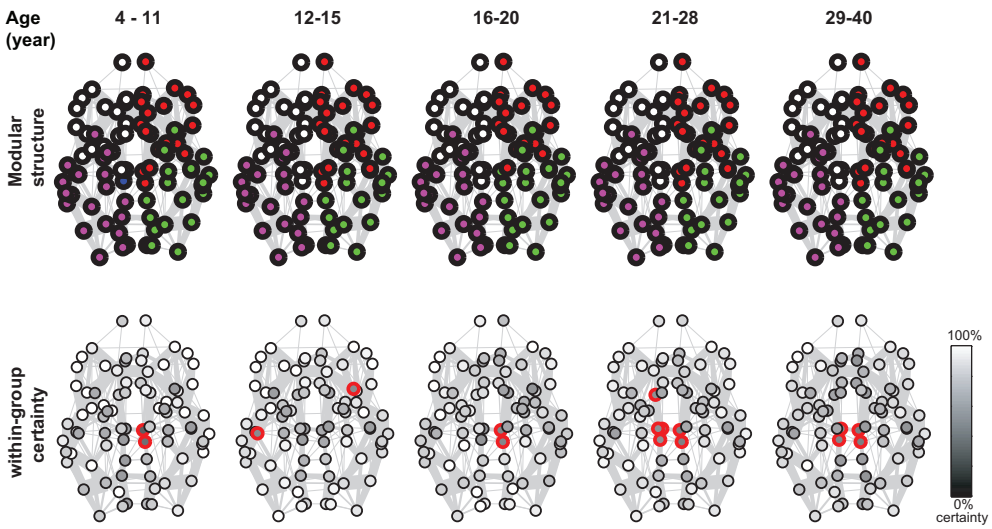

Figure 3.3.: Modular structure over four age groups (shown table 3.1): 4-11 y/o (A & E), 12-15 y/o (B & F), 16-19 y/o (C & G), and 20-28 y/o (D & H). For each group, we selected the representative participant which showed the smallest average normalized mutual information (NMI), and matched all the other participants to the representative participant, maximizing overlaps between modular memberships. Then we counted the most frequently occurred community membership over each group (upper row, A, B, C, and D) and showed the ratio of the most-frequently occurred community membership to the number of participants in each group as a certainty of averaging (within-group certainty, bottom row, E, F, G, and H). In the upper row, the community structure is largely unchanged with left anterior (purple), left posterior (white), right anterior (red), and right posterior (green) modules. . The left anterior module (white) was located on the frontal lobe and extended to the parietal lobe and temporal lobe, while left posterior module (purple) resided in the left occipital and parietal lobes. Right anterior module (red) in the frontal lobe and extended to the right temporal lobe occasionally, while right posterior (green) resides mostly in the occipital lobe and extended to the parietal and temporal lobes. The left central module (blue) was very small in the youngest age group (two nodes). In the bottom row, the whiter circles represent more certain modular membership assignment, where red circle showed the nodes whose average certainty is below 50%. In the modular organization of the youngest group, there were only two nodes in the green module but it does not mean that there were only two nodes in the particular module. The number of nodes in the green module varied from 0 to 13; there were very high variability thus having very low certainty; consistent results were only for two nodes but the module is much larger for each individual member of that age group.

3.3.2.2. Within-module strength and Participation coefficient

Twenty out of 82 ROIs (24.4%) showed significant changes in within-module strengths and participation coefficients (FDR corrected). Overall changes were asymmetric between hemispheres, affecting homologous ROIs either in the left or right hemisphere. Ten of the 24 ROIs (42%) characterized by age effects were areas in subcortical regions, such as the basal ganglia, thalamus and nucleus accumbens (Table 3.2). Specifically within-module strengths decreased while participation coefficients increased, indicating that with development connections involving basal ganglia decreased within its module while connections to the surrounding modules/regions decreased. In contrast, eight ROIs within the anterior cingulate cortex and the paralimbic division (Mesulam, 2000) were mainly characterized by increased within-module connectivity with age.

Table 3.2.: ROIs with age effect in within-module strength (WMS) and participation coefficient (PC)

	Increased	**Decreased**	**Sex-specific**
WMS	**lh.caudalanteriorcingulate (F)** lh.entorhinal (T) lh.parahippocampal (T) **rh.caudalanteriorcingulate (F)** **rh.rostralanteriorcingulate (F)**	**lh.thalamus** **lh.accumbens** **rh.putamen** (f >m) **rh.pallidum**	**lh.putamen** m: decreased rh.paracentral (F) m:Increased
PC	**lh.putamen** **lh.pallidum** **rh.caudate** **rh.putamen** (m >f) **rh.pallidum** (m >f)	**rh.caudalanteriorcingulate (F)** rh.paracentral (F) **rh.posteriorcingulate (P)**	lh.medialorbitofrontal (F) m: increased rh.insula (m >f)

Note: Basal ganglia showing a more distributed network and anterior cingulate cortex showed a more focused connectivity within its module (Blue: cingulate cortex, Black(bold): subcortical areas, F: frontal lobe, P: parietal lobe, T: temporal lobe, O: occipital lobe, lh: left hemisphere, rh: right hemisphere, f: female, m: male, FDR corrected, with a q level of 0.05).

3.3.2.3. Within vs. between module analysis

Modular membership and modularity Q stayed relatively stable during development although there were some ROIs that showed significant changes in terms of inter- vs. intra-modules connectivity (Section 3.3.2.2, Table 3.2). This can be realized when changes occurred mainly within modules. The decreasing slopes of streamline count for intra- and inter-module edges differed (repeated measures GLM, $F_{(1,119)} = 33.186$, $p < 10^{-7}$). The reduction of streamlines occurred within modules ($\beta_1 = -61.25$, $t_{(118)} = -6.321$, $p < 10^{-8}$, Figure 3.4B) but not between modules ($t_{(118)} = -1.831$, $p = 0.0696$, Figure 3.4B). This preference was not fully explained by the higher proportion of intra-module edges (χ^2 test, $p < 10^{-6}$).

3.3.2.4. Individual edge analysis

To identify edge-specific age effects, we investigated 128 edges found in all participants (total number of edges: 396 ± 20), of which 64 edges showed significant age-related changes. The findings were consistent across different tractography parameters (Figure 3.12). First, 57 edges (89%) showed developmental changes: Fifty-five edges (86%) showed a reduced number of streamlines while only 2 (3%) had an increased streamline count (Figure 3.4C & 3.6A, Table 3.4). Reduction of streamlines was most pronounced in the frontal lobe; increased number of streamlines only occurred for two connections (3%) of cingulate cortex. These changes for both genders mainly occurred in the frontal and parietal lobe.

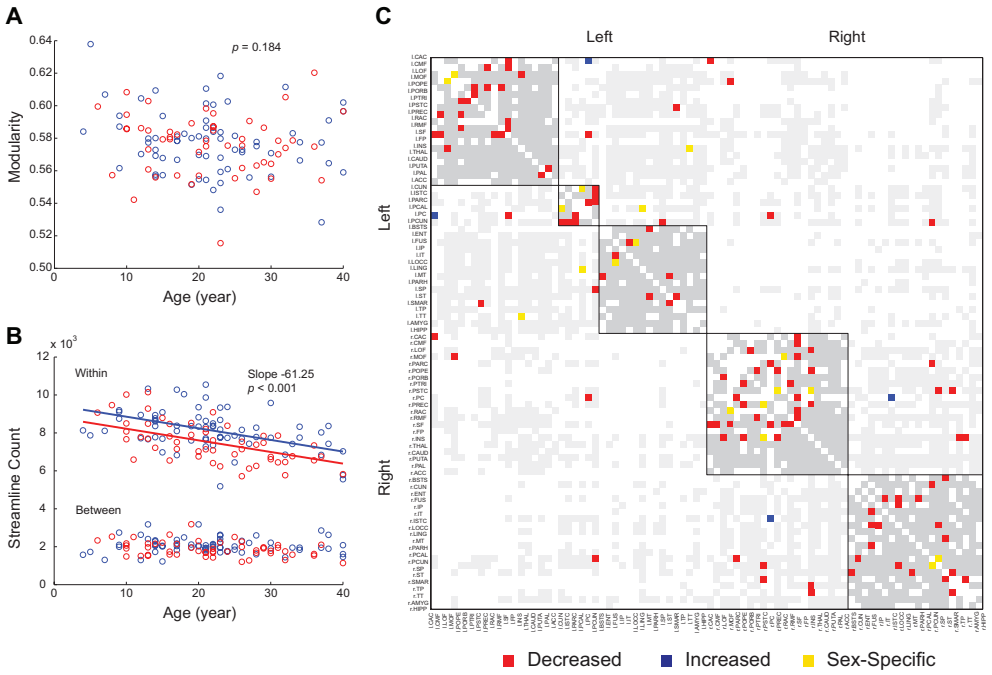

Figure 3.4.: Modular organisation. A. modularity Q, B. Streamline count in within vs. between module edges, and C individual edge analysis (Grey: intra-module edges and Light grey: inter-module edges, both without changes over age; Red: edges with a decreased streamline count, Blue: edges with an increased streamline count and Yellow: edges with sex-specific changes). When multiple lines were drawn, the lines are parallel unless otherwise noted. A list of all changes is provided in Table 3.3 for sex-specific changes and Table 3.4 for age effect.

3.3.2.5. Sex-specific age-related changes

Unlike developmental changes for both males and females, only several network properties showed sex-specific developmental changes. While both male and females lost short streamlines, only female participants were characterized by a decrease in long streamlines. However, this decrease was less pronounced than the reduction in short streamlines ($\beta_1 = -21.229$, $t_{(50)} = -3.372$, $p = 0.001$, Figure 3.2F). While global modular organisation did not show sex differences, three regions out of 20 showed sex-specific developmental changes in within-

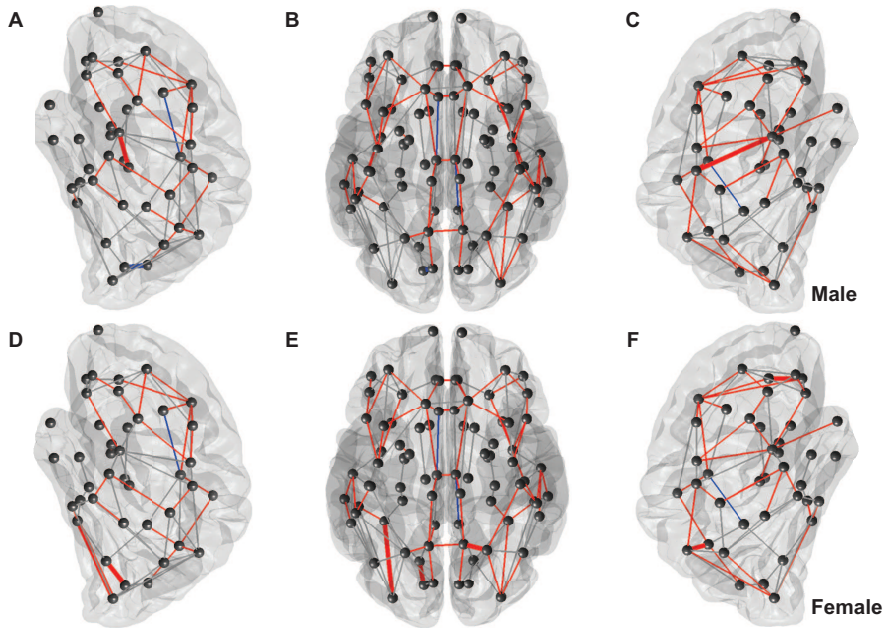

Figure 3.5.: Sex-specific developmental changes in individual edge analysis for male (A, B, and C) and for female subjects (D, E, and F), where red edges represent significant decrease, blue edges indicate significant increases over development, grey edges illustrate the tested edges that all subjects shared in common and the sex-specific changes were emphasised by the thick edges. A &C: sagittal views of the left hemisphere, B & D: transverse view, and C & F: sagittal views of the right hemisphere, of male and female brains, respectively. A. Two edges showed age-related changes; one in the temporal lobe lost streamlines and the other edge in the occipital lobe gained streamlines. C. An edge in the parietal lobe lost streamlines. D. Two edges in the temporal and the occipital lobes lost streamlines. F. Two edges in the frontal and parietal lobes lost streamlines.

module strength and participation coefficients (Table 3.2). In the individual fibre tract analysis, changes that only affected one gender occurred in seven fibre tracts (11%) (Figure 3.4C, 3.5 and 3.7B, Table 3.3). There were four edges with age-effect only in females, and three edges only in males, mostly involving occipital and parietal regions.

Table 3.3.: Edges with sex-specific age-related changes

ROI (node)	Lobe	ROI (node)	Lobe	Sex	Slope	FDR adjusted P
lh.cuneus	O	lh.pericalcarine	O	Male	1.035	0.0002
lh.fusiform	T	lh.lateraloccipital	O	Female	-0.9	0.041
lh.lingual	O	lh.pericalcarine	O	Female	-0.535	0.041
lh.transversetemporal	T	lh.insula		Male	-0.908	0.0002
rh.postcentral	P	rh.insula		Male	-0.747	0.001
rh.medialorbitofrontal	F	rh.rostralanteriorcingulate	P	Female	-0.769	0.0003
rh.precuneus	P	rh.superiorparietal	P	Female	-1.351	0.023
F:1	P:4	T:2	O:5			

3.3.2.6. Differences independent of age

Males had approximately 800 more streamlines than females across age ($t_{(118)} = -3.949$, $p < 0.001$, Figure 3.2A) mainly due to larger brain size. In particular, males had larger number of streamlines for within-module edges (Figure 3.9). Although males showed a substantially larger number of streamlines, male and female participants demonstrated comparable edge density ($t_{(118)} = -0.880$, $p = 0.381$, Figure 3.2B) as well as global efficiency (Global: $t_{(118)} = 1.598$, $p = 0.113$, Figure 3.2D). However, females showed higher local efficiency than males (Local: $t_{(118)} = 2.891$, $p = 0.005$, Figure 3.2E). Modularity ($t_{(118)} = -0.409$, $p = 0.684$, Figure 3.4A) and overall modular organisation based on NMI also did not differ between genders ($p = 0.177$). Most ROIs did not show gender differences in within-module strength and participation coefficient except 4 ROIs (Table 3.2).

3.4. Discussion

In this study, we investigated changes in structural connectivity between ages of 4 and 40 years from DTI data in cortical and subcortical regions. Previous

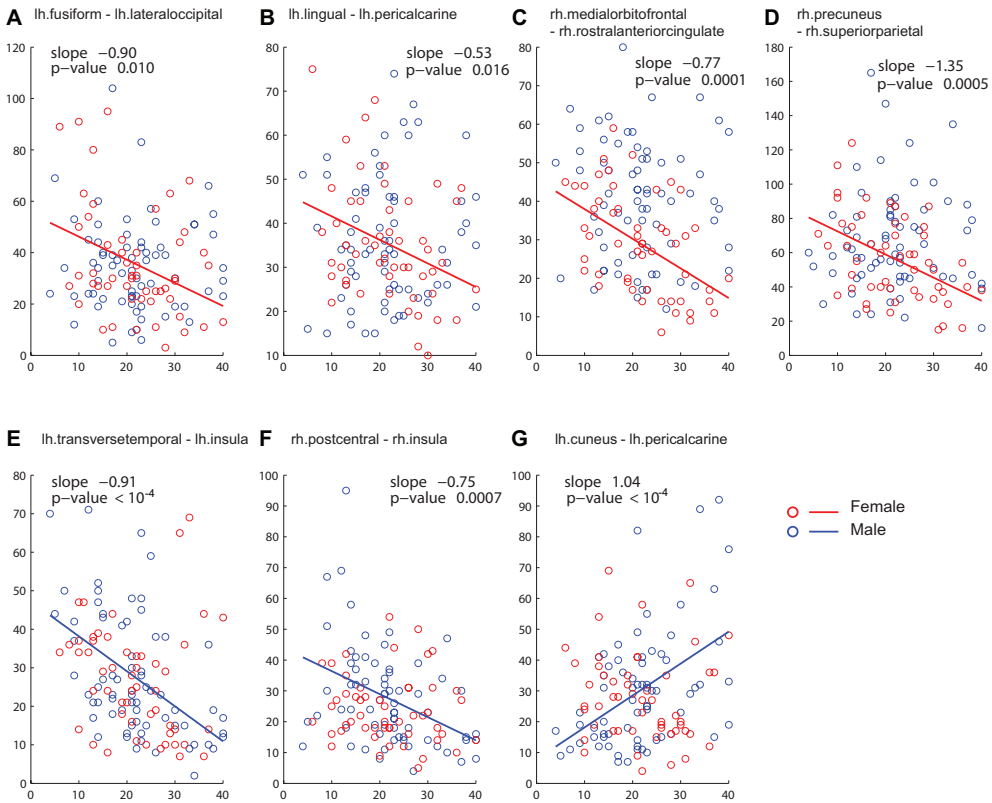

Figure 3.6.: Sex-specific developmental changes. A-G: scatter plots of streamline count with relevant fitted lines. Red: Female, Blue: Male. Upper panel: The four fibre tracts demonstrating age effects only for females Lower panel: the three fibre tracts displaying age effects only for males. Lh: left hemisphere, rh: right hemisphere. A. The fibre tract between lh.fusiform and lh.lateraloccipital showing a reduction of streamline counts only for females. B. The fibre tract between lh.lingual and lh.pericalcarine with a decreased number of streamlines for females, C. rh.medialorbitofrontal - rh.rostralanteriorcingulate, D. rh.precuneus - rh.superiorparietal, E. The fibre tract between lh.transversetemporal and lh.insula with a reduced number of streamlines over age only for males, F. rh.postcentral - rh.insula, G. lh.cuneus - lh.pericalcarine. The rate of change per year and corresponding p value is included in the figure and FDR-adjusted p-values can be found in Table 3.3.

studies had shown that the human brain undergoes vast structural changes involving alterations in the topology of structural and functional connectivity. Yet, core properties such as small-world topology and modular organisation were retained throughout development (Fair *et al.*, 2009; Gong *et al.*, 2009;

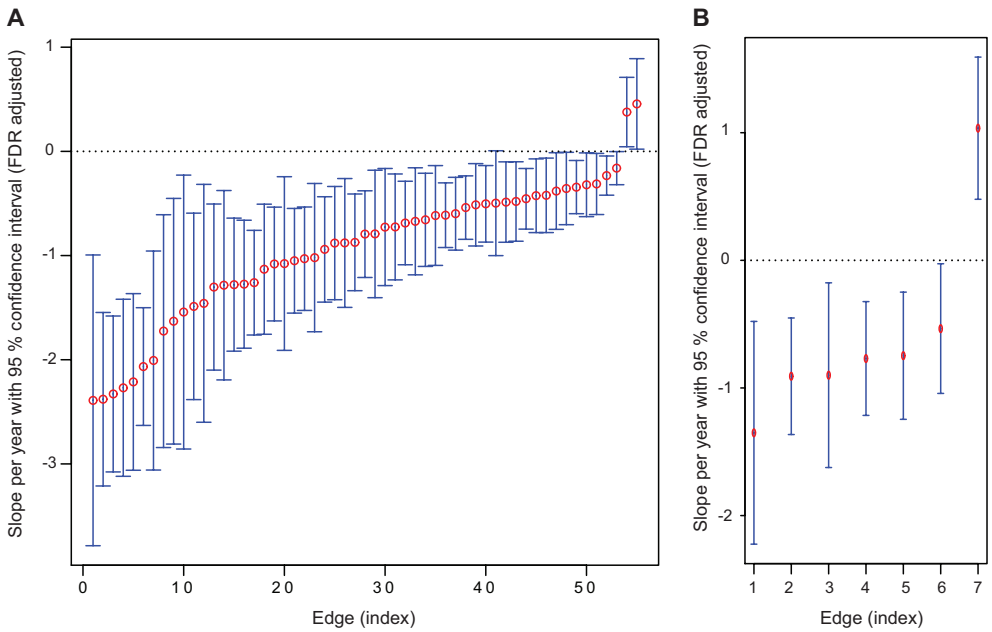

Figure 3.7.: Individual edge slopes representing age effect per year with FDR adjusted confidence intervals. A. Individual edge age effect for both genders. x-axis: indices of edges, y-axis: coefficients for age effect per year with FDR adjusted confidence intervals. The last two edges with positive slopes and confidence interval ranges are the edges with an increased streamline count and the others are the fibre tracts characterised by a decreased number of streamlines. B. Age-related sex effect. x-axis: indices of edges, First four edges show decreasing rate of streamline count for females and the rest three edges display age effect for males, y-axis: coefficients for age effect per year with FDR adjusted confidence intervals.

Supekar *et al.*, 2009; Hagmann *et al.*, 2010; Dennis *et al.*, 2013). Therefore, we examined if specific types of fibre tracts were preferentially affected, which might be conducive to conserving major topological features. Our results show that small-world features, the number of fibre tracts, and the modular organisation remained largely stable over age despite a significant reduction of streamlines in fibre tracts. This reduction preferentially affected fibre tracts that were relatively short, consisted of more streamlines and were within topological modules (Figure 3.8 A & B). Finally, streamline loss occurred at an earlier age in females than in males.

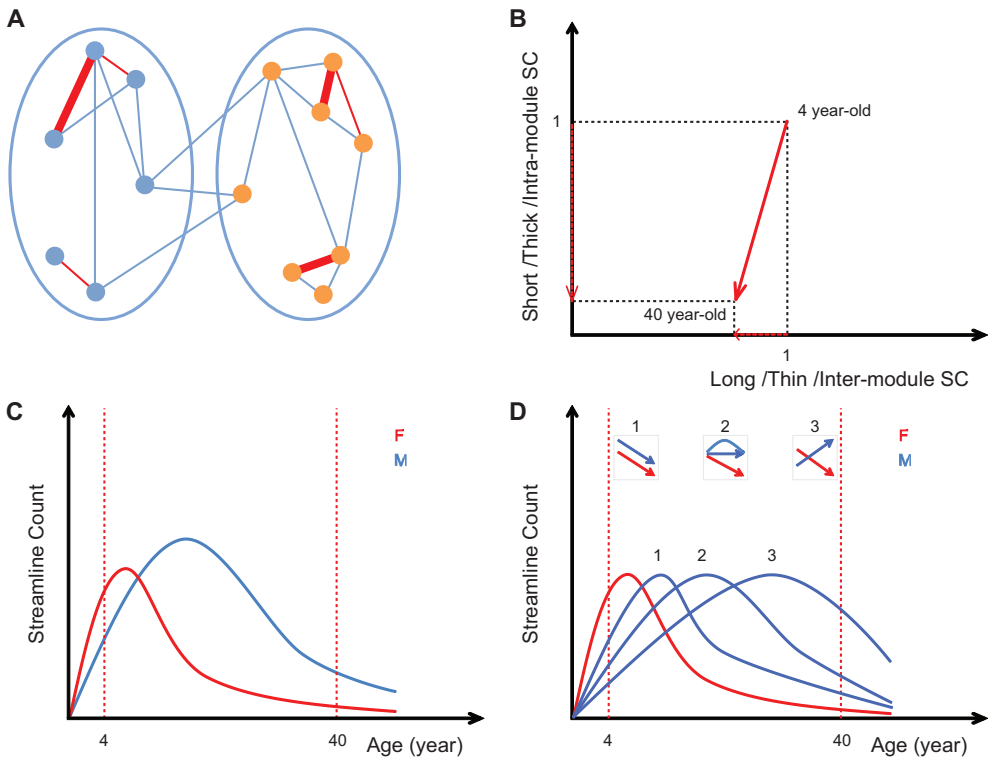

Figure 3.8.: A & B The schematic summary of the preferential reduction of thick, short and within-module streamlines over age. A. Location of change: Two ellipses represent left and right hemispheres and small circles inside hemispheres indicate ROIs. Lines connecting ROIs illustrate fibre tracts between ROIs. Red lines are where the reduction of streamlines occurred; thick, short or intra-module edges were mostly affected. B. Magnitude of change: Short, thick, or intra-module edges lost more streamlines than long, thin, or inter-module edges. X-axis: either long, thin, or inter-module streamline count (SC), y-axis: either short, thick, or intra-module SC. C & D: Hypothetical developmental curves for males (blue) and females (red). C. For the total streamline count based on the observation of our data (Figure 3.2A): a longer-lasting and higher peaked increase and a delayed decrease in males. D For individual edges: we observed sex-specific development (Figure 3.5C), which can be explained by three representative cases: if the two curves strongly overlap they show similar decreasing patterns (case 1), if one of the curves peaks later, one curve shows a decreasing pattern while the other curve is still increasing (case 3) or simply not decreasing yet (case 2). Therefore, depending on the time scale of the developmental trajectory, males and females may show different patterns.

Stable small-world and modular organisation with preferential streamline loss within short-distance, thick, and intra-modular fibre tracts

We found that fewer long-distance, thin, and inter-modular fibre tracts showed streamline loss than would be expected given how often such fibre tracts could have been affected by chance. This preferential streamline loss has several implications for the stable topological features that we observed. First, we found that small-world features were retained over age despite the overall reduction in the number of streamlines. A significant decrease in many long-distance streamlines would remove short-cuts and result in larger path lengths and reduced global efficiency while fewer connections between neighbours would decrease local clustering and local efficiency, disrupting small-world features of a brain network. However, global efficiency stayed comparable to that of rewired networks, local efficiency was much higher than in rewired networks across age, conserving small-world topology (Latora & Marchiori, 2001; Latora & Marchiori, 2003). We would therefore expect changes mainly in short-distance connectivity. Indeed, short streamlines were mostly affected and long-distance connectivity was rather preserved. Relatively conserved streamlines in long-distance fibre tracts could be achieved by strengthening long-range pathways in the brain network and a reduced number of streamlines in short fibre tracts could be due to weakening of short connections, which is consistent with previous findings from rs-fMRI and DTI-data (Fair *et al.*, 2009; Supekar *et al.*, 2009; Dosenbach *et al.*, 2010; Hagmann *et al.*, 2010).

Second, in line with previous rs-fMRI and DTI studies (Fair *et al.*, 2009; Hagmann *et al.*, 2010), modularity Q remained stable over age. We found that the global modular organisation and module membership of ROIs were unchanged with local changes especially in the basal ganglia. Therefore, local networks re-organized their relationships with other community members while keeping

the global community structure stable. This retained modular organisation (Kaiser & Hilgetag, 2010; Meunier *et al.*, 2010) might be crucial in keeping the balance between information integration and the segregation of separate processing streams (Sporns, 2011). Too many connections between modules would interfere with different processing demands, e.g., leading to interference between visual and auditory processing. In addition, more inter-module connections would also facilitate activity spreading potentially leading to large-scale activation as observed during epileptic seizures (Kaiser *et al.*, 2007; Kaiser & Hilgetag, 2010). However, because of the reduction of streamlines in intra-module edges, proportionally inter-module connections increased, indicating that brain network became a more distributed network rather than modular with age as observed in previous studies, which was associated with development of advanced cognitive abilities by enhancing integration of neural processing (Fair *et al.*, 2009; Supekar *et al.*, 2009; Hagmann *et al.*, 2010).

In summary, we find that long-distance and inter-modular connectivity is largely spared from the ongoing streamline losses during development, which is potentially beneficial for the observed stability of small-world and modular connectome features. Note that as connections between modules are not necessarily long-distance (Kaiser & Hilgetag, 2006), we found that only 47% of inter-modular fibre tracts also belong to the class of long-distance connections. Retaining long-distance and inter-modular fibres indicate that small-world features, such as the number of processing steps but also the balance between information integration and large-scale brain activity, are kept within a critical range during development (Kaiser & Hilgetag, 2006). Preserving this balance is crucial as changes in long-distance connectivity are a hallmark of neurodegenerative and neurodevelopmental disorders ranging from Alzheimer's disease (Ponten *et al.*, 2007; Stam *et al.*, 2007) to schizophrenia (Alexander-Bloch *et al.*,

2012). Therefore, stable topological network features might help to prevent cognitive deficits in pathological brains.

Another important implication of the reduced number of streamlines is the relationship to the number of edges within a network. Changes in streamline count can lead to a reduction of connections within a network if an edge comprised of few streamlines loses all its streamlines, thus reducing edge density. However, edge density did not significantly change during brain maturation. Therefore, several mechanisms are conceivable how the number of edges is maintained during development. One option is that newly emerging edges cancel out disappearing edges ("equilibrium-state"), which is biologically costly by removing already established connections and unlikely because new connections are established mostly early in the development. Alternatively, only the weight of an edge changes ("stable-state"). For the latter case, a reduction of streamlines in thin edges, which could result in the loss of the whole edge, needs to be prohibited. Indeed, we found that thick edges were mostly affected from the decreased streamlines, thus preserving the structure of the network. This is beneficial, as reducing thin fibres would necessitate an increase in synaptic weights or number of synapses to transmit the same amount of information. Reducing streamlines for thick fibres, on the other hand, has only a small effect on activity flow due to the large number of remaining streamlines.

Preferential streamline loss for frontal and subcortical regions

Changes in individual edges were most pronounced in the frontal lobe, a brain region that is characterized by protracted development until the 3rd and 4th decade of life as indicated by ongoing synaptic pruning and myelination (Benes *et al.*, 1994; Sowell *et al.*, 1999; Shaw *et al.*, 2008; Petanjek *et al.*, 2011). In addi-

tion, the fibre tract between putamen and pallidum in the basal ganglia for the left hemisphere was characterized by a reduced number of streamlines. Previous studies which examined GM volume (Sowell *et al.*, 1999) also found changes GM density in putamen and pallidum in post-adolescent brain development, which are involved in learning and neurodevelopment diseases (DeLong *et al.*, 1984; Alexander & Crutcher, 1990; Hokama *et al.*, 1995; Teicher *et al.*, 2000; Ell *et al.*, 2006; DeLong Mr, 2007; de Jong *et al.*, 2008; Farid & Mahadun, 2009). Furthermore, basal ganglia were characterized by decreased within-module strengths and increased participation coefficients over age. This suggests that connectivity to within these areas decreased relative to connections to outside of the basal ganglia, which is consistent with data from Supekar and colleagues (Supekar *et al.*, 2009) who demonstrated that subcortical functional connectivity in children had higher degree and efficiency than in adults.

This reorganisation of cortico-subcortical connectivity could be involved in the ongoing changes of cognition and behaviour during development. The basal ganglia involve regions that are crucially involved in neural circuits relevant for response-inhibition and reward modulation. Previous studies have shown that response inhibition improves significantly with age (Williams *et al.*, 1999) as well as reward modulation (Gardner & Steinberg, 2005). Unlike for the basal ganglia, the anterior cingulate cortex (ACC) was characterized by an increased connectivity within its module with age. This observation is consistent with functional connectivity of ACC that develops a more focal organisation with age (Kelly *et al.*, 2009). ACC has also shown to mature late through error-related ERPs (Santesso & Segalowitz, 2008).

Delayed streamline loss for males

Individual edge analysis revealed sex-specific age effects in the occipital and

parietal lobe but to a much lesser extent in the frontal lobe. This is consistent with a previous WM study where mainly the occipital lobe development varied with sex while the growth trajectory in the frontal lobe was similar for both genders (Baron-Cohen *et al.*, 2005; Lenroot *et al.*, 2007; Giedd, 2008; Perrin *et al.*, 2009). These results can be explained if we assume that the same mechanism of preferential streamline loss operates at different time-scales in males and females. Provided that males had a similar developmental curve but with a shifted peak (Figure 3.8C & D), we can explain the sex-specific changes. As expected from the shifted peak hypothesis (Figure 3.8 C & D), the total number of streamlines for males, but not females, remained stable at an earlier age range (4-28 years, not shown) while both genders showed streamline reductions in the age range 4 to 40 years old. This delayed developmental growth curve in streamline count can be related to later volume growth peaks for grey and white matter in males (Giedd *et al.*, 1997; Giedd & Rapoport, 2010) and earlier myelination for females (Benes *et al.*, 1994).

We only observed circumscribed sex-differences independent of age. Local efficiency was higher for females than males consistent to Gong and colleagues' finding (Gong *et al.*, 2009) and some ROIs showing higher within-module strength and lower participation coefficient for females can be related to higher local efficiency in females. Interestingly, absolute difference in the number of streamlines between genders was not uniformly distributed; males exhibited more streamlines for intra-module edges. This is consistent with the finding that males and females do not differ in the WM volume growth trajectory in corpus callosum (Giedd, 2008). However, this means proportionally females have more connections across hemispheres and between modules (DeLacoste-Utamsing & Holloway, 1982; Davatzikos & Resnick, 2002; Allen *et al.*, 2003).

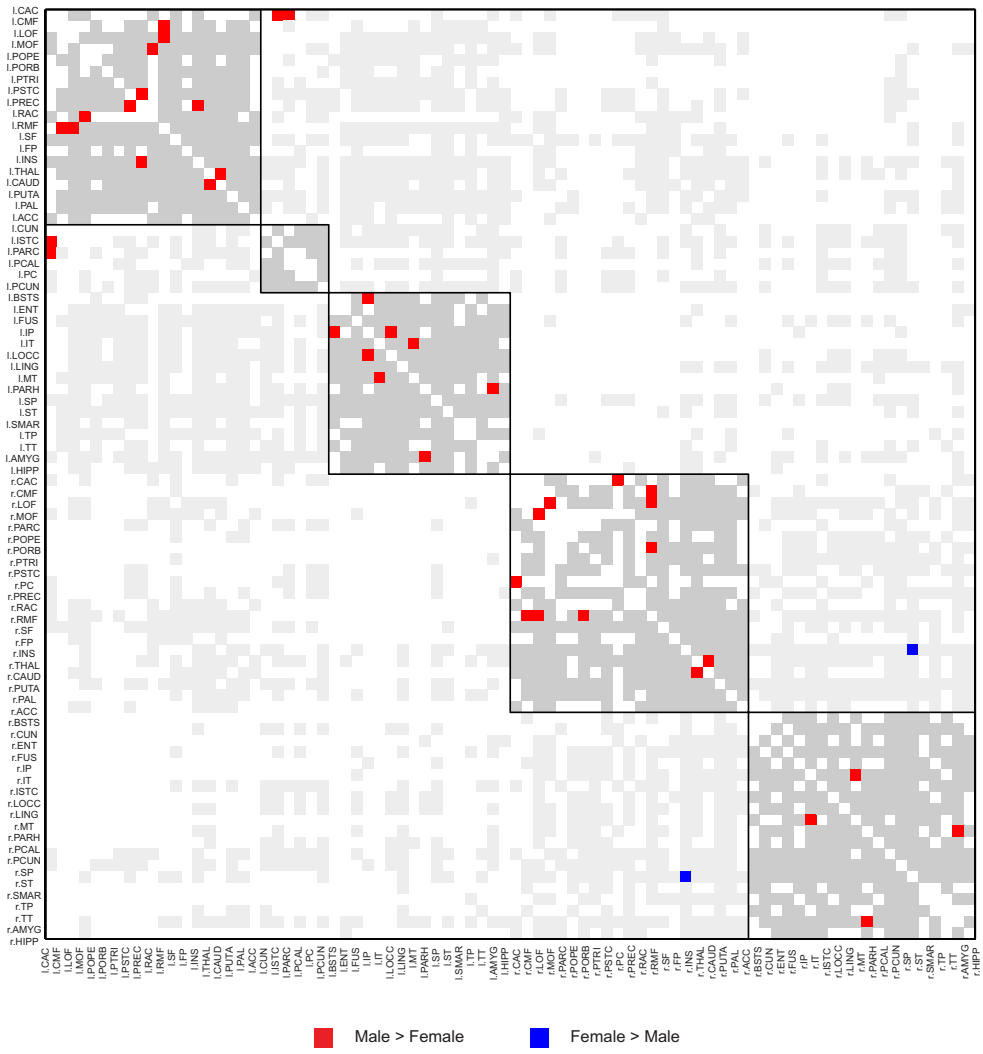

Figure 3.9.: Sex difference in the individual edges. Gender differences were observed mostly within modules and only within hemispheres. (Gray: edges connecting ROIs within modules and Light gray: edges between modules, both with no significant change over age; Red: edges with a larger number of streamlines for males than females; Blue: edges with a larger streamline count for females than males).

Structural correlates of streamline loss

The observed reduction in the total number of streamlines could be related to rs-fMRI developmental 'system-level pruning' (Supekar *et al.*, 2009), considering tight coupling between structural connectivity (SC) and functional connectivity (Honey *et al.*, 2009a; Honey *et al.*, 2010). As Supekar and colleagues suggested for functional connectivity (Supekar *et al.*, 2009), the decreased number of streamlines for short and intra-module connections in this study could be due to weakening of local connections through synaptic pruning and neuronal rewiring. These local processes prolong until adulthood and are major factors for anatomical developmental changes (Benes *et al.*, 1994; Petanjek *et al.*, 2011). The reduction of synapses and corresponding axons or axon collaterals could potentially also lead to a decreased number of streamlines within fibre tracts. Due to technical limitations of DTI, pruning of dendrites and intra-cortical connections cannot be detected. However, synaptic pruning in the prefrontal cortex for intra-cortical connections (Petanjek *et al.*, 2011) was mainly limited to children at younger ages than in our study (Petanjek *et al.*, 2011). In contrast, the pruning of long-distance connection, observable in DTI, occurs in developing rhesus monkeys, both at earlier and later stages of development (LaMantia & Rakic, 1990; LaMantia & Rakic, 1994; Luo & O'Leary, 2005). Considering both limitations of DTI (Jones & Leemans, 2011) and previous studies (Fair *et al.*, 2009; Supekar *et al.*, 2009; Dosenbach *et al.*, 2010), changes in cortico-cortical and subcortico-cortical projections might underlie our results but further investigations are needed to determine the contributions of these potential biological correlates.

Studies have shown that volume for WM fibre tracts increased with age (Faria *et al.*, 2010; Lebel & Beaulieu, 2011) and continued myelination also leads to an increase in WM volume, which could explain an increase in total WM

volume while undergoing a possible reduction of fibre tracts. Even though streamlines were reduced in our study, an increased myelination might still have taken place but might have been over-shadowed by axonal changes and vice versa. Greater amounts of myelination would generate higher FA values (Mädler *et al.*, 2008; Faria *et al.*, 2010), leading to an increase in the number of detected streamlines. For example, even if the number of axonal projections were reduced the remaining fibres with an increased myelination could be detected easily by tractography and compensate the lost fibre tracts, leading to no changes in the number of streamlines. Thus, the balance between myelination and axonal pruning may have contributed to our final results. The reduction in streamlines with age cannot be attributable to ongoing changes in the number of seed voxels used for tractography as this number was unaffected by age.

Other factors affecting tractography include axon diameter distributions (See detailed discussion (Jones, 2010; Jones *et al.*, 2013) and fibre curvature changes. If many fibre tracts became more curved over age, as DTI normally does not track highly curved trajectories, the number of streamlines of the fibre tract could decrease. However, most of the fibre tracts (edges) that we tested did not change their curvature over age (83%, 106 out of 128) only 22 edges (17%) showed changed curvature over development. Out of these 22, only half showed curvature increase. For a single edge do we find streamline decrease while curvature increased ruling out curvature as a confounding factor of our results.

Possible scenarios to explain the reduction in the streamline count

We suggested our observation of a reduced number of streamlines might be explained by prolonged synaptic pruning concomitant with myelination increase (i). However, there are other possible explanations (ii-v). (i) Decrease in the

actual axonal projections from synaptic pruning or cell death; (ii) An edge (fibre tract) became more curved so could not be detected by our tractography algorithm (this is a well-known problem for DTI network reconstruction) ; (iii) Less homogeneity of fibre directions would result in lower Fractional anisotropy, preventing fibre tracts from reconstructed by tractography ; (iv) Myelination reduction would lower fractional anisotropy or (v) Enlarged axonal diameter would also lower fractional anisotropy, which make axon bundles less likely to be detectable .

Regarding (ii), we cannot resolve the issue of limitation in finding highly curved fibres using DTI but we did test the role of the angular threshold for fibre tract reconstruction. The comparison between the original 35- degree and the more relaxed 45-degree criterion showed similar results confirming our earlier conclusions. While highly-curved fibres might still go undetected even with the relaxed criterion, we can test for the impact of curvature on our results by investigating whether edges characterised by a decreasing number of streamlines became more curved or not. If so, higher curvature streamlines that cannot be detected at old age might explain part of the loss of streamlines during development. On the other hand, if we do not find any changes in curvature of edges over age, we can conclude that the reduction in the streamline count cannot be explained by stronger curvature. Edges we tested did not show any systematic or consistent relationship between their curvatures and the age effects. Curvature of a fibre tract was estimated by dividing the trajectory length of fibre tract by the Euclidean distance between the centres of mass between a pair of nodes. Out of 128 edges, 21 edges showed significant curvature changes over age using GLM. Eleven edges were characterised by increased curvatures and 10 showed decreased curvatures. One edge with an increased curvature lost streamline count over age, with which we need to interpret the

result with caution because it would be difficult to tell whether the decreased streamline count was from the higher curvature or from the loss of axonal projections. Interestingly, six fibre tracts with decreased curvature were also the edges that lost streamlines over age. These edges became straighter but lost streamline count over age, which can be stronger evidence showing the reduction in the number of streamlines was not from the changes in curvatures. For (iii): Less homogeneity of fibre directions, which means a smaller number (or a proportion) of streamlines with similar directions, or more crossing fibres. It is a possibility if we assume that axonal projections decrease over age because the reduction in the streamline count could change the proportions of fibre directions within voxels. However, the formation of maps between cortical areas, an on-going event during brain development, would increase the homogeneity of fibres (von der Malsburg, 1973). Homogeneity is also expected from anatomical findings of fibre lengths between two maps that are as short as possible (Chklovskii & Koulakov, 2004) (iv): Previous studies reported that myelination increases so we can exclude this possibility. (v): Dilation of axon diameters is in principal possible. As the brain size enlarges, axonal fibres might lengthen and to obtain the same conduction velocity axons may need to widen their diameters or increase myelination or both. In our study, we did not observe any significant lengthening of fibre tracts; rather, the lengths of fibre tracts remained relatively stable for those older than 10 years of age (Spearman's $\rho = 0.1704$, $p = 0.0617$). Therefore, this scenario is less likely to explain the overall reduction in the streamline count.

The relationship between the length of a fibre tract and its weight (streamline count)

The brain is connected in a way that the total wiring length is optimally short with a few long-distance connections, which benefits efficient communications

between brain regions while spending a lesser amount of resources (Kaiser & Hilgetag, 2006; Bullmore & Sporns, 2012). Likewise, to shorten total connection length, long fibre tracts may consist of fewer streamlines than short-range ones. However, this tendency was not a simple negative correlation; short edges showed a wide spectrum of different weights and 'thick' fibre tracts with many streamlines could be long too (Figure 3.10). Thus long fibre tracts are not always 'thinner' edges. In addition, there were more thicker and shorter edges within modules than between modules but they showed much overlapping areas in the scatterplot (Figure 3.10) indicating within module edges are not always short and between module fibre tracts can be also short. Within-module fibre tracts were comprised of more short edges than between-module edges in general (Figure 3.10 inset) but not necessarily short. We found that only 47% of inter-modular fibre tracts also belongs to the class of long-distance connections and 43% of thin fibre tracts were also long distance-connections. Therefore, we analysed all three types of fibre tracts independently and connected with small-world topology, modular organization and edge density, respectively in the main text.

Limitations

Even though the current study comprises a large dataset, there are several inherent limitations. First, the subjects were unequally distributed across ages. Having subjects at ages between 4 and 40 years may not be optimal for detecting major changes as small-world and modular features are established during the first two years (Fan *et al.*, 2011; Yap *et al.*, 2011a). Our focus, however, was not the major structural changes but the continuous development while keep the network economic (Vértes *et al.*, 2012) and stable. Second, studies with network approaches use different definitions for weight and different normalization schemes complicating the comparison between studies. We used

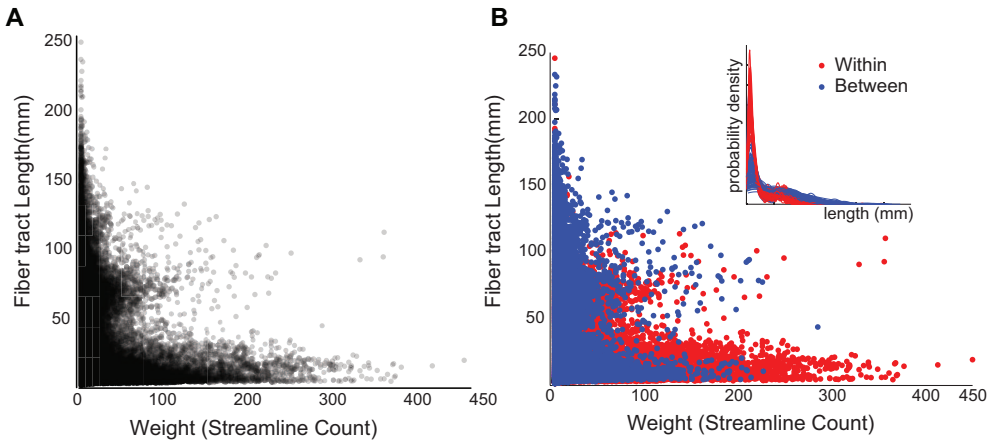

Figure 3.10.: The relationship among between the average length of an edge and its weight (streamline count) A. Scatterplot. Darker areas have more data points. Short fibre tracts tend to have larger number of streamlines and the fibre tract with many streamlines ('thick') is more likely to be short-range. However, the tendency was not a simple negative correlation. B. Scatterplot differentiating intra- and inter-module fibre tracts. Inset: the probability density estimate for fibre tracts according to lengths using kernel smoothing density. Within module fibre tracts were comprised of more short edges than between module edges. Each line represents a participant. Red: edges within modules, Blue: edges between modules.

absolute number of streamlines as weights; however, our results are consistent with previous studies with slightly different weight definitions (Gong *et al.*, 2009; Hagmann *et al.*, 2010). Third, our DTI approach will not resolve crossing fibres (See discussion in Section 5.2.2). However, the shorter recording time of this data are an advantage when measuring connectivity in children. Modelling through probabilistic tracking with crossing fibres (Behrens *et al.*, 2007; Jbabdi & Johansen-Berg, 2011) would therefore be a future research direction. Although streamlines do not directly correspond to axonal projections (Jones, 2010; Jones *et al.*, 2013), we found our results were consistent with previous anatomical studies (Benes *et al.*, 1994; Sowell *et al.*, 1999; Gong *et al.*, 2009; Perrin *et al.*, 2009). Finally, our particular linear model approach may be vulnerable to changes in the age range (Fjell *et al.*, 2010; Reiss *et al.*, 2014), more flexible

models such as penalized spline models have been suggested (Reiss *et al.*, 2014; Alexander-Bloch *et al.*, 2014; Wood, 2006; Green & Silverman, 1993; Faraway, 2005); nonetheless, our polynomial model was good enough to answer our hypotheses.

3.5. Conclusion

The human brain undergoes vast structural changes during development. Nonetheless brain networks develop in a way that preserves its topological (small-world/modular) and spatial (long-distance connectivity) organisation to secure its capability of integration of information and individual processing of modules. This present study showed how brain connectivity changed during development in terms of fibre tracts as well as global network features. We showed preferential decreases in the number of streamlines for thick, short-distance, and within-module/within-hemisphere fibre tracts. These changes may not necessarily occur at the same time for males and females; males seem to show a delayed start in the prolonged development of white and grey matter. However, although with different time courses between genders, the global topological features ensuring healthy brain development apply to both genders. Therefore, brain networks maintain their topological stability during brain development by preferentially modifying structural connectivity.

In this chapter, I found that the brain network may ensure the normative trajectory of connectivity development by selectively changing fibre tracts over age. In the following chapter, combining microscopic and macroscopic brain network development, I provide a connectome maturation hypothesis, in particular, concerning short/long-distance connectivity.

Table 3.4.: Fibre tracts with age-related changes for both genders.

ROI (node)	Lobe	ROI (node)	Lobe	Slope	FDR adjusted P	
lh.bankssts	T	lh.middletemporal	T	-0.941	0.001	
lh.caudalanteriorcingulate	F	rh.caudalanteriorcingulate	F	-0.487	0.017	Inter-hemispheric
lh.caudalanteriorcingulate	F	lh.superiorfrontal	F	-1.542	0.024	Symmetric
lh.caudalmiddlefrontal	F	lh.precentral	F	-1.458	0.016	
lh.caudalmiddlefrontal	F	lh.superiorfrontal	F	-1.26	<10 -4	Symmetric
lh.cuneus	O	lh.precuneus	P	-1.488	0.002	Symmetric
lh.fusiform	T	lh.inferiortemporal	T	-0.356	0.043	Symmetric
lh.isthmuscingulate	P	lh.precuneus	P	-0.726	0.016	
lh.lateralorbitofrontal	F	lh.insula		-2.008	0.001	Symmetric
lh.medialorbitofrontal	F	rh.medialorbitofrontal	F	-1.03	0.0003	Inter-hemispheric
lh.middletemporal	T	lh.superiortemporal	T	-0.513	0.016	Symmetric
lh.paracentral	F	lh.precuneus	P	-2.213	<10 -5	Symmetric
lh.paracentral	F	lh.posteriorcingulate	P	-0.671	0.016	Symmetric
lh.parsopercularis	F	lh.parstriangularis	F	-0.343	0.014	Symmetric
lh.parsopercularis	F	lh.precentral	F	-2.269	<10 -5	Symmetric
lh.parsopercularis	F	lh.rostralmiddlefrontal	F	-0.455	0.004	Symmetric
lh.parsorbitalis	F	lh.parstriangularis	F	-1.077	0.016	
lh.postcentral	P	lh.supramarginal	P	-0.381	0.041	
lh.posteriorcingulate	P	lh.superiorfrontal	F	-1.285	0.01	
lh.posteriorcingulate	P	rh.posteriorcingulate	P	-1.303	0.003	Inter-hemispheric
lh.precuneus	P	rh.precuneus	P	-0.599	0.002	Inter-hemispheric
lh.precuneus	P	lh.superiorparietal	P	-0.504	0.012	
lh.putamen		lh.pallidum		-1.02	0.009	Subcortical
lh.rostralanteriorcingulate	F	lh.superiorfrontal	F	-1.63	0.012	Symmetric
lh.rostralmiddlefrontal	F	lh.superiorfrontal	F	-1.275	0.0003	Symmetric
lh.superiortemporal	T	lh.supramarginal	P	-1.725	0.004	Symmetric
rh.bankssts	T	rh.superiortemporal	T	-0.688	0.001	
rh.caudalanteriorcingulate	F	rh.superiorfrontal	F	-1.081	0.0004	Symmetric
rh.caudalmiddlefrontal	F	rh.superiorfrontal	F	-0.422	0.024	Symmetric
rh.cuneus	O	rh.precuneus	P	-0.426	0.021	Symmetric

ROI (node)	Lobe	ROI (node)	Lobe	Slope	FDR adjusted P	
rh.fusiform	T	rh.inferiortemporal	T	-0.725	0.004	Symmetric
rh.fusiform	T	rh.lateraloccipital	O	-0.161	0.045	
rh.fusiform	T	rh.parahippocampal	T	-2.39	0.002	
rh.inferiorparietal	P	rh.lateraloccipital	O	-1.131	0.001	
rh.lateraloccipital	O	rh.superiorparietal	P	-0.657	0.007	
rh.lateralorbitofrontal	F	rh.parsorbitalis	F	-0.794	0.001	
rh.lateralorbitofrontal	F	rh.insula		-0.616	0.016	Symmetric
rh.medialorbitofrontal	F	rh.superiorfrontal	F	-0.879	0.01	
rh.middletemporal	T	rh.superiortemporal	T	-0.54	0.001	Symmetric
rh.paracentral	F	rh.posteriorcingulate	P	-0.481	0.017	Symmetric
rh.paracentral	F	rh.precuneus	P	-0.873	0.001	Symmetric
rh.parsopercularis	F	rh.parstriangularis	F	-1.05	0.0003	Symmetric
rh.parsopercularis	F	rh.precentral	F	-0.313	0.04	Symmetric
rh.parsopercularis	F	rh.insula		-0.321	0.016	
rh.parstriangularis	F	rh.rostralmiddlefrontal	F	-2.066	<10 -5	Symmetric
rh.postcentral	P	rh.superiorparietal	P	-0.613	0.0002	
rh.postcentral	P	rh.supramarginal	P	-0.88	0.002	Symmetric
rh.posteriorcingulate	P	rh.superiorfrontal	F	-0.497	0.017	
rh.precentral	F	rh.insula		-2.379	$< 10^{-5}$	
rh.rostralanteriorcingulate	F	rh.superiorfrontal	F	-0.232	0.016	Symmetric
rh.rostralmiddlefrontal	F	rh.superiorfrontal	F	-0.793	0.016	Symmetric
rh.superiortemporal	T	rh.supramarginal	P	-0.56	0.046	Symmetric
rh.supramarginal	P	rh.transversetemporal	T	-1.279	0.0004	
rh.temporalpole	T	rh.insula		-0.254	0.007	
rh.transversetemporal	T	rh.insula		-2.329	$< 10^{-5}$	
F:50	P:27		T:20	O:5		
lh.caudalanteriorcingulate	F	lh.posteriorcingulate	P	0.377	0.012	
rh.isthmuscingulate	P	rh.posteriorcingulate	P	0.456	0.034	
F:1	P:3		T:0	O:0		

Note: Decreased connections: Interhemispheric connections and a subcortical fiber tract showing a decreased number of streamlines are bolded. Increased connections (the penultimate two rows): The last row of each section gives an overview of how often different lobes participate in these changes. (F: Frontal lobe, P: Parietal lobe, T: Temporal lobe, O: Occipital lobe). p-values were adjusted by FDR with a q level 0.05 (Benjamini & Hochberg, 1995; Benjamini *et al.*, 2005; Jung *et al.*, 2011)

3.6. Appendix

3.6.1. Overall anatomical changes in brain volumes

The overall anatomical changes in volume would inevitably affect topological and spatial features in the structural connectivity. Thus, before examining topological and spatial features of the structural connectivity in human developing brain, we explored volume changes. White matter volume (WMV), gray matter volume (GMV, cortical + subcortical) and intracranial volume (ICV) were tested with a general linear model (Eq.(3.2) - Eq.(3.4) , Table 3.5). All showed a significant gender difference ($p < 0.001$). On average, males had larger brain volumes than females. WMV increased over age but the increasing rate slowed down after age 10 ($p = 0.001$), whereas GMV decreased significantly with increasing age ($\beta_1 = -4171.981 mm^3$/year, $p < 0.001$), while ICV did not show any age effect ($p = 0.069$). In all cases, no significant gender and age interaction effect were observed so all models are fitted without the interaction term.

Table 3.5.: Linear model analysis on white matter volume (WMV), gray matter volume (GMV) and intracranial volume (ICV): t-values with degrees of freedom (df) and p-values (two-sided, $\alpha = 0.05$) are provided in the table.

	Gender t ($df = 118$)	p	Age t ($df = 118$)	p
WMV	-5.457	< 0.001	2.777	0.006
GMV	-5.975	< 0.001	-6.249	< 0.001
ICV	-6.776	< 0.001	-0.418	0.677

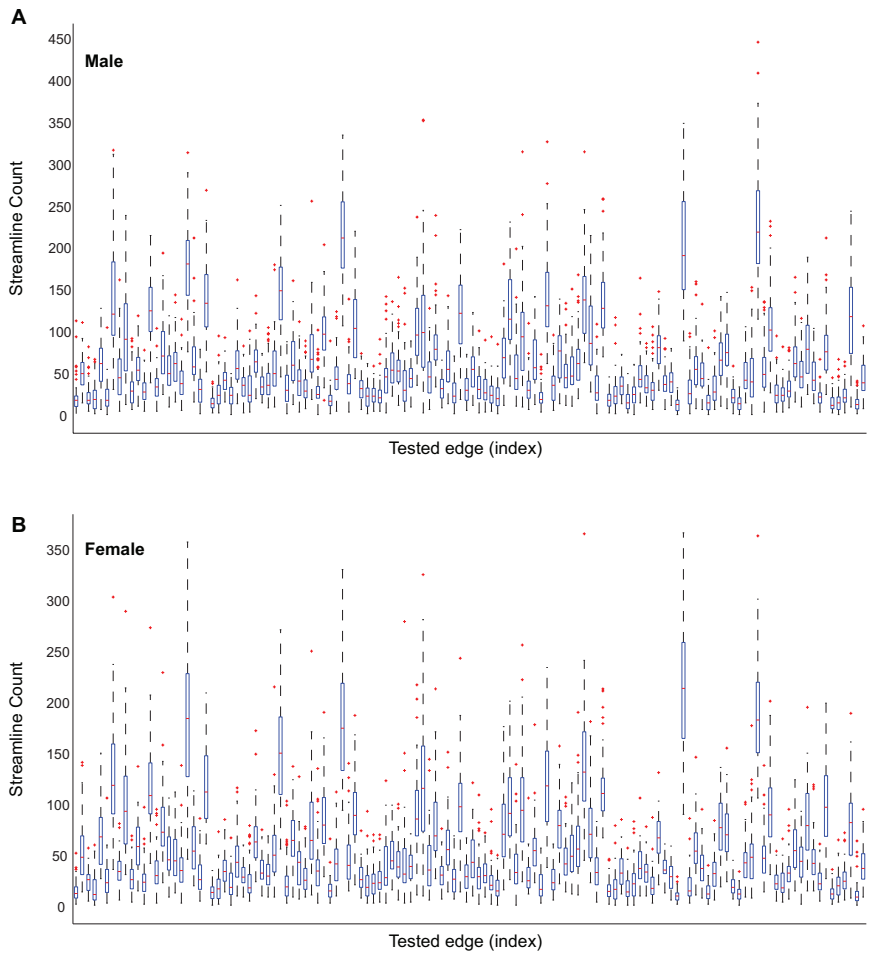

Figure 3.11.: Streamline count range. A. Streamline count ranges for individual edges (Male) B. Streamline count ranges for individual edges (Female), 128 tested edges shared by all participants with box plots. Red cross: outliers.

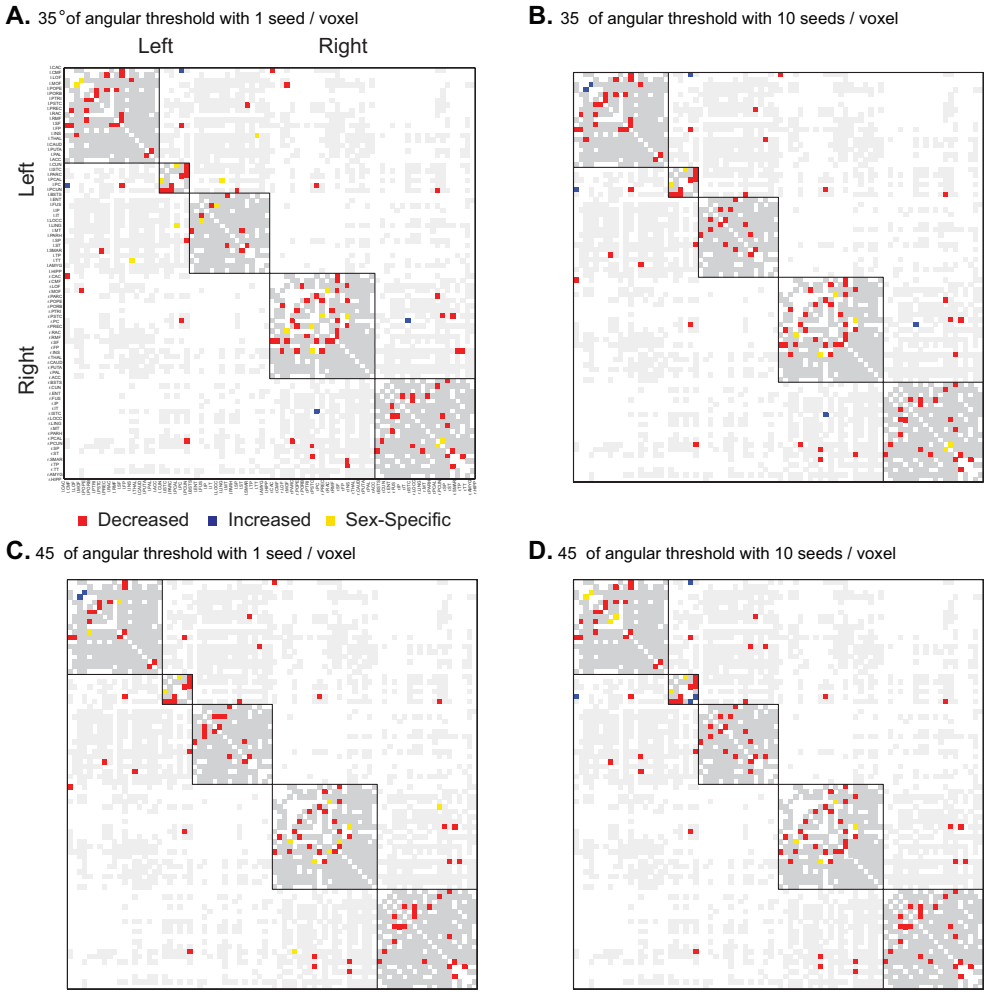

Figure 3.12.: Individual edge analysis with 35 and 45 degrees of angular threshold and single and ten random seeds tracking. First row: 35 degrees of angular threshold, Second row: 45 degrees of angular threshold. Left column: a single seed at the centre per voxel, Right column: ten random seeds tracking per voxel.

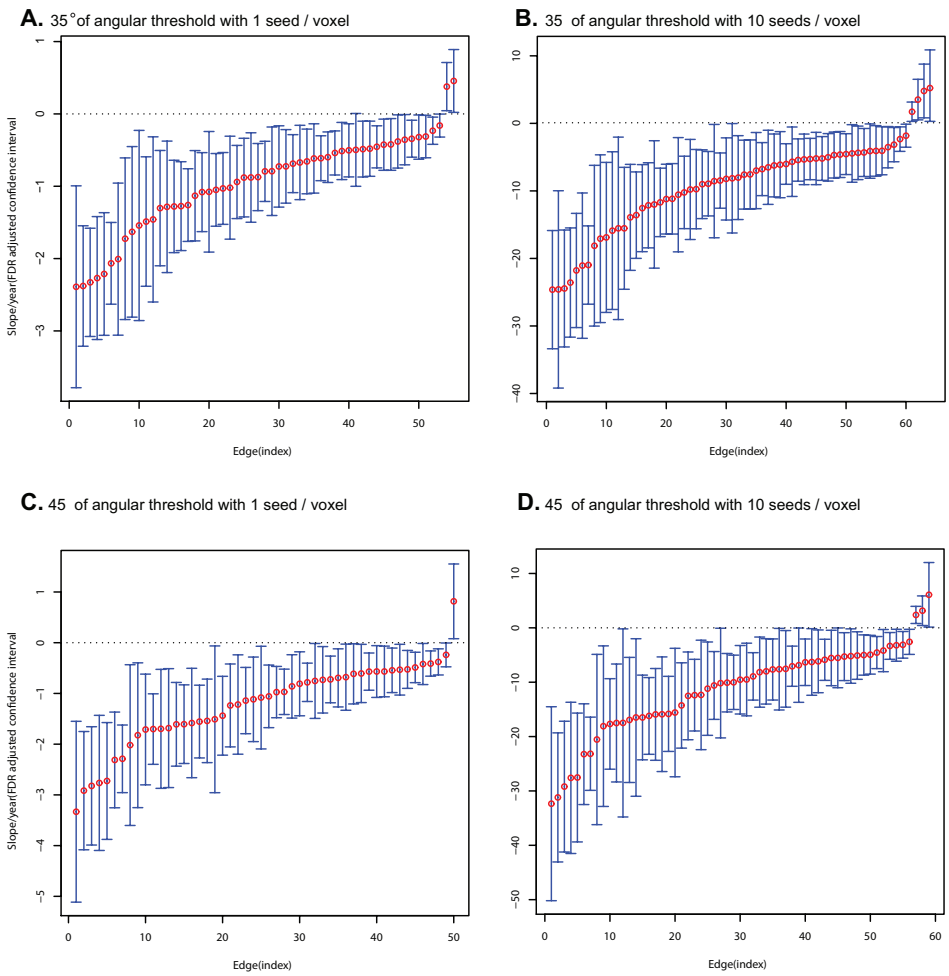

Figure 3.13.: Slopes with FDR adjusted confidence intervals for the edges with age effects for both genders with four different tracking parameters. First row: 35 degrees of angular threshold, Second row: 45 degrees of angular threshold. Left column: a single seed at the centre per voxel, Right column: ten random seeds tracking per voxel. Slopes are represented as sorted and different tracking parameters resulted in different number of testable edges that all participants shared, leading to slightly different results. The result with 10 random seeds tracking demonstrated approximately 10-fold slopes than the resulting slopes with the original parameters (35 degrees with a single tracking per voxel).

Table 3.6.: Pair-wise comparison of modular organization (uncorrected p-values)

Age group			
4-11 vs. 12-15	14-15 vs. 16-19	16-19 vs. 20-28	20-28 vs. 29-40
P = 0.1561	P = 0.2140	P = 0.3414	P = 0.1119
lh.medialorbitofrontal: p = 0.035	lh.medialorbitofrontal: p = 0.031	lh.medialorbitofrontal: p = 0.046	lh.medialorbitofrontal: p = 0.008
lh.inferiorparietal: p = 0.043	lh.superiorfrontal: p = 0.049	lh.postcentral: p = 0.022	lh.bankssts: p = 0.045
lh.superiorparietal: p = 0.043	rh.inferiorparietal: p = 0.025	rh.bankssts: p = 0.046	lh.caudalanteriorcingulate: p = 0.018
rh.parahippocampal: p = 0.044	rh.precentral: p = 0.049	rh.caudalmiddlefrontal: p = 0.023	lh.entorhinal: p = 0.039
rh.paracentral: p = 0.048		rh.postcentral: p = 0.024	lh.lingual: p = 0.043
rh.postcentral: p = 0.005		rh.transversetemporal: p = 0.019	lh.parahippocampal: p = 0.013
rh.posteriorcingulate: p = 0.025		rh.amygdala: p = 0.017	lh.parsopercularis: p = 0.028
		rh.hippocampus: p = 0.048	lh.precentral: p = 0.039
			lh.rostralanteriorcingulate: p = 0.002
			lh.superiorfrontal: p = 0.009
			rh.caudalmiddlefrontal: p = 0.006
			rh.parsopercularis: p = 0.020
			rh.rostralanteriorcingulate: p = 0.035
			rh.rostralmiddlefrontal: p = 0.026
			rh.superiorfrontal: p = 0.032

Table 3.7.: Abbreviation of ROI names

Abbreviated name	Full name
BSTS	banks of the superior temporal sulcus
CAC	caudal anterior cingulate
CMF	caudal middle frontal
CUN	cuneus
ENT	entorhinal
FUS	fusiform
IP	inferior parietal
IT	inferior temporal
ISTC	isthmus of the cingulate
LOCC	lateral occipital
LOF	lateral orbitofrontal
LING	lingual
MOF	medial orbitofrontal
MT	middle temporal
PARH	parahippocampal
PARC	paracentral
POPE	pars opercularis
PORB	pars orbitalis
PTRI	pars triangularis
PCAL	peri-calcarine
PSTC	postcentral
PC	posterior cingulate
PREC	precentral
PCUN -	precuneus
RAC	rostral anterior cingulate
RMF	rostral middle frontal
SF	superior frontal
SP	superior parietal
ST	superior temporal
SMAR	supra-marginal
FP	frontal pole
TP	temporal pole
TT	transverse temporal
INS	insula
THAL	thalamus
CAUD	caudate
PUTA	putamen
PAL	pallidum
AMYG	amygdala
HIPP	hippocampus
ACC	accumbens

Part IV.

Two-stage connectome maturation

4. Two-stage connectome maturation: Establishment and refinement of functional modules

In this chapter, I will propose a hypothesis encompassing both microscopic and macroscopic features of brain network development. First, I introduce that during development quantities of neurons, synapses and axons first increases followed by a selective reduction of features later on to mature towards its final stage. This selective removal is also found in macroscopic scale brain networks estimated from neuroimaging technique such as fMRI and DTI. I connect these two different 'pruning' processes and propose that there are two stages of this process. In addition, I claim that this two-stage connectome maturation may explain certain features of neurodevelopmental disorders such as Autistic Spectrum Disorder (ASD), schizophrenia or epilepsy.

4.1. Introduction

While the removal of neurons and connections during developmental pruning is well studied at the local cellular level, recent results also indicate the reduction of global connectivity between brain regions. These results on the human developing connectome are based on observing brain connectivity over the life span ranging from *in utero* recordings and newborns to children and adults (Lim *et al.*, 2013; Betzel *et al.*, 2014; Bassett *et al.*, 2008; Fair *et al.*, 2009; Gong

et al., 2009; Supekar *et al.*, 2009; Hagmann *et al.*, 2010; Tymofiyeva *et al.*, 2013; Fan *et al.*, 2011; Yap *et al.*, 2011a; van den Heuvel *et al.*, 2014). In part IV, I propose that there are two stages of human connectome maturation: first, an early stage from birth during childhood where highly inter-connected sets of brain areas, or modules are formed by mainly removing connections, or which are often long-distance, between modules and, second, a later stage starting in the teenager years where the connectome is further refined by removing connections, mostly short-distance, within modules. First, I discuss the role of 'pruning' from a network perspective. Selective elimination of connections helps the nervous system to re-organize its network from a transient and redundant structure to an efficient and economic network. Eliminating over- or ill-produced connections, structural and functional modules arise during early development that allow specialization, e.g., processing vision or sound. In later development, functions and connections are refined; for example, enabling better cognitive control and self-regulation for the adult brain. Second, we discuss the two stages of connectome maturation in terms of short- versus long-distance connections. Early establishment of the brain network forms structural and functional modules by removing long-distance connections while during a second stage connection within modules are refined. In part III, structural connectivity changes in late childhood through adulthood (Lim *et al.*, 2013) showed that connections between modules, most of which are long-distance and many of which run between hemispheres, remain largely unchanged preserving the modular organization that arises early on. On the other hand, short-distance connections, that are mostly within modules and hemispheres, get refined during this stage. Therefore, successful removal or preservation of connections at the right stage is crucial for healthy development. Finally, I argue that alterations during each stage might lead to different

cognitive deficits. Over- or under-pruning during the first and/or the second stage would lead to fewer or more short- and/or long-distance connections, resulting in pronounced changes in modular organization. Given the two stages, any pathological changes to long-distance connectivity would predominantly occur during the first stage. Indeed, a poorly developed corpus callosum has been associated with childhood-onset schizophrenia and epilepsy while autism spectrum disorders, that arise early, have decreased long-range connectivity. Loss of refinement in the second stage, on the other hand, may hinder memory and skill formation. It may also cause adult-onset epilepsy due to excessive excitatory synapses leading to an imbalance between excitation and inhibition. At the same stage, failure to maintain long-distance connections may lead to adult-onset schizophrenia.

4.2. Less is more?

Initial exuberance of production followed by selective elimination is one of the major developmental characteristics in the vertebrate nervous system (Cowan *et al.*, 1984; Huttenlocher, 1979; Innocenti & Price, 2005). Neuronal density is highest around birth about double that of an adult brain (Cowan *et al.*, 1984); Synaptic density is at its highest around 1-2 year old and decreases throughout maturation (Huttenlocher, 1979; Huttenlocher, 1990; LaMantia & Rakic, 1990; LaMantia & Rakic, 1994; Luo & O'Leary, 2005); grey matter volume and thickness peaks around 10 years old and decreases through adulthood and the reduction of cortical thickness and volume over age has been positively correlated with better cognitive performance (Giedd *et al.*, 1999b; Gogtay *et al.*, 2004). Gyrification of cortex peaks around five and six postnatal months and

gradually decreases throughout adulthood (Armstrong *et al.*, 1995; Klein *et al.*, 2014a; Raznahan *et al.*, 2011; Su *et al.*, 2013). These phenomena cannot be explained independently and in particular, pruning of synapse, dendrites and axons is suspected to be the major underlying driving force for developmental anatomical changes in the brain (Gogtay *et al.*, 2004; Sowell, 2004; White *et al.*, 2010).

4.3. Pruning and protracted remodelling throughout development

Selective elimination of connections, or pruning helps the nervous system to re-organize its network from a transient and redundant structure to an efficient and economic network, which provides neural plasticity for learning and memory and for repairing damaged circuits (Low & Cheng, 2006; Luo & O'Leary, 2005) (4.1). Computational models have also demonstrated that brain networks become more efficient by selectively eliminating synapses (Chechik *et al.*, 1998; Chechik *et al.*, 1999). Previously, it was believed that this pruning process only continues until puberty (Huttenlocher, 1979). Recent findings, however, demonstrated that synaptic pruning prolongs into third decade of a lifetime especially in prefrontal areas (Petanjek *et al.*, 2011).

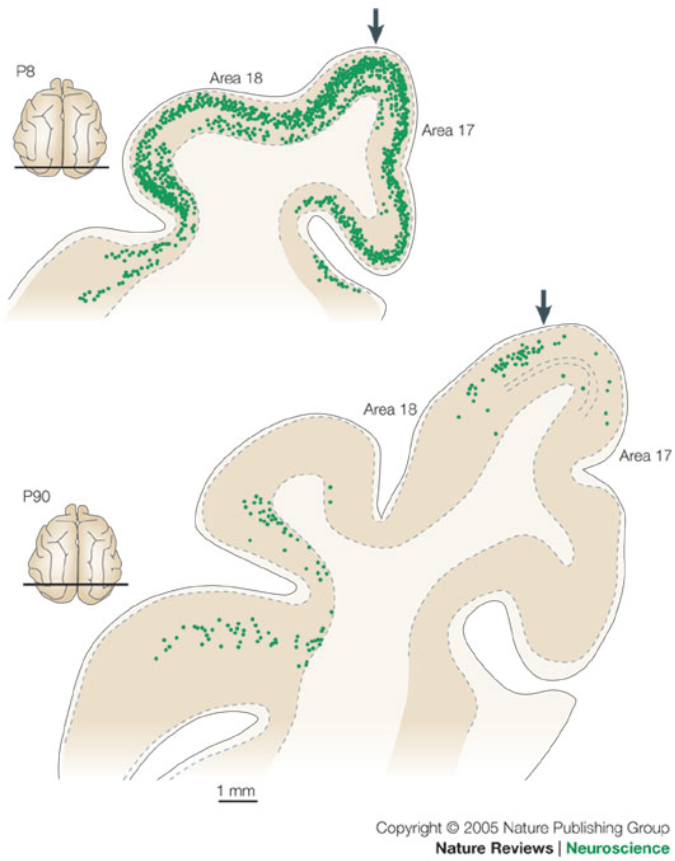

Figure 4.1.: By day 90 the origin of the projection has become focused by two regions, whereas the first postnatal week the whole of area 17 and other visual areas were involved, Reprinted by permission from Macmillan Publishers Ltd: Nature Reviews Neuroscience (Innocenti & Price, 2005), copyright (2005).

4.4. Abnormal pruning and imbalance between excitation and inhibition

Pruning in various levels from dendritic spines to long-range axon fibres is generally considered as part of normal development and time course of this process varies depending on brain areas (Huttenlocher & Dabholkar, 1997; Innocenti & Price, 2005; LaMantia & Rakic, 1990). Various neurodevelopmental and neurodegenerative disorders have been related to abnormal pruning of neural tissues, synapses (4.2). Here we mainly focus on selective elimination process during maturation. The hyper-pruning hypothesis regarding schizophrenia has been held for a long time (Boksa, 2012; Keshavan *et al.*, 1994). Failure to prune away weak synapses has been shown to impede the construction of synaptic multiplicity, which results in weakening of long-range functional connectivity correlated with autism-associated behaviour in knockout mice (Paolicelli *et al.*, 2011; Zhan *et al.*, 2014). Failure of pruning excitatory synapses during postnatal development causes hyper-excitability (Bozzi *et al.*, 2012; Caleo, 2009; Chu *et al.*, 2010; Galvan *et al.*, 2000; Zhou *et al.*, 2009) resulting from the imbalance between excitatory and inhibitory synapses in autism (Rubenstein & Merzenich, 2003), social dysfunction (Yizhar *et al.*, 2011) and epilepsy (Stief *et al.*, 2007).

4.5. Macroscopic scale of pruning

Interestingly, large-scale brain connectivity studies have also observed 'macroscopic pruning', which can be viewed as indirect evidence of pruning of synapses, axons or dendrites influencing large-scale brain connectivity. Previous studies using graph-theoretical measures found that there seems to be over-connectivity

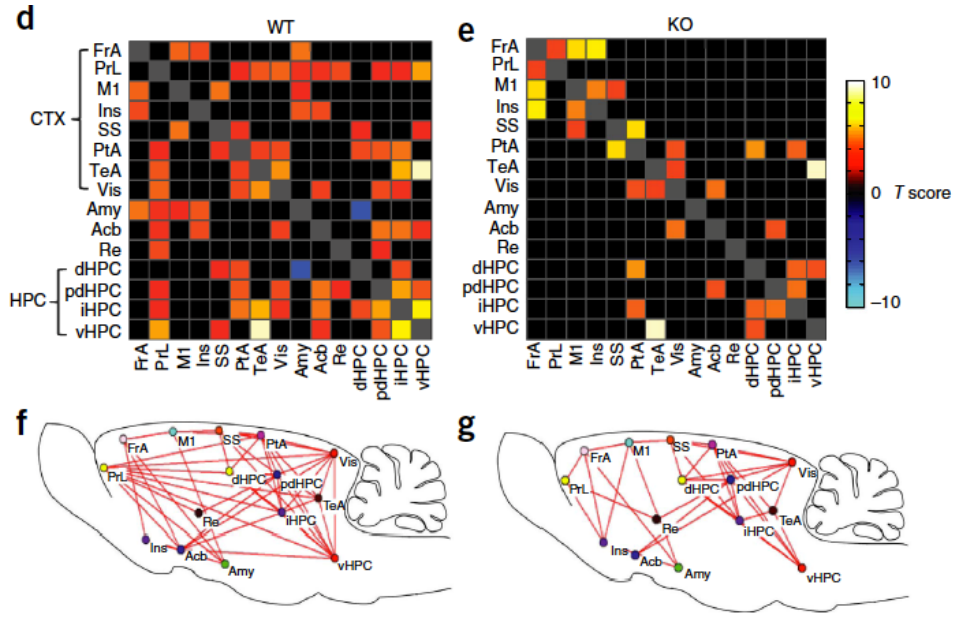

Figure 4.2.: Abnormal pruning and failure of developing long-range functional connectivity; Adapted by permission from Macmillan Publishers Ltd: Nature neuroscience ((Caleo, 2009)), copyright (2014)

in the early developmental stage and 'pruning' of connectivity follows during development (Lim *et al.*, 2013; Menon, 2013; Supekar *et al.*, 2009); brain undergoes selective remodelling by weakening or eliminating short-range connectivity while strengthening and maintaining long-range connections leading to a more efficient and integrated network (Fair *et al.*, 2009; Hagmann *et al.*, 2010; Huang *et al.*, 2013; Supekar *et al.*, 2009). In particular, this selective refinement of a brain network appears to focus on specific type of fibre tracts such as short, intra-module and interhemispheric fibre tracts similar to selective synaptic pruning, which allows brain network to maintain it core topological properties such as small-worldness and modular organization (Lim *et al.*, 2013). Neonates also have small-world topology with a hierarchical and modular structure if not perfect yet (Fan *et al.*, 2011; Yap *et al.*, 2011a). Interestingly, the changes before or around birth seem to be the opposite of those observed from childhood

to adulthood (Smyser *et al.*, 2010; Tymofiyeva *et al.*, 2013; van den Heuvel *et al.*, 2014). Baby connectome studies showed that modularity and clustering coefficient increase from preterm to term babies (Tymofiyeva *et al.*, 2013; van den Heuvel *et al.*, 2014), whereas modularity and clustering coefficient decrease during adolescence and adulthood leading to a more distributed and integrated network (Fair *et al.*, 2009; Hagmann *et al.*, 2010), which may result from eliminating diffusive and less accurate connections. Increased connectivity in congenital blind people can be related to deficient synaptic pruning resulting from absence of visual experiences (Wang *et al.*, 2014). Another example of long-distance connection elimination in early development is that children show stronger inter-hemisperic co-activation between homotopic areas than adults do indicating homotopic long-range connections between hemispheres become weaker during maturation.

4.6. Abnormal macroscopic pruning

Neurodevelopmental diseases and brain connectivity

Analogous to abnormal synaptic pruning, brain connectome studies both in structural and functional connectivity reported aberrant connectivity possibly caused from imperfect maturation of a brain network in neurodevelopmental diseases such as schizophrenia, autistic spectrum and epilepsy (Belmonte, 2004; Boksa, 2012; Keshavan *et al.*, 1994; Paolicelli *et al.*, 2011; Zhou *et al.*, 2009). Schizophrenia has been thought of as a neurodevelopmental disease caused by disconnectivity (Boksa, 2012) especially in the frontal and temporal lobes (Pettersson-Yeo *et al.*, 2011); connectome studies have found both increased and decreased connectivity in schizophrenic patients (Fornito *et al.*, 2012),

however; decreased connectivity has been reported consistently across all stages of schizophrenia and in various modalities (Pettersson-Yeo *et al.*, 2011); child-onset schizophrenia patients showed less short-range functional connections than healthy controls (Alexander-Bloch *et al.*, 2012) leading to decreased modularity and clustering coefficients in patients (Alexander-Bloch *et al.*, 2010) whereas late-onset patients displayed lack of long-distance connections (Bollobás, 1998). People with autistic spectrum disorder (ASD) showed decreased long-distance connectivity between frontal and posterior and increased connectivity in short-distance connectivity (Anagnostou & Taylor, 2011; Belmonte, 2004; Williams & Minshew, 2007) and also agenesis of corpus callosum (Lau et al., 2013, Paul, 2011). ASD and schizophrenic patients have shown to have a decreased functional interhemispheric connectivity (Barttfeld *et al.*, 2011; Guo *et al.*, 2014; Hoptman *et al.*, 2012), indicating there might have been hyper-pruning of commissural connections. Epilepsy is also associated with deceased long-distance connectivity and increased short-distance connectivity (Bernhardt *et al.*, 2011; Bonilha *et al.*, 2012; DeSalvo *et al.*, 2013), although not as consistent as previous two disorders and also idiopathic epileptic patients suffer from under-developed white matter (Hermann *et al.*, 2006; Hutchinson *et al.*, 2010) impeding long-range connectivity development.

4.7. Two-stage Connectome Maturation

Here we propose a two-stage hypothesis for macroscopic refinement of connectivity during development (Figure 4.3 1). First stage of 'pruning' from around 1-2 years after exuberance of new formation of synapses eliminates mainly long-range connections that are also very likely to be inter-module connections,

which accentuate modular structure from a more random-like network, which can be related to massive long-range axon elimination during early development resulting from genetic pre-programmed cues and also external sensory input (LaMantia & Rakic, 1990; O'Leary, 1992; O'Leary & Koester, 1993). After establishing the modular structure by eliminating over-abundant transient long connections, the brain network focuses on delineating a detailed configuration by removing unnecessary short-range connections within modules over a prolonged period from childhood to young adulthood and maintaining/strengthening long-distance connections (Fair *et al.*, 2009; Hagmann *et al.*, 2010; Lim *et al.*, 2013; Supekar *et al.*, 2009). This refinement can be influenced by experiences and education and also by genetic propensity, which results in better performance in complex cognitive tasks with a more efficient brain network.

Here, we discuss mainly about macroscopic refinement during development; however, it cannot be thought of as a stand-alone analogous process independent of synaptic pruning, rather this macroscopic pruning is attributable to synaptic pruning. The two stages both involve synaptic pruning and strengthening of axons by increased myelination, however the first stage may be dominated by synaptic pruning of long connections and the second stage may be mainly dependent on strengthening and maintaining of long-range connections and calibrating local (short) connections. During development, new synapses and axons can be also established by learning and memory. The net process, however, is governed by refinement of connectivity by reducing connections. This two-stage hypothesis can be thought as an analogous process of the retaining small-scale axon elimination ability after critical period of long-range axon pruning in retinal ganglion cells' axons to the dorsal lateral geniculate nucleus (Muir-Robinson *et al.*, 2002; Ruthazer *et al.*, 2003). Aberrant developmental trajectories of schizophrenia, ASD and epilepsy can be explained in terms of

short and long-distance connectivity during two-stage maturation (Figure 4.4 2). Although it may seem to over-simplify them as each disorder involves various etiologies, similar features of the trajectories can explain phenotypical similarities of the disorders. ASD and schizophrenia affect overlapping areas of the brain, so some researchers argue that child-onset schizophrenia may be a subtype of ASD. Moreover, ASD and epilepsy have comorbidity around 30% (Canitano, 2007; Mannion & Leader, 2014). For example, over-connectivity both in short and long-range connections in ASD and epilepsy in the second stage of maturation can be associated with ASD children who also become epileptic later on.

4.8. Conclusion

Analogous to synaptic remodelling during development, we can also consider connectivity pruning at the global level, which is not random but rather selective, focusing specific type of fibre tracts. Furthermore, we can divide this systematic refinement of a brain network into two stages: first stage mainly focuses on long-range connection removal and the second stage refines local networks by removing/weakening short-distance connections while maintaining/strengthening long-distance connections. Using two-stage connectome hypothesis, we summarise aberrant structural connectivity development in three neurodevelopmental disorders: schizophrenia, ASD and epilepsy. We suggest that considering two stages of connectome maturation elucidate connectome development both in healthy and unhealthy brain networks. Together, I provide a new framework for the cognitive development in health and disease linked to changes in connectome organization. This is timely as connectome

data related to development is only recently becoming available through the Developing Connectome project, twin studies within the Human Connectome Project, and ongoing longitudinal studies. This framework is unique and novel in linking local pruning with network re-organization, explaining how spatial and topological features change over time, and establishing two stages of connectome maturation. It also proposes a link between the developmental stage at which alternations occur, the changes in connectome organization at that stage, and the cognitive deficits that result.

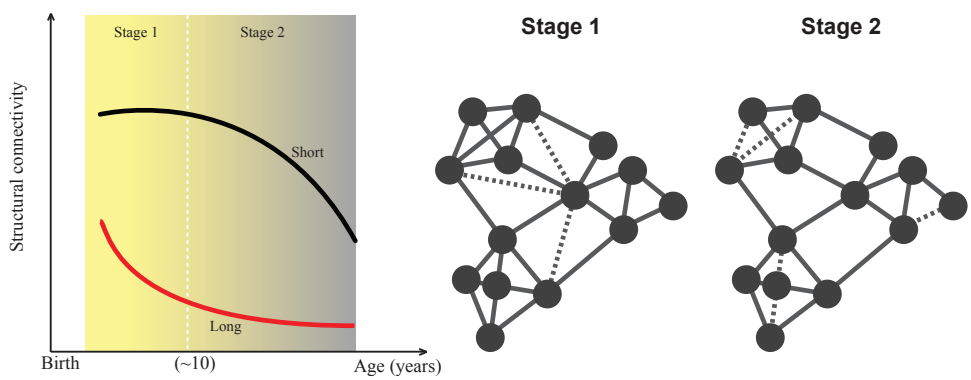

Figure 4.3.: Two-stage connectome maturation. Note that changes in stage 1 are dominated by long-distance (or inter-modular) connectivity and changes in stage 2 occur mainly for short-distance connectivity. black solid line: short-distance (intra-modular) connectivity;red solid line: long-distance connectivity; white dashed vertical line: approximate boundary between stage 1 and stage 2 around 10 years, although it may change depending on gender and brain area differences; x-axis: age (years), y-axis: structural connectivity. Black circles: Brain areas or neurons (nodes), solid lines: connections between nodes, dashed lines: connections that would be pruned away.

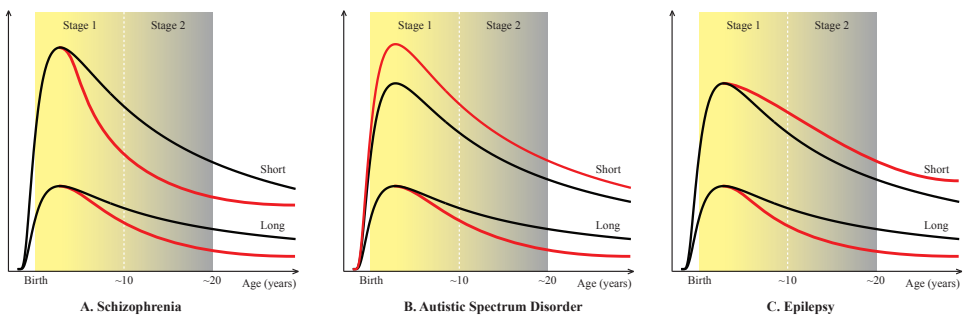

Figure 4.4.: A. Schizophrenia;B. Autistic Spectrum Disorder;C. Epilepsy. black solid line: Healthy connectome maturation;red solid line: hypothetical pathological connectome maturation; white dashed vertical line: approximate boundary between stage 1 and stage 2 around 10 years, although it may change depending on gender and brain area differences; x-axis: age (years), y-axis: structural connectivity.

Part V.

General discussion and outlook

5. Discussion and outlook

In this chapter, I will summarise main findings of the thesis and I will discuss advantages and limitations of the methods that I used as well as introducing alternatives. Finally, I will discuss the implication of my studies and outlook.

5.1. Summary and context

In this work, I investigated how structural connectivity of the human brain develops in both microscopic and macroscopic scales and based on the findings I suggest an hypothesis providing testable predictions for future studies as well as new insights for neurodevelopmental disorders.

In part II for the microscopic neuronal network development, I explored how neuronal network develops in particular with the constraints on developmental time windows of axon growth. I demonstrated that different time windows for axon growth could lead to distinct topological and spatial characteristics, which was validated using *C. elegans* connectivity data. Previous studies have focused on guidance cues (Sperry, 1963; Yamamoto *et al.*, 2002; Yu *et al.*, 2012; Franze, 2013; Scheiffele *et al.*, 2000; Dickson, 2002) to explain the mechanism of synaptogenesis. Although crucial (van Ooyen, 2011; Dickson, 2002; Gotz *et al.*, 1992; Butz *et al.*, 2014; Butz & van Ooyen, 2013; Van Ooyen *et al.*, 1995; Butz *et al.*, 2009), they cannot fully explain certain features of synaptic connectivity in particular for short-range connectivity during early development (Kaufman *et al.*, 2006; Baruch *et al.*, 2008; Verhage *et al.*, 2000; Packer *et al.*,

2013; Packer & Yuste, 2011; Price *et al.*, 2011; Kaiser *et al.*, 2009). Peters' rule (Braitenberg & Schüz, 1998) suggests that synapse formation in brain circuitry mainly depends on the overlap of geometrical locations of specific axons and dendrites in the absence of guidance cues (Binzegger *et al.*, 2004; van Pelt & van Ooyen, 2013; McAssey *et al.*, 2014; van Ooyen *et al.*, 2014; Hill *et al.*, 2012; Packer & Yuste, 2011). Time windows of development for connections between brain regions influence the topology of cortical connectivity (Kaiser *et al.*, 2007; Nisbach & Kaiser, 2007; Varier & Kaiser, 2011; Yu *et al.*, 2009; Yu *et al.*, 2012; Deguchi *et al.*, 2011; Druckmann *et al.*, 2014). Computational models (van Ooyen, 2003; van Ooyen, 2011) have been developed (Kaiser *et al.*, 2009; Willshaw & von der Malsburg, 1976; Perin *et al.*, 2013; Koene *et al.*, 2009; Godfrey *et al.*, 2009; Hennig *et al.*, 2009; Zubler & Douglas, 2009). In previous models; however, how different time windows of axon growth would affect the characteristics of the brain network organization was not systematically studied. Whereas previous studies dealt with time windows that operate on the population level, my study observes the effect of the timing of axon growth for individual neurons within a neural population. In summary, the findings show that the relative timing of connection formation within sub-graphs can already shape topological and spatial network properties. With timing for axon growth and synapse formation, this study introduces a mechanism that for early network formation before later refinement through activity-dependent factors. Together, this indicates that time windows for axon growth influence the topological and spatial properties of neuronal networks opening the possibility to a posteriori estimate of developmental mechanisms based on network properties of a developed network.

In part III for the macroscopic level of the whole brain network development, I investigated changes in whole brain connectivity with age. In this study, I

investigated changes in structural connectivity between ages of 4 to 40 years from DTI data in cortical and subcortical regions. Previous studies had shown that the human brain undergoes vast structural changes involving alterations in the topology of structural and functional connectivity, while core properties such as small-world topology and modular organisation were retained throughout development (Fair *et al.*, 2009; Gong *et al.*, 2009; Supekar *et al.*, 2009; Hagmann *et al.*, 2010; Dennis *et al.*, 2013). I demonstrated that the stability of the brain network may be realised by preferential detachment, that is, specific types of fibre tracts were preferentially affected. This approach differs from previous work in that, first, I investigated which type of fibre tracts showed changes during development as well as the resulting impact on network topology. Second, regions of interest (ROIs) included subcortical areas unlike previous studies of brain network development. Finally I provided evidence to explain sex differences during maturation, which is consistent with previous studies from a network perspective. In summary, we find that long-distance and inter-modular connectivity is largely spared from the ongoing streamline losses during development, which is potentially beneficial for the observed stability of small-world and modular connectome features. Retaining long-distance and inter-modular fibres indicate that small-world features, such as the number of processing steps but also the balance between information integration and large-scale brain activity, are kept within a critical range during development (Kaiser & Hilgetag, 2006). Preserving this balance is crucial as changes in long-distance connectivity are a hallmark of neurodegenerative and neurodevelopmental disorders ranging from Alzheimer's disease (Ponten *et al.*, 2007; Stam *et al.*, 2007) to schizophrenia (Alexander-Bloch *et al.*, 2012). Therefore, stable topological network features might help to prevent cognitive deficits in pathological brains.

Finally in part IV I discuss macroscopic refinement during development, proposing two-stage connectome maturation hypothesis. The two stages both involve synaptic pruning and strengthening of axons by increased myelination;the first stage may be dominated by synaptic pruning of long connections and the second stage may be mainly dependent on strengthening and maintaining of long-range connections and calibrating local (short) connections. I explained that aberrant developmental trajectories of neurodevelopmental disorders can be explained in terms of short and long-distance connectivity during two-stage maturation, suggesting similar features of the trajectories can explain phenotypical similarities of the disorders.

In the following sections, I will discuss the methodological issues of my studies and provide alternatives and their advantages and disadvantages.

5.2. Methodological consideration

5.2.1. Constructing networks from DWI

5.2.1.1. Definition of nodes and edges

Depending which parcellation schemes or atlases (Evans *et al.*, 2012) one chooses to use to define *nodes* and *edges*, the sizes of the networks change. This inevitably influences the graph measures (Section 1.1.1) that we calculate; they are dependent on the number of nodes and the average of degree of the network (Van Wijk *et al.*, 2010; Zalesky *et al.*, 2010). Therefore, when we compare networks using graph measures, we need to check whether the differences between networks are from different sizes of networks, in other

words, we need to correct the results considering the dependencies. Some studies examine graph measures as a function of threshold (Gong *et al.*, 2009; Achard & Bullmore, 2007) and others including this thesis (Kim *et al.*, 2014; Lim *et al.*, 2013) use surrogate rewired networks with the same number of nodes and degree distribution/strength distribution (Maslov & Sneppen, 2002; Rubinov & Sporns, 2011) or cost integration (Ginestet *et al.*, 2011). Future studies have yet to devise a better approach as each method has advantages and disadvantages.

5.2.1.2. Definition of weights

A weighted network can provide much richer information about the network that we investigate compared to binary networks because the same binary networks can be very different when the weights of the networks are different. While using a weighted network can provide us with more information, dealing with them is not an easy job. First of all, we need to decide how to define the weight of an edge. In part III, the streamline count was used to represent the connection strength between two nodes. However, the way we obtain streamline counts is confounded by individual brain volume differences, which was discussed in Section 3.4. Depending on the tractography methods, we may get streamline counts or probabilities and each method may be better suited to a certain normalization regarding brain volume or surface. These individual differences can be also accounted in the subsequent statistical models e.g., including covariates. Sometimes normalization based on brain volume or surface (Honey *et al.*, 2009a) may remove actual differences between patients and healthy controls, for instance, grey matter atrophy is one of the common phenomenon in neurological disorders and if we eliminate the volume differences

we may also remove the real difference between groups. Another example can be found in a recent study (Taylor *et al.*, 2015); the study showed that reduced surface areas of epileptic patients contributed more to the differences between groups. In which case, if we normalise the number of fibre tracts by the surface area, we might lose an important feature of the patient group. For probabilistic tractography, the connection probability from region A to B is not necessarily be the same as the connection probability from region B to A, the adjacency matrix is asymmetrical. The asymmetry of the graph, in other words, a directed graph has more information than an undirected graph; however, many studies use the average of the two probabilities (from A to B and from B to A) (Gong *et al.*, 2009) as DTI itself cannot provide directional information of fibre tracts. Since many studies use their own definitions of weights and weight normalization method, it is quite difficult to directly compare studies. For more discussion see (Sporns, 2014b; Fornito *et al.*, 2012).

5.2.2. Diffusion MRI: DTI and beyond

We would like to estimate the fibre orientation in the WM through DTI to investigate brain connectivity; however, DWI can be achieved in mm scale, while diameters of axons are in μm scale. Fitting a single tensor in each voxel further exacerbates this issue because using a single tensor can only represent one principal direction of fibres when in fact there can be multiple major fibre orientations. The following short discussion covers this issue and alternatives.

5.2.2.1. Other methods for fibre orientation estimation

More than 90% of WM voxels have multiple fibre orientation (Jeurissen *et al.*, 2010; Tournier *et al.*, 2011). The diffusion tensor model, however, cannot correctly resolve multiple fibre orientation issues in a single voxel. Therefore, there are other approaches such as multi-tensor model, Diffusion Spectrum Imaging and Q-Ball Imaging estimating diffusion orientation distribution function (dODF) and spherical deconvolution models estimating fibre orientation distribution (fODF). fODF is a probability distribution on the sphere, representing the proportion of fibres in the direction (each point on the sphere). However, fODF cannot be measured directly from our measurements since they are based on the diffusion of water molecules. dODF describes the probability distribution of diffusion of water molecules in each voxel.After we estimate the fibre orientations via tensor-based models, dODF or fODF, we 'connect' the local information into fibre tracts using tractography (1.2.2). As deterministic tractography approaches cannot provide *confidence* of the resulted pathways from the tractography, *probabilistic* tractography can be an alternative (Behrens *et al.*, 2003). For probabilistic tractography, the uncertainty of the fibre orientation, or orientation distribution function (ODF) needs to be estimated. uODF estimates the uncertainty of the fibre orientations from dMRI; the uncertainty representing our confidence that the true parameter lies within any particular area on the surface of the sphere, whereas fODF and dODF are more directly related to physical properties of the system. So far the tractography methods use *local* diffusivity information to find the path from a region to another region. We can ask another question to find the pathway: what is the path of least hindrance to diffusion that connects two regions? The maximum diffusivity of the path between two regions does not need to coincide with the local maximum

diffusivity, which means now the problem is global. This *global tractography* is robust against local effects (errors) from noise or modelling errors, for review (Mangin *et al.*, 2013).

5.2.2.2. Optimal parameter values and models

Another important topic is optimal parameters for DWI acquisition in particular b-value (Eq.(1.8), Eq.(1.9)) and subsequent models (or model-free methods). Higher b-value provides better angular contrast of DWI images (Descoteaux *et al.*, 2009; Jones *et al.*, 2013), thus beneficial for tractography; however, it reduces signal-to-noise ratio. Therefore, using multiple b-values (high b -values for better contrasts and low b -values for good signal-to-noise ratios) are used to resolve the issue. Unfortunately, mono-exponential decay assumption (see Section 1.2) breaks down when b -values higher than 1500 s/mm^2 (Clark & Le Bihan, 2000; Mulkern *et al.*, 1999; Beaulieu & Allen, 1994). This non-monoexponential diffusion decay poses an overfitting problem in the fibre orientation distribution and consequently would give false positive fibre tracts for tractography (Jbabdi *et al.*, 2012). Jbabdi and colleagues proposed a model using continuous gamma distribution diffusivities (Jbabdi *et al.*, 2012). For summary of models accounting for non-monoexponential diffusion decay, see (Jbabdi *et al.*, 2012; Mulkern *et al.*, 2009). Optimal b -value also changes depending on the methods for estimating fibre orientation distributions. For instance, So far most studies have used a b -value of 1000 s/mm^2, but more studies use multiple b-values to benefit both angular contrasts and SNR, we need to consider other models for future analysis (see also http://fsl.fmrib.ox.ac.uk/fsl/fslwiki/EDDY). For more information regarding other parameters such as the number of gradient directions and spatial resolution for DWI acquisition

can be well summarised here (Jones *et al.*, 2013).

In summary, investigating brain connectivity using DWI is quite promising to investigate WM structure noninvasively as long as we keep its limitations in mind and do not over-interpret the results than the methods can provide (Jones *et al.*, 2013; Thomas *et al.*, 2014).

5.3. Future outlook

In this section, I will briefly discuss future outlook of my studies.

- From Part II, future computational models for neuronal network development can benefit by incorporating developmental time window information as they play an important role to configure brain connectivity, although biological correlates or counterparts may be difficult to obtain for now. Developmental time windows may have hierarchical structure of different structures, for instance, the developmental time window of axon growth for a neuron as in my study may be influenced by its kind and its location of the brain. Future studies may investigate the structure of developmental time windows in more detail.

- From Part III and IV, one can continue to find an underlying mechanism to explain the preferential detachment of fibre tracts to find organising and re-organising principles (not necessarily the same) for a healthy mature connectome; is there a global objective function that our brain needs to optimize? Or is there only local adaptation to endogenous/exogenous factors? If somehow usual brain development encounters obstructions due to malnutrition, head injuries, or stressful environment, would brain

development principles help overcome some unexpected changes or would they exacerbate the problems? Would recovery be governed by global optimizations or local adaptation rules? Global principles and local rules may act on brain development together; however, depending on the weights of each forces, we may need to use different methods to intervene brain disorders.

- Investigating structural connectivity alone cannot address the organising and reorganising principles during brain development because structure and function influence each other, thus develop interactively. Previous studies developed models to infer structural connectivity from functional connectivity (Greicius *et al.*, 2009) and vice versa (Honey *et al.*, 2009b). However, the relationship between structural and functional connectivity is more complex than it seems (Uddin, 2013). Therefore, rather than simply predicting one from the other at a certain time point, one needs to have some starting testable hypotheses/principles regarding the interaction between structure and function. I believe that part III and IV can provide a good starting ground to achieve our goal.

- Finally, by unravelling principles of the brain connectivity development, we may be able to find possible causes to neurodevelopmental diseases and eventually be able to find optimal solutions to them.

Abbreviations

AAL	Automated Anatomical Labeling
ACC	Anterior Cingulate Cortex
AD	Axial Diffusivity
ADC	Apparent Diffusion Coefficient
AIC	Akaike Information Criterion
ASD	Autistic Spectrum Disorder
BA	Brodmann Area
BIC	Bayesian Information Criterion
dODF	Diffusion Orientation Distribution Function
DTI	Diffusion Tensor Imaging
DWI	Diffusion Weighted Imaging
EPI	Echo Planar Image
ERP	Event-Related Potential
F	Frontal Lobe
FA	Fractional Anisotropy
FACT	Fibre Assignment by Continuous Tracking
FDR	False Discovery Rate
fODF	Fibre Orientation Distribution Function
FoV	Field of View
GLM	General Linear Model
GM	Gray Matter
GMV	Gray Matter Volume
ICV	IntraCranial Volume
lh	Left hemisphere
MD	Mean Diffusivity
MNI	Montreal Neurological Institute
MR	Magnetic Resonance
MRI	Magnetic Resonance Imaging
NKI	Nathan Kline Institute
NMI	Normalized Mutual Information
O	Occipital Lobe
ODF	Orientation Distribution Function
P	Parietal Lobe
PC	Participation Coefficient
RD	Radial Diffusivity
rh	Right hemisphere
ROI	Region Of Interest
rs-fMRI	Resting-State Functional MRI
SC	Structural Connectivity
SNR	Signal-to-Noise Ratio
T	Temporal Lobe
TE	Echo Time
TR	Repetition Time
uODF	Uncertainty Orientation Distribution Function
WM	White Matter
WMS	Within-Module Strength
WMV	White Matter Volume

References

Achard, Sophie, & Bullmore, Ed. 2007. Efficiency and cost of economical brain functional networks. *PLoS computational biology*, **3**(2), e17.

Alexander, G. E., & Crutcher, M. D. 1990. Preparation for movement: neural representations of intended direction in three motor areas of the monkey. *J Neurophysiol*, **64**(1), 133–50.

Alexander-Bloch, A., Lambiotte, R., Roberts, B., Giedd, J., Gogtay, N., & Bullmore, E. 2012. The discovery of population differences in network community structure: New methods and applications to brain functional networks in schizophrenia. *NeuroImage*, **59**, 3889–3900.

Alexander-Bloch, Aaron F, Gogtay, Nitin, Meunier, David, Birn, Rasmus, Clasen, Liv, Lalonde, Francois, Lenroot, Rhoshel, Giedd, Jay, & Bullmore, Edward T. 2010. Disrupted modularity and local connectivity of brain functional networks in childhood-onset schizophrenia. *Frontiers in systems neuroscience*, **4**.

Alexander-Bloch, Aaron F, Vértes, Petra E, Stidd, Reva, Lalonde, François, Clasen, Liv, Rapoport, Judith, Giedd, Jay, Bullmore, Edward T, & Gogtay, Nitin. 2013. The Anatomical Distance of Functional Connections Predicts Brain Network Topology in Health and Schizophrenia. *Cerebral Cortex*, **23**(1), 127–138.

Alexander-Bloch, Aaron F, Reiss, Philip T, Rapoport, Judith, McAdams,

Harry, Giedd, Jay N, Bullmore, Ed T, & Gogtay, Nitin. 2014. Abnormal cortical growth in schizophrenia targets normative modules of synchronized development. *Biological psychiatry*, **76**(6), 438–446.

Allen, J. S., Damasio, H., Grabowski, T. J., Bruss, J., & Zhang, W. 2003. Sexual dimorphism and asymmetries in the gray-white composition of the human cerebrum. *Neuroimage*, **18**(4), 880–94.

Anagnostou, Evdokia, & Taylor, Margot J. 2011. Review of neuroimaging in autism spectrum disorders: what have we learned and where we go from here. *Mol Autism*, **2**(1), 4–4.

Andersen, Susan L. 2003. Trajectories of brain development: point of vulnerability or window of opportunity? *Neuroscience & Biobehavioral Reviews*, **27**(1-2), 3–18.

Andersson, Jesper L.R. 2014. Chapter 4 - Geometric Distortions in Diffusion MRI. *Pages 63 – 85 of:* Johansen-Berg, Heidi, & Behrens, Timothy E.J. (eds), *Diffusion MRI (Second Edition)*, second edition edn. San Diego: Academic Press.

Andersson, Jesper L.R., & Skare, Stefan. 2002. A Model-Based Method for Retrospective Correction of Geometric Distortions in Diffusion-Weighted EPI. *NeuroImage*, **16**(1), 177 – 199.

Andersson, Jesper L.R., Skare, Stefan, & Ashburner, John. 2003. How to correct susceptibility distortions in spin-echo echo-planar images: application to diffusion tensor imaging. *NeuroImage*, **20**(2), 870 – 888.

Armstrong, Este, Schleicher, Axel, Omran, Heyder, Curtis, Maria, & Zilles,

Karl. 1995. The ontogeny of human gyrification. *Cerebral Cortex*, **5**(1), 56–63.

Ascoli, Giorgio A. 2012. Potential connectomics complements the endeavour of 'no synapse left behind' in the cortex. *The Journal of physiology*, **590**(4), 651–652.

Assaf, Yaniv, & Cohen, Yoram. 2014. Chapter 9 - Inferring Microstructural Information of White Matter from Diffusion MRI. *Pages 185 – 208 of:* Johansen-Berg, Heidi, & Behrens, Timothy E.J. (eds), *Diffusion MRI (Second Edition)*, second edition edn. San Diego: Academic Press.

Baron-Cohen, S., Knickmeyer, R.C., & Belmonte, M.K. 2005. Sex differences in the brain: implications for explaining autism. *Science*, **310**(5749), 819–823.

Barrat, A., Barthelemy, M., Pastor-Satorras, R., & Vespignani, A. 2004. The architecture of complex weighted networks. *Proc Natl Acad Sci U S A*, **101**(11), 3747.

Bartsch, Andreas J., Biller, Armin, & Homola, György A. 2014. Chapter 23 - Presurgical Tractography Applications. *Pages 531 – 567 of:* Johansen-Berg, Heidi, & Behrens, Timothy E.J. (eds), *Diffusion MRI (Second Edition)*, second edition edn. San Diego: Academic Press.

Barttfeld, Pablo, Wicker, Bruno, Cukier, Sebastián, Navarta, Silvana, Lew, Sergio, & Sigman, Mariano. 2011. A big-world network in ASD: Dynamical connectivity analysis reflects a deficit in long-range connections and an excess of short-range connections. *Neuropsychologia*, **49**(2), 254 – 263.

Bartzokis, G., Beckson, M., Lu, P. H., Nuechterlein, K. H., Edwards, N., &

Mintz, J. 2001. Age-related changes in frontal and temporal lobe volumes in men: A magnetic resonance imaging study. *Archives of General Psychiatry*, **58**(5), 461–465.

Baruch, Leehod, Itzkovitz, Shalev, Golan-Mashiach, Michal, Shapiro, Ehud, & Segal, Eran. 2008. Using Expression Profiles of Caenorhabditis elegans Neurons To Identify Genes That Mediate Synaptic Connectivity. *PLoS Computational Biology*, **4**(7), e1000120.

Basser, Peter J, & Jones, Derek K. 2002. Diffusion-tensor MRI: theory, experimental design and data analysis–a technical review. *NMR in Biomedicine*, **15**(7-8), 456–467.

Basser, Peter J., & Özarslan, Evren. 2014. Chapter 1 - Introduction to Diffusion {MR}. *Pages 3 – 9 of:* Johansen-Berg, Heidi, & Behrens, Timothy E.J. (eds), *Diffusion MRI (Second Edition)*, second edition edn. San Diego: Academic Press.

Basser, Peter J, Mattiello, James, & LeBihan, Denis. 1994. MR diffusion tensor spectroscopy and imaging. *Biophysical journal*, **66**(1), 259–267.

Basser, Peter J, Pajevic, Sinisa, Pierpaoli, Carlo, Duda, Jeffrey, & Aldroubi, Akram. 2000. In vivo fiber tractography using DT-MRI data. *Magnetic resonance in medicine*, **44**(4), 625–632.

Bassett, Danielle S, Bullmore, Edward, Verchinski, Beth A, Mattay, Venkata S, Weinberger, Daniel R, & Meyer-Lindenberg, Andreas. 2008. Hierarchical organization of human cortical networks in health and schizophrenia. *The Journal of Neuroscience*, **28**(37), 9239–9248.

Beaulieu, Christian. 2014. Chapter 8 - The Biological Basis of Diffusion Anisotropy. *Pages 155 – 183 of:* Johansen-Berg, Heidi, & Behrens, Timothy E.J. (eds), *Diffusion MRI (Second Edition)*, second edition edn. San Diego: Academic Press.

Beaulieu, Christian, & Allen, Peter S. 1994. Determinants of anisotropic water diffusion in nerves. *Magnetic resonance in medicine*, **31**(4), 394–400.

Behrens, T. E., Berg, H. J., Jbabdi, S., Rushworth, M. F., & Woolrich, M. W. 2007. Probabilistic diffusion tractography with multiple fibre orientations: What can we gain? *Neuroimage*, **34**(1), 144–55.

Behrens, TEJ, Woolrich, MW, Jenkinson, M, Johansen-Berg, H, Nunes, RG, Clare, S, Matthews, PM, Brady, JM, & Smith, SM. 2003. Characterization and propagation of uncertainty in diffusion-weighted MR imaging. *Magnetic resonance in medicine*, **50**(5), 1077–1088.

Behrens, Timothy E.J., & Jbabdi, Saad. 2009. Chapter 15 - MR Diffusion Tractography. *Pages 333 – 351 of:* Behrens, Heidi Johansen-BergTimothy E.J. (ed), *Diffusion MRI*. San Diego: Academic Press.

Belmonte, M. K. 2004. Autism and Abnormal Development of Brain Connectivity. *Journal of Neuroscience*, **24**(42), 9228–9231.

Benes, Fm., Turtle, M., Khan, Y., & Farol, P. 1994. Myelination of a key relay zone in the hippocampal formation occurs in the human brain during childhood, adolescence, and adulthood. *Archives of General Psychiatry*, **51**(6), 477–484.

Bengtsson, H. 2007. *R. matlab-local and remote Matlab connectivity in R.* Tech.

rept. Technical report, Mathematical Statistics, Centre for MAthematical Sciences, Lund University, Sweden.

Benjamini, Y., & Hochberg, Y. 1995. Controlling the false discovery rate: a practical and powerful approach to multiple testing. *Journal of the Royal Statistical Society. Series B (Methodological)*, **57**(1), 289–300.

Benjamini, Yoav, Yekutieli, Daniel, Don, Edwards, Shaffer, Juliet Popper, Tamhane, Ajit C., Westfall, Peter H., & Holland, Burt. 2005. False Discovery Rate: Adjusted Multiple Confidence Intervals for Selected Parameters [with Comments, Rejoinder]. *Journal of the American Statistical Association*, **100**(469), 71–93.

Bernhardt, Boris C, Chen, Zhang, He, Yong, Evans, Alan C, & Bernasconi, Neda. 2011. Graph-theoretical analysis reveals disrupted small-world organization of cortical thickness correlation networks in temporal lobe epilepsy. *Cerebral cortex*, **21**(9), 2147–2157.

Betzel, Richard F, Byrge, Lisa, He, Ye, Goñi, Joaquín, Zuo, Xi-Nian, & Sporns, Olaf. 2014. Changes in structural and functional connectivity among resting-state networks across the human lifespan. *Neuroimage*, **102**, 345–357.

Bianconi, Ginestra. 2014. Multilayer networks: Dangerous liaisons? *Nature Physics*, **10**(10), 712–714.

Binzegger, Tom, Douglas, Rodney J., & Martin, Kevan A. C. 2004. A Quantitative Map of the Circuit of Cat Primary Visual Cortex. *J. Neurosci.*, **24**, 8441–8453.

Bodini, Benedetta, & Ciccarelli, Olga. 2014. Chapter 11 - Diffusion MRI in Neurological Disorders. *Pages 241 – 255 of:* Johansen-Berg, Heidi, & Behrens, Timothy E.J. (eds), *Diffusion MRI (Second Edition)*, second edition edn. San Diego: Academic Press.

Bodini, Benedetta, & Ciccarelliy, Olga. 2013. Diffusion MRI in neurological disorders. *Diffusion MRI: From Quantitative Measurement to In vivo Neuroanatomy*, 241.

Boksa, Patricia. 2012. Abnormal synaptic pruning in schizophrenia: Urban myth or reality? *Journal of psychiatry & neuroscience: JPN*, **37**(2), 75.

Bollobás, Béla. 1998. *Random graphs.* Springer.

Bonilha, L., Nesland, T., Martz, G. U., Joseph, J. E., Spampinato, M. V., Edwards, J. C., & Tabesh, A. 2012. Medial temporal lobe epilepsy is associated with neuronal fibre loss and paradoxical increase in structural connectivity of limbic structures. *J Neurol Neurosurg Psychiatry*, **83**(9), 903–9.

Bozzi, Yuri, Casarosa, Simona, & Caleo, Matteo. 2012. Epilepsy as a neurodevelopmental disorder. *Frontiers in psychiatry*, **3**.

Braitenberg, Valentino, & Schüz, Almut. 1998. *Cortex: statistics and geometry of neuronal connectivity.* Springer Berlin.

Brandes, Ulrik, & Erlebach, Thomas. 2005. *Network Analysis.* Lecture Notes in Computer Science. Heidelberg: Springer.

Bullmore, E., & Sporns, O. 2009. Complex brain networks: graph theoretical

analysis of structural and functional systems. *Nat Rev Neurosci*, **10**(3), 186–98.

Bullmore, Ed, & Sporns, Olaf. 2012. The economy of brain network organization. *Nature Reviews Neuroscience*, **13**(5), 336–349.

Butz, Markus, & van Ooyen, Arjen. 2013. A Simple Rule for Dendritic Spine and Axonal Bouton Formation Can Account for Cortical Reorganization after Focal Retinal Lesions. *PLoS computational biology*, **9**(10), e1003259.

Butz, Markus, Wörgötter, Florentin, & van Ooyen, Arjen. 2009. Activity-dependent structural plasticity. *Brain research reviews*, **60**(2), 287–305.

Butz, Markus, Steenbuck, Ines Derya, & van Ooyen, Arjen. 2014. Homeostatic structural plasticity increases the efficiency of small-world networks. *Frontiers in Synaptic Neuroscience*, **6**.

Caleo, Matteo. 2009. Epilepsy: synapses stuck in childhood. *Nature medicine*, **15**(10), 1126–1127.

Canitano, Roberto. 2007. Epilepsy in autism spectrum disorders. *European child & adolescent psychiatry*, **16**(1), 61–66.

Catani, Marco, & Budisavljević, Sanja. 2014. Chapter 22 - Contribution of Diffusion Tractography to the Anatomy of Language. *Pages 511 – 529 of:* Johansen-Berg, Heidi, & Behrens, Timothy E.J. (eds), *Diffusion MRI (Second Edition)*, second edition edn. San Diego: Academic Press.

Chechik, Gal, Meilijson, Isaac, & Ruppin, Eytan. 1998. Synaptic pruning

in development: A computational account. *Neural computation*, **10**(7), 1759–1777.

Chechik, Gal, Meilijson, Isaac, & Ruppin, Eytan. 1999. Neuronal regulation: A mechanism for synaptic pruning during brain maturation. *Neural Computation*, **11**(8), 2061–2080.

Chen, Beth L, Hall, David H, & Chklovskii, Dmitri B. 2006. Wiring optimization can relate neuronal structure and function. *Proceedings of the National Academy of Sciences of the United States of America*, **103**(12), 4723–4728.

Chklovskii, Dmitri B, & Koulakov, Alexei A. 2004. Maps in the brain: what can we learn from them? *Annu. Rev. Neurosci.*, **27**, 369–392.

Choe, Y, McCormick, BH, & Koh, W. 2004. Network connectivity analysis on the temporally augmented C. elegans web: A pilot study. *In: Soc Neurosci Abstr*, vol. 30.

Chu, Yunxiang, Jin, Xiaoming, Parada, Isabel, Pesic, Alexei, Stevens, Beth, Barres, Ben, & Prince, David A. 2010. Enhanced synaptic connectivity and epilepsy in C1q knockout mice. *Proceedings of the National Academy of Sciences*, **107**(17), 7975–7980.

Clark, Chris A, & Le Bihan, Denis. 2000. Water diffusion compartmentation and anisotropy at high b values in the human brain. *Magnetic Resonance in Medicine*, **44**(6), 852–859.

Cloutman, Lauren Louise, & Lambon Ralph, Matthew A. 2012. Connectivity-based structural and functional parcellation of the human cortex using diffusion imaging and tractography. *Frontiers in Neuroanatomy*, **6**(34).

Costa, Luciano da Fontoura, Rodrigues, F. A., Travieso, G., & Villas Boas, P. R. 2007. Characterization of complex networks: A survey of measurements. *Advances in Physics*, **56**(1), 167–242.

Counsell, Serena J., Ball, Gareth, Pandit, Anand, & Edwards, A. David. 2014. Chapter 13 - Diffusion Imaging in the Developing Brain. *Pages 283 – 300 of:* Johansen-Berg, Heidi, & Behrens, Timothy E.J. (eds), *Diffusion MRI (Second Edition)*, second edition edn. San Diego: Academic Press.

Cowan, W Maxwell, Fawcett, James W, O'Leary, Dennis D, & Stanfield, Brent B. 1984. Regressive events in neurogenesis. *Science*, **225**(4668), 1258–1265.

da Fontoura Costa, Luciano, Kaiser, Marcus, & Hilgetag, Claus C. 2007. Predicting the connectivity of primate cortical networks from topological and spatial node properties. *BMC Syst Biol*, **1**, 16.

Davatzikos, C., & Resnick, S. M. 2002. Degenerative age changes in white matter connectivity visualized in vivo using magnetic resonance imaging. *Cereb Cortex*, **12**(7), 767–71.

de Haan, W., van der Flier, W. M., Koene, T., Smits, L. L., Scheltens, P., & Stam, C. J. 2012. Disrupted modular brain dynamics reflect cognitive dysfunction in Alzheimer's disease. *NeuroImage*, **59**(4), 3085–3093.

de Jong, L. W., van der Hiele, K., Veer, I. M., Houwing, J. J., Westendorp, R. G., Bollen, E. L., de Bruin, P. W., Middelkoop, H. A., van Buchem, M. A., & van der Grond, J. 2008. Strongly reduced volumes of putamen and thalamus in Alzheimer's disease: an MRI study. *Brain*, **131**(Pt 12), 3277–85.

Deco, Gustavo, Ponce-Alvarez, Adrián, Hagmann, Patric, Romani, Gian Luca, Mantini, Dante, & Corbetta, Maurizio. 2014a. How Local Excitation–Inhibition Ratio Impacts the Whole Brain Dynamics. *The Journal of Neuroscience*, **34**(23), 7886–7898.

Deco, Gustavo, McIntosh, Anthony R, Shen, Kelly, Hutchison, R Matthew, Menon, Ravi S, Everling, Stefan, Hagmann, Patric, & Jirsa, Viktor K. 2014b. Identification of optimal structural connectivity using functional connectivity and neural modeling. *The Journal of Neuroscience*, **34**(23), 7910–7916.

Deguchi, Yuichi, Donato, Flavio, Galimberti, Ivan, Cabuy, Erik, & Caroni, Pico. 2011. Temporally matched subpopulations of selectively interconnected principal neurons in the hippocampus. *Nature neuroscience*, **14**(4), 495–504.

DeLacoste-Utamsing, C., & Holloway, R. L. 1982. Sexual dimorphism in the human corpus callosum. *Science*, **216**(4553), 1431–2.

DeLong, M. R., Alexander, G. E., Georgopoulos, A. P., Crutcher, M. D., Mitchell, S. J., & Richardson, R. T. 1984. Role of basal ganglia in limb movements. *Hum Neurobiol*, **2**(4), 235–44.

DeLong Mr, Wichmann T. 2007. Circuits and circuit disorders of the basal ganglia. *Archives of Neurology*, **64**(1), 20–24.

Dennis, E.L., Jahanshad, N., McMahon, K.L., de Zubicaray, G.I., Martin, N.G., Hickie, I.B., Toga, A.W., Wright, M.J., & Thompson, P.M. 2013. Development of Brain Structural Connectivity between Ages 12 and 30: A 4-

Tesla Diffusion Imaging Study in 439 Adolescents and Adults. *NeuroImage*, **64**(0), 671–684.

DeSalvo, Matthew N, Douw, Linda, Tanaka, Naoaki, Reinsberger, Claus, & Stufflebeam, Steven M. 2013. Altered Structural Connectome in Temporal Lobe Epilepsy. *Radiology*, **270**(3), 842–848.

Descoteaux, Maxime, Deriche, Rachid, Knosche, TR, & Anwander, Alfred. 2009. Deterministic and probabilistic tractography based on complex fibre orientation distributions. *Medical Imaging, IEEE Transactions on*, **28**(2), 269–286.

Desikan, R. S., Segonne, F., Fischl, B., Quinn, B. T., Dickerson, B. C., Blacker, D., Buckner, R. L., Dale, A. M., Maguire, R. P., Hyman, B. T., Albert, M. S., & Killiany, R. J. 2006. An automated labeling system for subdividing the human cerebral cortex on MRI scans into gyral based regions of interest. *Neuroimage*, **31**(3), 968–80.

Dickson, BJ. 2002. Molecular Mechanisms of Axon Guidance. *Science*, **298**(5600), 1959 – 1964.

Dosenbach, N.U.F., Nardos, B., Cohen, A.L., Fair, D.A., Power, J.D., Church, J.A., Nelson, S.M., Wig, G.S., Vogel, A.C., & Lessov-Schlaggar, C.N. 2010. Prediction of individual brain maturity using fMRI. *Science*, **329**(5997), 1358–1361.

Druckmann, Shaul, Feng, Linqing, Lee, Bokyoung, Yook, Chaehyun, Zhao, Ting, Magee, Jeffrey C, & Kim, Jinhyun. 2014. Structured Synaptic Connectivity between Hippocampal Regions. *Neuron*.

Duarte-Carvajalino, J. M., Jahanshad, N., Lenglet, C., McMahon, K. L., de Zubicaray, G. I., Martin, N. G., Wright, M. J., Thompson, P. M., & Sapiro, G. 2011. Hierarchical topological network analysis of anatomical human brain connectivity and differences related to sex and kinship. *Neuroimage*.

Easter, S. S., Jr., Purves, D., Rakic, P., & Spitzer, N. C. 1985. The changing view of neural specificity. *Science*, **230**(4725), 507–511.

Edgar, Julia M., & Griffiths, Ian R. 2014. Chapter 7 - White Matter Structure: A Microscopist's View. *Pages 127 – 153 of:* Johansen-Berg, Heidi, & Behrens, Timothy E.J. (eds), *Diffusion MRI (Second Edition)*, second edition edn. San Diego: Academic Press.

Ell, S. W., Marchant, N. L., & Ivry, R. B. 2006. Focal putamen lesions impair learning in rule-based, but not information-integration categorization tasks. *Neuropsychologia*, **44**(10), 1737–51.

Engel, Jerome, Thompson, Paul M, Stern, John M, Staba, Richard J, Bragin, Anatol, & Mody, Istvan. 2013. Connectomics and epilepsy. *Current opinion in neurology*, **26**(2), 186–194.

Essen, David C. Van, Jbabdi, Saad, Sotiropoulos, Stamatios N., Chen, Charles, Dikranian, Krikor, Coalson, Tim, Harwell, John, Behrens, Timothy E.J., & Glasser, Matthew F. 2014. Chapter 16 - Mapping Connections in Humans and Non-Human Primates: Aspirations and Challenges for Diffusion Imaging. *Pages 337 – 358 of:* Johansen-Berg, Heidi, & Behrens, Timothy E.J. (eds), *Diffusion MRI (Second Edition)*, second edition edn. San Diego: Academic Press.

Evans, Alan C, Janke, Andrew L, Collins, D Louis, & Baillet, Sylvain. 2012. Brain templates and atlases. *Neuroimage*, **62**(2), 911–922.

Fair, D. A., Cohen, A. L., Power, J. D., Dosenbach, N. U., Church, J. A., Miezin, F. M., Schlaggar, B. L., & Petersen, S. E. 2009. Functional brain networks develop from a "local to distributed" organization. *PLoS Comput Biol*, **5**(5), e1000381.

Fan, Y., Shi, F., Smith, J.K., Lin, W., Gilmore, J.H., & Shen, D. 2011. Brain anatomical networks in early human brain development. *NeuroImage*, **54**(3), 1862–1871.

Faraway, Julian J. 2005. *Extending the linear model with R: generalized linear, mixed effects and nonparametric regression models*. CRC press.

Faria, Andreia V., Zhang, Jiangyang, Oishi, Kenichi, Li, Xin, Jiang, Hangyi, Akhter, Kazi, Hermoye, Laurent, Lee, Seung-Koo, Hoon, Alexander, Stashinko, Elaine, Miller, Michael I., van Zijl, Peter C. M., & Mori, Susumu. 2010. Atlas-based analysis of neurodevelopment from infancy to adulthood using diffusion tensor imaging and applications for automated abnormality detection. *NeuroImage*, **52**(2), 415–428.

Farid, F., & Mahadun, P. 2009. Schizophrenia-like psychosis following left putamen infarct: a case report. *Journal of medical case reports*, **3**(1), 1–3.

Fischl, B., Salat, D. H., Busa, E., Albert, M., Dieterich, M., Haselgrove, C., van der Kouwe, A., Killiany, R., Kennedy, D., Klaveness, S., Montillo, A., Makris, N., Rosen, B., & Dale, A. M. 2002. Whole brain segmentation: automated labeling of neuroanatomical structures in the human brain.

Neuron, **33**(3), 341–55.

Fischl, B., van der Kouwe, A., Destrieux, C., Halgren, E., Segonne, F., Salat, D. H., Busa, E., Seidman, L. J., Goldstein, J., Kennedy, D., Caviness, V., Makris, N., Rosen, B., & Dale, A. M. 2004. Automatically parcellating the human cerebral cortex. *Cereb Cortex*, **14**(1), 11–22.

Fjell, Anders M, Walhovd, Kristine B, Westlye, Lars T, Østby, Ylva, Tamnes, Christian K, Jernigan, Terry L, Gamst, Anthony, & Dale, Anders M. 2010. When does brain aging accelerate? Dangers of quadratic fits in cross-sectional studies. *Neuroimage*, **50**(4), 1376–1383.

Fornito, A., Zalesky, A., Pantelis, C., & Bullmore, E. T. 2012. Schizophrenia, neuroimaging and connectomics. *Neuroimage*, **62**(4), 2296–314.

Franze, Kristian. 2013. The mechanical control of nervous system development. *Development*, **140**(15), 3069–3077.

Galvan, Cynthia D, Hrachovy, Richard A, Smith, Karen L, & Swann, John W. 2000. Blockade of neuronal activity during hippocampal development produces a chronic focal epilepsy in the rat. *The Journal of Neuroscience*, **20**(8), 2904–2916.

Gao, Wei, Gilmore, John H, Giovanello, Kelly S, Smith, Jeffery Keith, Shen, Dinggang, Zhu, Hongtu, & Lin, Weili. 2011. Temporal and spatial evolution of brain network topology during the first two years of life. *PloS one*, **6**(9), e25278.

Garcia, Guadalupe C, Lesne, Annick, Hütt, Marc-Thorsten, & Hilgetag, Claus C. 2012. Building blocks of self-sustained activity in a simple deterministic

model of excitable neural networks. *Frontiers in computational neuroscience*, **6**.

Gardner, Margo, & Steinberg, Laurence. 2005. Peer influence on risk taking, risk preference, and risky decision making in adolescence and adulthood: An experimental study. *Developmental psychology*, **41**(4), 625–635.

Giedd, Jay N., & Rapoport, Judith L. 2010. Structural MRI of Pediatric Brain Development: What Have We Learned and Where Are We Going? *Neuron*, **67**(5), 728–734.

Giedd, Jay N, Blumenthal, Jonathan, Jeffries, Neal O, Castellanos, F Xavier, Liu, Hong, Zijdenbos, Alex, Paus, Tomáš, Evans, Alan C, & Rapoport, Judith L. 1999a. Brain development during childhood and adolescence: a longitudinal MRI study. *Nature neuroscience*, **2**(10), 861–863.

Giedd, J.N. 2008. The teen brain: insights from neuroimaging. *Journal of Adolescent Health*, **42**(4), 335–343.

Giedd, J.N., Castellanos, F.X., Rajapakse, J.C., Vaituzis, A.C., & Rapoport, J.L. 1997. Sexual dimorphism of the developing human brain. *Progress in Neuro-Psychopharmacology and Biological Psychiatry*, **21**(8), 1185–1201.

Giedd, J.N., Jeffries, N.O., Blumenthal, J., Castellanos, FX, Vaituzis, A.C., Fernandez, T., Hamburger, S.D., Liu, H., Nelson, J., & Bedwell, J. 1999b. Childhood-onset schizophrenia: progressive brain changes during adolescence. *Biological psychiatry*, **46**(7), 892–8.

Gigerenzer, Gerd, & Marewski, Julian N. 2015. Surrogate Science: The Idol

of a Universal Method for Scientific Inference. *Journal of Management*, **41**(2), 421–440.

Ginestet, Cedric E, Nichols, Thomas E, Bullmore, Ed T, & Simmons, Andrew. 2011. Brain network analysis: separating cost from topology using cost-integration. *PloS one*, **6**(7), e21570.

Godfrey, Keith B., Eglen, Stephen J., & Swindale, Nicholas V. 2009. A Multi-Component Model of the Developing Retinocollicular Pathway Incorporating Axonal and Synaptic Growth. *PLoS Computational Biology*, **5**(12), e1000600.

Gogtay, Nitin, Giedd, Jay N, Lusk, Leslie, Hayashi, Kiralee M, Greenstein, Deanna, Vaituzis, A Catherine, Nugent, Tom F, Herman, David H, Clasen, Liv S, & Toga, Arthur W. 2004. Dynamic mapping of human cortical development during childhood through early adulthood. *Proceedings of the National Academy of Sciences of the United States of America*, **101**(21), 8174–8179.

Gong, G., Rosa-Neto, P., Carbonell, F., Chen, Z. J., He, Y., & Evans, A. C. 2009. Age- and Gender-Related Differences in the Cortical Anatomical Network. *Journal of Neuroscience*, **29**(50), 15684–15693.

Gong, Gaolang, He, Yong, Chen, Zhang J, & Evans, Alan C. 2012. Convergence and divergence of thickness correlations with diffusion connections across the human cerebral cortex. *Neuroimage*, **59**(2), 1239–1248.

Gotz, M, Novak, NINO, Bastmeyer, MARTIN, & Bolz, JíÂÂŽÂÂěRGEN. 1992. Membrane-bound molecules in rat cerebral cortex regulate thalamic

innervation. *Development*, **116**(3), 507–519.

Green, Peter J, & Silverman, Bernard W. 1993. *Nonparametric regression and generalized linear models: a roughness penalty approach*. CRC Press.

Greicius, Michael D, Supekar, Kaustubh, Menon, Vinod, & Dougherty, Robert F. 2009. Resting-state functional connectivity reflects structural connectivity in the default mode network. *Cerebral cortex*, **19**(1), 72–78.

Guimera, R., & Amaral, L. A. 2005. Cartography of complex networks: modules and universal roles. *J Stat Mech*, **2005**(P02001), nihpa35573.

Guo, Wenbin, Xiao, Changqing, Liu, Guiying, Wooderson, Sarah C, Zhang, Zhikun, Zhang, Jian, Yu, Liuyu, & Liu, Jianrong. 2014. Decreased resting-state interhemispheric coordination in first-episode, drug-naive paranoid schizophrenia. *Progress in Neuro-Psychopharmacology and Biological Psychiatry*, **48**, 14–19.

Hagmann, P., Sporns, O., Madan, N., Cammoun, L., Pienaar, R., Wedeen, V. J., Meuli, R., Thiran, J. P., & Grant, P. E. 2010. White matter maturation reshapes structural connectivity in the late developing human brain. *Proceedings of the National Academy of Sciences of the United States of America*, **107**(44), 19067–72.

Hall, D. H., & Altun, Z. F. 2008. *C. elegans atlas*. Cold Spring Harbor, N.Y: Cold Spring Harbor Laboratory Press.

Harary, Frank. 2008. *Graph Theory*. Addison-Wesley, Reading, MA.

Haynes, Robin L, Borenstein, Natalia S, Desilva, Tara M, Folkerth, Rebecca D,

Liu, Lena G, Volpe, Joseph J, & Kinney, Hannah C. 2005. Axonal development in the cerebral white matter of the human fetus and infant. *Journal of Comparative Neurology*, **484**(2), 156–167.

Hellwig, Bernhard. 2000. A Quantitative Analysis of the Local Connectivity Between Pyramidal Neurons in Layers 2/3 of the Rat Visual Cortex. *Biol. Cybern.*, **82**, 111–121.

Hennig, M. H., Adams, C., Willshaw, D., & Sernagor, E. 2009. Early-Stage Waves in the Retinal Network Emerge Close to a Critical State Transition between Local and Global Functional Connectivity. *Journal of Neuroscience*, **29**(4), 1077–1086.

Hermann, Bruce, Jones, Jana, Sheth, Raj, Dow, Christian, Koehn, Monica, & Seidenberg, Michael. 2006. Children with new-onset epilepsy: neuropsychological status and brain structure. *Brain*, **129**(10), 2609–2619.

Hilgetag, C. C., Burns, G. A. P. C., O'Neill, M. A., Scannell, J. W., & Young, M. P. 2000. Anatomical Connectivity Defines the Organization of Clusters of Cortical Areas in the Macaque Monkey and the Cat. *Phil. Trans. R. Soc. Lond. B*, **355**, 91–110.

Hill, Sean L, Wang, Yun, Riachi, Imad, Schürmann, Felix, & Markram, Henry. 2012. Statistical connectivity provides a sufficient foundation for specific functional connectivity in neocortical neural microcircuits. *Proceedings of the National Academy of Sciences*, **109**(42), E2885–E2894.

Hokama, H., Shenton, M. E., Nestor, P. G., Kikinis, R., Levitt, J. J., Metcalf, D., Wible, C. G., O'Donnell, B. F., Jolesz, F. A., & McCarley, R. W.

1995. Caudate, putamen, and globus pallidus volume in schizophrenia: a quantitative MRI study. *Psychiatry Res*, **61**(4), 209–29.

Holland, Dominic, Kuperman, Joshua M., & Dale, Anders M. 2010. Efficient correction of inhomogeneous static magnetic field-induced distortion in Echo Planar Imaging. *NeuroImage*, **50**(1), 175 – 183.

Homae, F., Watanabe, H., Otobe, T., Nakano, T., Go, T., Konishi, Y., & Taga, G. 2010. Development of Global Cortical Networks in Early Infancy. *Journal of Neuroscience*, **30**(14), 4877–4882.

Honey, C. J., Sporns, O., Cammoun, L., Gigandet, X., Thiran, J. P., Meuli, R., & Hagmann, P. 2009a. Predicting human resting-state functional connectivity from structural connectivity. *Proc Natl Acad Sci U S A*, **106**(6), 2035–40.

Honey, Christopher J., Thivierge, Jean-Philippe, & Sporns, Olaf. 2010. Can structure predict function in the human brain? *Neuroimage*, **52**(3), 766–776.

Honey, CJ, Sporns, O, Cammoun, Leila, Gigandet, Xavier, Thiran, Jean-Philippe, Meuli, Reto, & Hagmann, Patric. 2009b. Predicting human resting-state functional connectivity from structural connectivity. *Proceedings of the National Academy of Sciences*, **106**(6), 2035–2040.

Hoptman, Matthew J, Zuo, Xi-Nian, D'Angelo, Debra, Mauro, Cristina J, Butler, Pamela D, Milham, Michael P, & Javitt, Daniel C. 2012. Decreased interhemispheric coordination in schizophrenia: a resting state fMRI study. *Schizophrenia research*, **141**(1), 1–7.

Hrabe, Jan, Kaur, Gurjinder, & Guilfoyle, David N. 2007. Principles and limitations of NMR diffusion measurements. *Journal of medical physics/Association of Medical Physicists of India*, **32**(1), 34.

Huang, Hao, Shu, Ni, Mishra, Virendra, Jeon, Tina, Chalak, Lina, Wang, Zhiyue J, Rollins, Nancy, Gong, Gaolang, Cheng, Hua, & Peng, Yun. 2013. Development of Human Brain Structural Networks Through Infancy and Childhood. *Cerebral Cortex*, bht335.

Hubbard, Penny L., & Parker, Geoffrey J.M. 2014. Chapter 20 - Validation of Tractography. *Pages 453 – 480 of:* Johansen-Berg, Heidi, & Behrens, Timothy E.J. (eds), *Diffusion MRI (Second Edition)*, second edition edn. San Diego: Academic Press.

Hutchinson, Elizabeth, Pulsipher, Dalin, Dabbs, Kevin, Sheth, Raj, Jones, Jana, Seidenberg, Michael, Meyerand, Elizabeth, & Hermann, Bruce. 2010. Children with new-onset epilepsy exhibit diffusion abnormalities in cerebral white matter in the absence of volumetric differences. *Epilepsy research*, **88**(2), 208–214.

Huttenlocher, Peter R. 1979. Synaptic density in human frontal cortex-developmental changes and effects of aging. *Brain research*, **163**(2), 195.

Huttenlocher, Peter R. 1984. Synapse elimination and plasticity in developing human cerebral cortex. *American journal of mental deficiency*, **88**(5), 488–496.

Huttenlocher, Peter R. 1990. Morphometric study of human cerebral cortex development. *Neuropsychologia*, **28**(6), 517–527.

Huttenlocher, Peter R., & Dabholkar, Arun S. 1997. Regional differences in synaptogenesis in human cerebral cortex. *The Journal of Comparative Neurology*, **387**(2), 167–178.

Innocenti, Giorgio M, & Price, David J. 2005. Exuberance in the development of cortical networks. *Nature Reviews Neuroscience*, **6**(12), 955–965.

Jbabdi, S., & Johansen-Berg, H. 2011. Tractography: Where Do We Go from Here? *Brain Connectivity*, **1**(3), 169–183.

Jbabdi, Saad. 2014. Chapter 25 - Imaging Structure and Function. *Pages 585 – 605 of:* Johansen-Berg, Heidi, & Behrens, Timothy E.J. (eds), *Diffusion MRI (Second Edition)*, second edition edn. San Diego: Academic Press.

Jbabdi, Saad, Woolrich, Mark William, & Behrens, Timothy Edward John. 2009. Multiple-subjects connectivity-based parcellation using hierarchical Dirichlet process mixture models. *NeuroImage*, **44**(2), 373–384.

Jbabdi, Saad, Sotiropoulos, Stamatios N, Savio, Alexander M, Graña, Manuel, & Behrens, Timothy EJ. 2012. Model-based analysis of multishell diffusion MR data for tractography: How to get over fitting problems. *Magnetic Resonance in Medicine*, **68**(6), 1846–1855.

Jeurissen, B, Leemans, A, Tournier, JD, Jones, DK, & Sijbers, J. 2010. Estimating the number of fiber orientations in diffusion MRI voxels: a constrained spherical deconvolution study. *Proceedings of the International Society for Magnetic Resonance in Medicine. Stockholm, Sweden*, 573.

Johansen-Berg, Heidi, & Behrens, Timothy EJ. 2009. *Diffusion MRI: From quantitative measurement to in-vivo neuroanatomy.* Academic Press.

Johansen-Berg, Heidi, & Behrens, Timothy E.J. (eds). 2014a. Copyright. *Pages iv – of:* Johansen-Berg, Heidi, & Behrens, Timothy E.J. (eds), *Diffusion MRI (Second Edition)*, second edition edn. San Diego: Academic Press.

Johansen-Berg, Heidi, & Behrens, Timothy E.J. (eds). 2014b. Front Matter. *Pages iii – of:* Johansen-Berg, Heidi, & Behrens, Timothy E.J. (eds), *Diffusion MRI (Second Edition)*, second edition edn. San Diego: Academic Press.

Johansen-Berg, Heidi, & Behrens, Timothy E.J. (eds). 2014c. Index. *Pages 607 – 614 of:* Johansen-Berg, Heidi, & Behrens, Timothy E.J. (eds), *Diffusion MRI (Second Edition)*, second edition edn. San Diego: Academic Press.

Jones, Derek K. 2009. Chapter 3 - Gaussian Modeling of the Diffusion Signal. *Pages 87 – 104 of:* Johansen-Berg, Heidi, & Behrens, Timothy E.J. (eds), *Diffusion MRI*, second edition edn. San Diego: Academic Press.

Jones, Derek K. 2010. Challenges and limitations of quantifying brain connectivity in vivo with diffusion MRI. *Imaging*, **2**(3), 341–355.

Jones, Derek K, Knösche, Thomas R, & Turner, Robert. 2013. White matter integrity, fiber count, and other fallacies: the do's and don'ts of diffusion MRI. *Neuroimage*, **73**, 239–254.

Jones, DerekK, & Leemans, Alexander. 2011. Diffusion Tensor Imaging. *Pages 127–144 of:* Modo, Michel, & Bulte, Jeff W. M. (eds), *Magnetic Resonance Neuroimaging*. Methods in Molecular Biology, vol. 711. New York, NY: Humana Press.

Jones, DK, & Pierpaoli, C. 2005. Contribution of cardiac pulsation to variability

of tractography results. *Page 222 of: Proc Intl Soc Magn Reson Med*, vol. 13.

Jung, Klaus, Friede, Tim, & Beißbarth, Tim. 2011. Reporting FDR analogous confidence intervals for the log fold change of differentially expressed genes. *BMC bioinformatics*, **12**(1), 288.

Kadane, Joseph B., & Lazar, Nicole A. 2004. Methods and Criteria for Model Selection. *Journal of the American Statistical Association*, **99**(465), 279–290.

Kaiser, M., & Hilgetag, C. C. 2004. Edge vulnerability in neural and metabolic networks. *Biol Cybern*, **90**(5), 311–7.

Kaiser, M., & Hilgetag, C. C. 2010. Optimal hierarchical modular topologies for producing limited sustained activation of neural networks. *Front Neuroinformatics*, **4**, 8.

Kaiser, M., Hilgetag, C. C., & van Ooyen, A. 2009. A simple rule for axon outgrowth and synaptic competition generates realistic connection lengths and filling fractions. *Cereb Cortex*, **19**(12), 3001–10.

Kaiser, Marcus. 2011. A Tutorial in Connectome Analysis: Topological and Spatial Features of Brain Networks. *Neuroimage*, **57**(3), 892–907.

Kaiser, Marcus, & Hilgetag, Claus C. 2006. Nonoptimal Component Placement, but Short Processing Paths, due to Long-Distance Projections in Neural Systems. *PLoS Computational Biology*, **2**(7), e95.

Kaiser, Marcus, & Hilgetag, Claus C. 2007. Development of multi-cluster

cortical networks by time windows for spatial growth. *Neurocomputing*, **70**, 1829–1832.

Kaiser, Marcus, & Varier, Sreedevi. 2011. Evolution and Development of Brain Networks: From Caenorhabditis elegans to Homo sapiens. *Network: Computation in Neural Systems*, **22**, 143–147.

Kaiser, Marcus, Goerner, Matthias, & Hilgetag, Claus C. 2007. Criticality of spreading dynamics in hierarchical cluster networks without inhibition. *New Journal of Physics*, **9**(5), 110.

Kaiser, Marcus, Hilgetag, Claus C, & Kötter, Rolf. 2010. Hierarchy and dynamics of neural networks. *Frontiers in neuroinformatics*, **4**.

Kaufman, A, Dror, G, Meilijson, I, & Ruppin, E. 2006. Gene Expression of C. elegans Neurons Carries Information on Their Synaptic Connectivity. *PLoS Computational Biology*, **2**(12), e167.

Kelly, AM Clare, Di Martino, Adriana, Uddin, Lucina Q, Shehzad, Zarrar, Gee, Dylan G, Reiss, Philip T, Margulies, Daniel S, Castellanos, F Xavier, & Milham, Michael P. 2009. Development of anterior cingulate functional connectivity from late childhood to early adulthood. *Cerebral Cortex*, **19**(3), 640–657.

Kelsch, Wolfgang, Sim, Shuyin, & Lois, Carlos. 2010. Watching synaptogenesis in the adult brain. *Annual review of neuroscience*, **33**, 131–149.

Keshavan, Matcheri S, Anderson, Stewart, & Pettergrew, Jay W. 1994. Is schizophrenia due to excessive synaptic pruning in the prefrontal cortex?

The Feinberg hypothesis revisited. *Journal of psychiatric research*, **28**(3), 239–265.

Kim, Dae-Jin, Davis, Elysia Poggi, Sandman, Curt A., Sporns, Olaf, O'Donnell, Brian F., Buss, Claudia, & Hetrick, William P. 2014. Longer gestation is associated with more efficient brain networks in preadolescent children. *NeuroImage*, **100**(0), 619 – 627.

Kingsley, Peter B. 2006a. Introduction to diffusion tensor imaging mathematics: Part I. Tensors, rotations, and eigenvectors. *Concepts in Magnetic Resonance Part A*, **28**(2), 101–122.

Kingsley, Peter B. 2006b. Introduction to diffusion tensor imaging mathematics: Part II. Anisotropy, diffusion-weighting factors, and gradient encoding schemes. *Concepts in Magnetic Resonance Part A*, **28**(2), 123–154.

Kingsley, Peter B. 2006c. Introduction to diffusion tensor imaging mathematics: Part III. Tensor calculation, noise, simulations, and optimization. *Concepts in Magnetic Resonance Part A*, **28**(2), 155–179.

Klein, Daniel, Rotarska-Jagiela, Anna, Genc, Erhan, Sritharan, Sharmili, Mohr, Harald, Roux, Frederic, Han, Cheol E, Kaiser, Marcus, Singer, Wolf, & Uhlhaas, Peter J. 2014a. Adolescent brain maturation and cortical folding: evidence for reductions in gyrification. *PloS one*, **9**(1), e84914.

Klein, Johannes C, Behrens, Timothy EJ, Robson, Matthew D, Mackay, Clare E, Higham, Desmond J, & Johansen-Berg, Heidi. 2007. Connectivity-based parcellation of human cortex using diffusion MRI: establishing reproducibility, validity and observer independence in BA 44/45 and SMA/pre-SMA.

Neuroimage, **34**(1), 204–211.

Klein, Johannes C., Behrens, Timothy E.J., & Johansen-Berg, Heidi. 2014b. Chapter 21 - Connectivity Fingerprinting of Gray Matter. *Pages 481 – 509 of:* Johansen-Berg, Heidi, & Behrens, Timothy E.J. (eds), *Diffusion MRI (Second Edition)*, second edition edn. San Diego: Academic Press.

Koene, Randal A, Tijms, Betty, van Hees, Peter, Postma, Frank, de Ridder, Alexander, Ramakers, Ger JA, van Pelt, Jaap, & van Ooyen, Arjen. 2009. NETMORPH: a framework for the stochastic generation of large scale neuronal networks with realistic neuron morphologies. *Neuroinformatics*, **7**(3), 195–210.

Kropf, S., Heuer, H., Gruning, M., & Smalla, K. 2004. Significance test for comparing complex microbial community fingerprints using pairwise similarity measures. *J Microbiol Methods*, **57**(2), 187–95.

Krottje, Johannes K., & Van Ooyen, A. 2007. A mathematical framework for modelling axon guidance. *Bulletin of Mathematical Biology*, **69**, 3–31.

Kubicki, M., Westin, C-F., Pasternak, O., & Shenton, M.E. 2014. Chapter 15 - Diffusion Tensor Imaging and its Application to Schizophrenia and Related Disorders. *Pages 317 – 334 of:* Johansen-Berg, Heidi, & Behrens, Timothy E.J. (eds), *Diffusion MRI (Second Edition)*, second edition edn. San Diego: Academic Press.

LaMantia, Anthony S, & Rakic, P. 1994. Axon overproduction and elimination in the anterior commissure of the developing rhesus monkey. *Journal of Comparative Neurology*, **340**(3), 328–336.

LaMantia, AS, & Rakic, P. 1990. Axon overproduction and elimination in the corpus callosum of the developing rhesus monkey. *The Journal of neuroscience*, **10**(7), 2156–2175.

Latora, V., & Marchiori, M. 2001. Efficient behavior of small-world networks. *Physical Review Letters*, **87**(19), 198701.

Latora, Vito, & Marchiori, Massimo. 2003. Economic small-world behavior in weighted networks. *The European Physical Journal B-Condensed Matter and Complex Systems*, **32**(2), 249–263.

Lau, Yolanda C, Hinkley, Leighton BN, Bukshpun, Polina, Strominger, Zoe A, Wakahiro, Mari LJ, Baron-Cohen, Simon, Allison, Carrie, Auyeung, Bonnie, Jeremy, Rita J, & Nagarajan, Srikantan S. 2013. Autism traits in individuals with agenesis of the corpus callosum. *Journal of autism and developmental disorders*, **43**(5), 1106–1118.

Lazar, Mariana, & Alexander, Andrew L. 2003. An error analysis of white matter tractography methods: synthetic diffusion tensor field simulations. *Neuroimage*, **20**(2), 1140–1153.

Le Bihan, Denis, Breton, E, *et al.* 1985. Imagerie de diffusion in-vivo par résonance magnétique nucléaire. *Comptes-Rendus de l'Académie des Sciences*, **93**(5), 27–34.

Lebel, C., & Beaulieu, C. 2011. Longitudinal development of human brain wiring continues from childhood into adulthood. *The Journal of neuroscience : the official journal of the Society for Neuroscience*, **31**(30), 10937–47.

Leicht, E. A., & Newman, M. E. 2008. Community structure in directed

networks. *Phys Rev Lett*, **100**(11), 118703.

Lemon, Jim. 2006. Plotrix: a package in the red light district of R. *R-news*, **6**(4), 8–12.

Lenroot, R.K., Gogtay, N., Greenstein, D.K., Wells, E.M., Wallace, G.L., Clasen, L.S., Blumenthal, J.D., Lerch, J., Zijdenbos, A.P., & Evans, A.C. 2007. Sexual dimorphism of brain developmental trajectories during childhood and adolescence. *Neuroimage*, **36**(4), 1065–1073.

Li, Wen-Chang, Cooke, Tom, Sautois, Bart, Soffe, Stephen, Borisyuk, Roman, & Roberts, Alan. 2007. Axon and dendrite geography predict the specificity of synaptic connections in a functioning spinal cord network. *Neural Development*, **2**(1), 17.

Li, Yonghui, Liu, Yong, Li, Jun, Qin, Wen, Li, Kuncheng, Yu, Chunshui, & Jiang, Tianzi. 2009. Brain anatomical network and intelligence. *PLoS computational biology*, **5**(5), e1000395.

Lim, Sol, & Kaiser, Marcus. 2015. Developmental time windows for axon growth influence neuronal network topology. *Biological cybernetics*, **109**(2), 275–286.

Lim, Sol, Han, C.E., Uhlhaas, P. J., & Kaiser, Marcus. 2013. Preferential detachment during human brain development: Age- and sex-specific structural connectivity in Diffusion Tensor Imaging (DTI). *Cereb Cortex*, **Advanced online**.

Low, Lawrence K, & Cheng, Hwai-Jong. 2006. Axon pruning: an essential step underlying the developmental plasticity of neuronal connections. *Philosoph-*

ical Transactions of the Royal Society B: Biological Sciences, **361**(1473), 1531–1544.

Luo, Liqun, & O'Leary, Dennis DM. 2005. Axon retraction and degeneration in development and disease. *Annu. Rev. Neurosci.*, **28**, 127–156.

Mädler, Burkhard, Drabycz, Sylvia A, Kolind, Shannon H, Whittall, Kenneth P, & MacKay, Alexander L. 2008. Is diffusion anisotropy an accurate monitor of myelination?: Correlation of multicomponent T2 relaxation and diffusion tensor anisotropy in human brain. *Magnetic resonance imaging*, **26**(7), 874–888.

Mangin, J-F, Fillard, Pierre, Cointepas, Yann, Le Bihan, Denis, Frouin, Vincent, & Poupon, Cyril. 2013. Toward global tractography. *NeuroImage*, **80**, 290–296.

Mannion, Arlene, & Leader, Geraldine. 2014. Epilepsy in autism spectrum disorder. *Research in Autism Spectrum Disorders*, **8**(4), 354–361.

Markram, Henry, Lübke, Joachim, Frotscher, Michael, Roth, Arnd, & Sakmann, Bert. 1997. Physiology and anatomy of synaptic connections between thick tufted pyramidal neurones in the developing rat neocortex. *The Journal of physiology*, **500**(2), 409–440.

Maslov, Sergei, & Sneppen, Kim. 2002. Specificity and Stability in Topology of Protein Networks. *Science*, **296**(5569), 910–913.

McAssey, Michael P, Bijma, Fetsje, Tarigan, Bernadetta, van Pelt, Jaap, van Ooyen, Arjen, & de Gunst, Mathisca. 2014. A Morpho-Density Approach to Estimating Neural Connectivity. *PLOS ONE*, **9**(1), e86526.

Menon, Vinod. 2013. Developmental pathways to functional brain networks: emerging principles. *Trends in cognitive sciences*, **17**(12), 627–640.

Merboldt, Klaus-Dietmar, Hanicke, Wolfgang, & Frahm, Jens. 1985. Self-diffusion NMR imaging using stimulated echoes. *Journal of Magnetic Resonance (1969)*, **64**(3), 479–486.

Messé, Arnaud, Hütt, Marc-Thorsten, König, Peter, & Hilgetag, Claus C. 2015. A closer look at the apparent correlation of structural and functional connectivity in excitable neural networks. *Scientific reports*, **5**.

Mesulam, M.M. 2000. *Principles of behavioral and cognitive neurology.* New york, NY: Oxford University Press, USA.

Meunier, D., Lambiotte, R., & Bullmore, E. T. 2010. Modular and hierarchically modular organization of brain networks. *Front Neurosci*, **4**, 200.

Miller, Karla L. 2014. Chapter 3 - Diffusion Acquisition: Pushing the Boundaries. *Pages 35 – 61 of:* Johansen-Berg, Heidi, & Behrens, Timothy E.J. (eds), *Diffusion MRI (Second Edition)*, second edition edn. San Diego: Academic Press.

Morecraft, Robert J., Ugolini, Gabriella, Lanciego, José L., Wouterlood, Floris G., & Pandya, Deepak N. 2014. Chapter 17 - Classic and Contemporary Neural Tract-Tracing Techniques. *Pages 359 – 399 of:* Johansen-Berg, Heidi, & Behrens, Timothy E.J. (eds), *Diffusion MRI (Second Edition)*, second edition edn. San Diego: Academic Press.

Morgan, Joshua L, Soto, Florentina, Wong, Rachel OL, & Kerschensteiner,

Daniel. 2011. Development of cell type-specific connectivity patterns of converging excitatory axons in the retina. *Neuron*, **71**(6), 1014–1021.

Mori, S., & Barker, P. B. 1999. Diffusion magnetic resonance imaging: its principle and applications. *Anat Rec*, **257**(3), 102–9.

Mori, Susumu, & van Zijl, Peter. 2002. Fiber tracking: principles and strategies–a technical review. *NMR in Biomedicine*, **15**(7-8), 468–480.

Mori, Susumu, & Zhang, Jiangyang. 2006. Principles of Diffusion Tensor Imaging and Its Applications to Basic Neuroscience Research. *Neuron*, **51**(5), 527 – 539.

Moseley, ME, Cohen, Y, Mintorovitch, J, Chileuitt, L, Shimizu, H, Kucharczyk, J, Wendland, MF, & Weinstein, PR. 1990. Early detection of regional cerebral ischemia in cats: comparison of diffusion-and T2-weighted MRI and spectroscopy. *Magnetic Resonance in Medicine*, **14**(2), 330–346.

Muir-Robinson, Gianna, Hwang, Bryan J, & Feller, Marla B. 2002. Retinogeniculate axons undergo eye-specific segregation in the absence of eye-specific layers. *The Journal of neuroscience*, **22**(13), 5259–5264.

Mulkern, Robert V, Gudbjartsson, Hakon, Westin, Carl-Fredrik, Zengingonul, Hale Pinar, Gartner, Werner, Guttmann, Charles RG, Robertson, Richard L, Kyriakos, Walid, Schwartz, Richard, Holtzman, David, *et al.* 1999. Multi-component apparent diffusion coefficients in human brain^2. *NMR Biomed*, **12**, 51–62.

Mulkern, Robert V, Haker, Steven J, & Maier, Stephan E. 2009. On high

b diffusion imaging in the human brain: ruminations and experimental insights. *Magnetic resonance imaging*, **27**(8), 1151–1162.

Newman, M. E. 2006. Modularity and community structure in networks. *Proc Natl Acad Sci U S A*, **103**(23), 8577–82.

Newman, M. E. J. 2003. The Structure and Function of Complex Networks. *SIAM Review*, **45**(2), 167–256.

Nicosia, Vincenzo, Vértes, Petra E, Schafer, William R, Latora, Vito, & Bullmore, Edward T. 2013. Phase transition in the economically modeled growth of a cellular nervous system. *Proceedings of the National Academy of Sciences*, **110**(19), 7880–7885.

Nir, Talia, Jahanshad, Neda, Jack, Clifford R, Weiner, Michael W, Toga, Arthur W, & Thompson, Paul M. 2012. Small world network measures predict white matter degeneration in patients with early-stage mild cognitive impairment. *Biomedical Imaging (ISBI), 2012 9th IEEE International Symposium*, 1405–1408.

Nisbach, F., & Kaiser, M. 2007. Developmental time windows for spatial growth generate multiple-cluster small-world networks. *European Physical Journal B*, **58**(2), 185–191.

Nooner, K.B., Colcombe, S., Tobe, R., Mennes, M., Benedict, M., Moreno, A., Panek, L., Brown, S., Zavitz, S., & Li, Q. 2012. The NKI-Rockland Sample: A Model for Accelerating the Pace of Discovery Science in Psychiatry. *Frontiers in Neuroscience*, **6**, 152.

O'Leary, Dennis DM. 1992. Development of connectional diversity and specificity

in the mammalian brain by the pruning of collateral projections. *Current opinion in neurobiology*, **2**(1), 70–77.

O'Leary, Dennis DM, & Koester, Susan E. 1993. Development of projection neuron types, axon pathways, and patterned connections of the mammalian cortex. *Neuron*, **10**(6), 991–1006.

Packer, Adam M, & Yuste, Rafael. 2011. Dense, unspecific connectivity of neocortical parvalbumin-positive interneurons: a canonical microcircuit for inhibition? *The Journal of Neuroscience*, **31**(37), 13260–13271.

Packer, Adam M, McConnell, Daniel J, Fino, Elodie, & Yuste, Rafael. 2013. Axo-dendritic overlap and laminar projection can explain interneuron connectivity to pyramidal cells. *Cerebral Cortex*, **23**(12), 2790–2802.

Paolicelli, Rosa C, Bolasco, Giulia, Pagani, Francesca, Maggi, Laura, Scianni, Maria, Panzanelli, Patrizia, Giustetto, Maurizio, Ferreira, Tiago Alves, Guiducci, Eva, & Dumas, Laura. 2011. Synaptic pruning by microglia is necessary for normal brain development. *Science*, **333**(6048), 1456–1458.

Parker, Christopher S, Deligianni, Fani, Cardoso, M Jorge, Daga, Pankaj, Modat, Marc, Dayan, Michael, Clark, Chris A, Ourselin, Sebastien, & Clayden, Jonathan D. 2014. Consensus between Pipelines in Structural Brain Networks. *PloS one*, **9**(10), e111262.

Passingham, Richard. 2014. Foreword. *Pages ix – x of:* Johansen-Berg, Heidi, & Behrens, Timothy E.J. (eds), *Diffusion MRI (Second Edition)*, second edition edn. San Diego: Academic Press.

Paul, Lynn K. 2011. Developmental malformation of the corpus callosum: a

review of typical callosal development and examples of developmental disorders with callosal involvement. *Journal of neurodevelopmental disorders*, **3**(1), 3–27.

Paus, Tomáš, Zijdenbos, Alex, Worsley, Keith, Collins, D Louis, Blumenthal, Jonathan, Giedd, Jay N, Rapoport, Judith L, & Evans, Alan C. 1999. Structural maturation of neural pathways in children and adolescents: in vivo study. *Science*, **283**(5409), 1908–1911.

Perin, R, Telefont, M, & Markram, H. 2013. Computing the size and number of neuronal clusters in local circuits. *Frontiers in neuroanatomy*, **7**, 1.

Perin, Rodrigo, Berger, Thomas K, & Markram, Henry. 2011. A synaptic organizing principle for cortical neuronal groups. *Proceedings of the National Academy of Sciences*, **108**(13), 5419–5424.

Perrin, J. S., Leonard, G., Perron, M., Pike, G. B., Pitiot, A., Richer, L., Veillette, S., Pausova, Z., & Paus, T. 2009. Sex differences in the growth of white matter during adolescence. *Neuroimage*, **45**(4), 1055–66.

Petanjek, Zdravko, Judaš, Miloš, Kostović, Ivica, & Uylings, Harry BM. 2008. Lifespan alterations of basal dendritic trees of pyramidal neurons in the human prefrontal cortex: a layer-specific pattern. *Cerebral Cortex*, **18**(4), 915–929.

Petanjek, Zdravko, Judaš, Miloš, Šimić, Goran, Rašin, Mladen Roko, Uylings, Harry BM, Rakic, Pasko, & Kostović, Ivica. 2011. Extraordinary neoteny of synaptic spines in the human prefrontal cortex. *Proceedings of the National Academy of Sciences*, **108**(32), 13281–13286.

Pettersson-Yeo, William, Allen, Paul, Benetti, Stefania, McGuire, Philip, & Mechelli, Andrea. 2011. Dysconnectivity in schizophrenia: where are we now? *Neuroscience & Biobehavioral Reviews*, **35**(5), 1110–1124.

Pipe, Jim. 2014. Chapter 2 - Pulse Sequences for Diffusion-Weighted MRI. *Pages 11 – 34 of:* Johansen-Berg, Heidi, & Behrens, Timothy E.J. (eds), *Diffusion MRI (Second Edition)*, second edition edn. San Diego: Academic Press.

Ponten, S., Bartolomei, F., & Stam, C. 2007. Small-world networks and epilepsy: Graph theoretical analysis of intracerebrally recorded mesial temporal lobe seizures. *Clinical Neurophysiology*, **118**(4), 918–927.

Price, David, Jarman, Andrew P, Mason, John O, & Kind, Peter C. 2011. *Building brains: An introduction to neural development.* John Wiley & Sons.

Purves, D., & Lichtman, J. W. 1980. Elimination of synapses in the developing nervous system. *Science*, **210**(4466), 153–157.

R Core Team. 2014. *R: A Language and Environment for Statistical Computing.* R Foundation for Statistical Computing, Vienna, Austria.

Rakic, P., Bourgeois, J. P., Eckenhoff, M. F., Zecevic, N., & Goldman-Rakic, P. S. 1986. Concurrent overproduction of synapses in diverse regions of the primate cerebral cortex. *Science*, **232**(4747), 232–235.

Rakic, Pasko. 2002. Neurogenesis in Adult Primate Neocortex: An Evaluation of the Evidence. *Nature Rev. Neurosci.*, **3**, 65–71.

Raznahan, Armin, Shaw, Phillip, Lalonde, Francois, Stockman, Mike, Wallace, Gregory L, Greenstein, Dede, Clasen, Liv, Gogtay, Nitin, & Giedd, Jay N. 2011. How does your cortex grow? *The Journal of Neuroscience*, **31**(19), 7174–7177.

Reis, Saulo DS, Hu, Yanqing, Babino, Andrés, Andrade Jr, José S, Canals, Santiago, Sigman, Mariano, & Makse, Hernán A. 2014. Avoiding catastrophic failure in correlated networks of networks. *Nature Physics*, **10**(10), 762–767.

Reiss, Philip T, Huang, Lei, Chen, Yin-Hsiu, Huo, Lan, Tarpey, Thaddeus, & Mennes, Maarten. 2014. Massively parallel nonparametric regression, with an application to developmental brain mapping. *Journal of Computational and Graphical Statistics*, **23**(1), 232–248.

Robinson, Emma C, Jbabdi, Saad, Glasser, Matthew F, Andersson, Jesper, Burgess, Gregory C, Harms, Michael P, Smith, Stephen M, Van Essen, David C, & Jenkinson, Mark. 2014. MSM: A new flexible framework for Multimodal Surface Matching. *Neuroimage*, **100**, 414–426.

Ropireddy, D., & Ascoli, G. A. 2011. Potential Synaptic Connectivity of Different Neurons onto Pyramidal Cells in a 3D Reconstruction of the Rat Hippocampus. *Frontiers in Neuroinformatics*, **5**, 5.

Rubenstein, JLR, & Merzenich, MM. 2003. Model of autism: increased ratio of excitation/inhibition in key neural systems. *Genes, Brain and Behavior*, **2**(5), 255–267.

Rubinov, M., & Sporns, O. 2010. Complex network measures of brain connec-

tivity: Uses and interpretations. *Neuroimage*, **52**(3), 1059–1069.

Rubinov, M., & Sporns, O. 2011. Weight-conserving characterization of complex functional brain networks. *Neuroimage*.

Rushworth, Matthew F.S., Sallet, Jérôme, Boorman, Erie D., & Mars, Rogier B. 2014. Chapter 24 - Comparing Connections in the Brains of Humans and Other Primates Using Diffusion-Weighted Imaging. *Pages 569 – 584 of:* Johansen-Berg, Heidi, & Behrens, Timothy E.J. (eds), *Diffusion MRI (Second Edition)*, second edition edn. San Diego: Academic Press.

Ruthazer, Edward S, Akerman, Colin J, & Cline, Hollis T. 2003. Control of axon branch dynamics by correlated activity in vivo. *Science*, **301**(5629), 66–70.

Sakai, Nozomi, & Kaprielian, Zaven. 2012. Guidance of longitudinally projecting axons in the developing central nervous system. *Frontiers in Molecular Neuroscience*, **5**.

Salat, David H. 2014. Chapter 12 - Diffusion Tensor Imaging in the Study of Aging and Age-Associated Neural Disease. *Pages 257 – 281 of:* Johansen-Berg, Heidi, & Behrens, Timothy E.J. (eds), *Diffusion MRI (Second Edition)*, second edition edn. San Diego: Academic Press.

Samsonovich, Alexei V., & Ascoli, Giorgio A. 2003. Statistical morphological analysis of hippocampal principal neurons indicates cell-specific repulsion of dendrites from their own cell. *Journal of Neuroscience Research*, **71**(2), 173–187.

Santesso, Diane L, & Segalowitz, Sidney J. 2008. Developmental Differences in

Error-Related ERPs in Middle-to Late-Adolescent Males. *Developmental psychology*, **44**(1), 205–217.

Sarkar, D. 2008. *Lattice: multivariate data visualization with R.* New York, NY: Springer Verlag.

Scheiffele, Peter, Fan, Jinhong, Choih, Jenny, Fetter, Richard, & Serafini, Tito. 2000. Neuroligin expressed in nonneuronal cells triggers presynaptic development in contacting axons. *Cell*, **101**(6), 657–669.

Scholz, Jan, Tomassini, Valentina, & Johansen-Berg, Heidi. 2014. Chapter 14 - Individual Differences in White Matter Microstructure in the Healthy Brain. *Pages 301 – 316 of:* Johansen-Berg, Heidi, & Behrens, Timothy E.J. (eds), *Diffusion MRI (Second Edition)*, second edition edn. San Diego: Academic Press.

Schüz, Almut, Chaimow, Denis, Liewald, Daniel, & Dortenman, Monika. 2006. Quantitative aspects of corticocortical connections: a tracer study in the mouse. *Cerebral cortex*, **16**(10), 1474–1486.

Seunarine, Kiran K, & Alexander, Daniel C. 2009. Multiple fibers: beyond the diffusion tensor. *Diffusion MRI: From quantitative measurement to in vivo neuroanatomy*, **1**.

Shaw, P., Kabani, N.J., Lerch, J.P., Eckstrand, K., Lenroot, R., Gogtay, N., Greenstein, D., Clasen, L., Evans, A., & Rapoport, J.L. 2008. Neurodevelopmental trajectories of the human cerebral cortex. *Journal of Neuroscience*, **28**(14), 3586–3594.

Shi, Feng, Wang, Li, Peng, Ziwen, Wee, Chong-Yaw, & Shen, Dinggang. 2013.

Altered Modular Organization of Structural Cortical Networks in Children with Autism. *PloS one*, **8**(5), e63131.

Smith, Stephen M., Jenkinson, Mark, Woolrich, Mark W., Beckmann, Christian F., Behrens, Timothy E.J., Johansen-Berg, Heidi, Bannister, Peter R., Luca, Marilena De, Drobnjak, Ivana, Flitney, David E., Niazy, Rami K., Saunders, James, Vickers, John, Zhang, Yongyue, Stefano, Nicola De, Brady, J. Michael, & Matthews, Paul M. 2004. Advances in functional and structural MR image analysis and implementation as FSL. *NeuroImage*, **23, Supplement 1**(0), S208 – S219. Mathematics in Brain Imaging.

Smith, Stephen M., Kindlmann, Gordon, & Jbabdi, Saad. 2014. Chapter 10 - Cross-Subject Comparison of Local Diffusion MRI Parameters. *Pages 209 – 239 of:* Johansen-Berg, Heidi, & Behrens, Timothy E.J. (eds), *Diffusion MRI (Second Edition)*, second edition edn. San Diego: Academic Press.

Smyser, Christopher D, Inder, Terrie E, Shimony, Joshua S, Hill, Jason E, Degnan, Andrew J, Snyder, Abraham Z, & Neil, Jeffrey J. 2010. Longitudinal analysis of neural network development in preterm infants. *Cerebral cortex*, bhq035.

Soares, Jose, Marques, Paulo, Alves, Victor, & Sousa, Nuno. 2013. A hitchhiker's guide to Diffusion Tensor Imaging. *Frontiers in Neuroscience*, **7**(31).

Sowell, E. R. 2004. Longitudinal Mapping of Cortical Thickness and Brain Growth in Normal Children. *Journal of Neuroscience*, **24**(38), 8223–8231.

Sowell, Elizabeth R, Thompson, Paul M, Tessner, Kevin D, & Toga, Arthur W. 2001. Mapping continued brain growth and gray matter density reduction

in dorsal frontal cortex: inverse relationships during postadolescent brain maturation. *The Journal of Neuroscience*, **21**(22), 8819–8829.

Sowell, Elizabeth R, Thompson, Paul M, Leonard, Christiana M, Welcome, Suzanne E, Kan, Eric, & Toga, Arthur W. 2004. Longitudinal mapping of cortical thickness and brain growth in normal children. *The Journal of Neuroscience*, **24**(38), 8223–8231.

Sowell, E.R., Thompson, P.M., Holmes, C.J., Jernigan, T.L., & Toga, A.W. 1999. In vivo evidence for postadolescent brain maturation in frontal and striatal regions. *Nature neuroscience*, **2**, 859–860.

Sperry, Roger W. 1963. Chemoaffinity in the Orderly Growth of Nerve Fiber Pattern and Connections. *Proc. Natl. Acad. Sci. USA*, **50**, 703–710.

Sporns, Olaf. 2011. The Non-Random Brain: Efficiency, Economy, and Complex Dynamics. *Frontiers in Computational Neuroscience*, **5**, 5.

Sporns, Olaf. 2014a. Chapter 18 - The Human Connectome: Linking Structure and Function in the Human Brain. *Pages 401 – 428 of:* Johansen-Berg, Heidi, & Behrens, Timothy E.J. (eds), *Diffusion MRI (Second Edition)*, second edition edn. San Diego: Academic Press.

Sporns, Olaf. 2014b. Contributions and challenges for network models in cognitive neuroscience. *Nature neuroscience*, **17**(5), 652–660.

Stam, C. J., Jones, B. F., Nolte, G., Breakspear, M., & Scheltens, P. 2007. Small-world networks and functional connectivity in Alzheimer's disease. *Cereb Cortex*, **17**(1), 92–9.

Stejskal, EO, & Tanner, JE. 1965. Spin diffusion measurements: spin echoes in the presence of a time-dependent field gradient. *The journal of chemical physics*, **42**(1), 288–292.

Stepanyants, A., Hof, P. R., & Chklovskii, D. B. 2002. Geometry and structural plasticity of synaptic connectivity. *Neuron*, **34**(2), 275–88.

Stief, F, Zuschratter, W, Hartmann, K, Schmitz, D, & Draguhn, A. 2007. Enhanced synaptic excitation–inhibition ratio in hippocampal interneurons of rats with temporal lobe epilepsy. *European Journal of Neuroscience*, **25**(2), 519–528.

Su, Shu, White, Tonya, Schmidt, Marcus, Kao, Chiu-Yen, & Sapiro, Guillermo. 2013. Geometric computation of human gyrification indexes from magnetic resonance images. *Human brain mapping*, **34**(5), 1230–1244.

Supekar, Kaustubh, Musen, Mark, & Menon, Vinod. 2009. Development of large-scale functional brain networks in children. *PLoS biology*, **7**(7), e1000157.

Sur, M., & Leamey, C. A. 2001. Development and Plasticity of Cortical Areas and Networks. *Nature Rev. Neurosci.*, **2**, 251–262.

Suter, HP. 2011. xlsReadWrite: Natively Read and Write Excel Files(.xls). *R package version*, **1**(1).

Tamnes, C. K., Ostby, Y., Fjell, A. M., Westlye, L. T., Due-Tonnessen, P., & Walhovd, K. B. 2010. Brain maturation in adolescence and young adulthood: regional age-related changes in cortical thickness and white matter volume and microstructure. *Cerebral Cortex*, **20**(3), 534–48.

Taylor, DG, & Bushell, MC. 1985. The spatial mapping of translational diffusion coefficients by the NMR imaging technique. *Physics in Medicine and Biology*, **30**(4), 345.

Taylor, Peter N, Han, Cheol E, Schoene-Bake, Jan-Christoph, Weber, Bernd, & Kaiser, Marcus. 2015. Structural connectivity changes in temporal lobe epilepsy: Spatial features contribute more than topological measures. *NeuroImage: Clinical*.

Team, R Development Core. 2011. R: A Language and Environment for Statistical Computing. *R Foundation for Statistical Computing*.

Teicher, M.H., Anderson, C.M., Polcari, A., Glod, C.A., Maas, L.C., & Renshaw, P.F. 2000. Functional deficits in basal ganglia of children with attention-deficit/hyperactivity disorder shown with functional magnetic resonance imaging relaxometry. *Nature Medicine*, **6**(4), 470–473.

Thomas, Cibu, Frank, Q Ye, Irfanoglu, M Okan, Modi, Pooja, Saleem, Kadharbatcha S, Leopold, David A, & Pierpaoli, Carlo. 2014. Anatomical accuracy of brain connections derived from diffusion MRI tractography is inherently limited. *Proceedings of the National Academy of Sciences*, **111**(46), 16574–16579.

Torrey, Henry C. 1956. Bloch equations with diffusion terms. *Physical Review*, **104**(3), 563.

Tournier, Jacques-Donald, Mori, Susumu, & Leemans, Alexander. 2011. Diffusion tensor imaging and beyond. *Magnetic Resonance in Medicine*, **65**(6), 1532–1556.

Tymofiyeva, Olga, Hess, Christopher P, Ziv, Etay, Lee, Patricia N, Glass, Hannah C, Ferriero, Donna M, Barkovich, A James, & Xu, Duan. 2013. A DTI-based template-free cortical connectome study of brain maturation. *PloS one*, **8**(5), e63310.

Uddin, Lucina Q. 2013. Complex relationships between structural and functional brain connectivity. *Trends in cognitive sciences*, **17**(12), 600–602.

van den Heuvel, M. P., Stam, C. J., Kahn, R. S., & Hulshoff Pol, H. E. 2009. Efficiency of Functional Brain Networks and Intellectual Performance. *Journal of Neuroscience*, **29**(23), 7619–7624.

van den Heuvel, Martijn P, Kersbergen, Karina J, de Reus, Marcel A, Keunen, Kristin, Kahn, René S, Groenendaal, Floris, de Vries, Linda S, & Benders, Manon JNL. 2014. The neonatal connectome during preterm brain development. *Cerebral Cortex*, bhu095.

Van Ooyen, A, Van Pelt, J, & Corner, MA. 1995. Implications of activity dependent neurite outgrowth for neuronal morphology and network development. *Journal of Theoretical Biology*, **172**(1), 63–82.

van Ooyen, Arjen. 2001. Competition in the development of nerve connections: a review of models. *Network: Computation in Neural Systems*, **12**(1), 1–47.

van Ooyen, Arjen. 2003. *Modeling Neural Development*. MIT Press.

van Ooyen, Arjen. 2011. Using theoretical models to analyse neural development. *Nature Reviews Neuroscience*, **12**(6), 311–326.

van Ooyen, Arjen, P. Graham, Bruce, & J.A. Ramakers, Ger. 2001. Competition

for tubulin between growing neurites during development. *Neurocomputing*, **38**(0), 73–78.

van Ooyen, Arjen, Carnell, Andrew, de Ridder, Sander, Tarigan, Bernadetta, Mansvelder, Huibert D, Bijma, Fetsje, de Gunst, Mathisca, & van Pelt, Jaap. 2014. Independently outgrowing neurons and geometry-based synapse formation produce networks with realistic synaptic connectivity. *PloS one*, **9**(1), e85858.

van Pelt, Jaap, & van Ooyen, Arjen. 2013. Estimating neuronal connectivity from axonal and dendritic density fields. *Frontiers in computational neuroscience*, **7**.

Van Wijk, Bernadette CM, Stam, Cornelis J, & Daffertshofer, Andreas. 2010. Comparing brain networks of different size and connectivity density using graph theory. *PloS one*, **5**(10), e13701.

Varier, Sreedevi, & Kaiser, Marcus. 2011. Neural development features: Spatio-Temporal development of the Caenorhabditis elegans neuronal network. *PLoS Comput Biol*, **7**, e1001044.

Varshney, Lav R, Chen, Beth L, Paniagua, Eric, Hall, David H, & Chklovskii, Dmitri B. 2011. Structural properties of the Caenorhabditis elegans neuronal network. *PLoS computational biology*, **7**(2), e1001066.

Verhage, M., Maia, A. S., Plomp, J. J., Brussaard, A. B., Heeroma, J. H., Vermeer, H., Toonen, R. F., Hammer, R. E., van den Berg, T. K., Missler, M., Geuze, H. J., & Sudhof, T. C. 2000. Synaptic assembly of the brain in the absence of neurotransmitter secretion. *Science*, **287**(5454), 864–869.

Vértes, Petra E, Alexander-Bloch, Aaron F, Gogtay, Nitin, Giedd, Jay N, Rapoport, Judith L, & Bullmore, Edward T. 2012. Simple models of human brain functional networks. *Proceedings of the National Academy of Sciences*, **109**(15), 5868–5873.

von der Malsburg, Chr. 1973. Self-organization of orientation sensitive cells in the striate cortex. *Kybernetik*, **14**(2), 85–100.

Wang, Dawei, Qin, Wen, Liu, Yong, Zhang, Yunting, Jiang, Tianzi, & Yu, Chunshui. 2014. Altered resting-state network connectivity in congenital blind. *Human brain mapping*, **35**(6), 2573–2581.

Wang, R., Benner, T., Sorensen, A. G., & Wedeen, V. J. 2007. *Diffusion Toolkit: A Software Package for Diffusion Imaging Data Processing and Tractography.*

Watts, D. J., & Strogatz, S. H. 1998. Collective Dynamics of 'small-World' Networks. *Nature*, **393**, 440–442.

Weisberg, S., & Fox, J. 2011. *An R companion to applied regression.* Second edn. Thousand Oaks,CA: Sage Publications, Inc.

Westlye, Lars T, Walhovd, Kristine B, Dale, Anders M, Bjørnerud, Atle, Due-Tønnessen, Paulina, Engvig, Andreas, Grydeland, Håkon, Tamnes, Christian K, Østby, Ylva, & Fjell, Anders M. 2009. Life-span changes of the human brain white matter: diffusion tensor imaging (DTI) and volumetry. *Cerebral cortex*, bhp280.

White, Tonya, Su, Shu, Schmidt, Marcus, Kao, Chiu-Yen, & Sapiro, Guillermo.

2010. The development of gyrification in childhood and adolescence. *Brain and cognition*, **72**(1), 36–45.

Williams, Benjamin R, Ponesse, Jonathan S, Schachar, Russell J, Logan, Gordon D, & Tannock, Rosemary. 1999. Development of inhibitory control across the life span. *Developmental psychology*, **35**(1), 205.

Williams, Diane L, & Minshew, Nancy J. 2007. Understanding autism and related disorders: what has imaging taught us? *Neuroimaging Clinics of North America*, **17**(4), 495–509.

Willshaw, D. J., & von der Malsburg, C. 1976. How patterned neural connections can be set up by self-organization. *Proc R Soc Lond B Biol Sci*, **194**(1117), 431–45.

Wood, Simon. 2006. *Generalized additive models: an introduction with R*. CRC press.

Yamamoto, N., Tamada, A., & Murakami, F. 2002. Wiring of the brain by a range of guidance cues. *Prog Neurobiol*, **68**(6), 393–407.

Yap, P. T., Fan, Y., Chen, Y., Gilmore, J. H., Lin, W., & Shen, D. 2011a. Development trends of white matter connectivity in the first years of life. *PLoS ONE*, **6**(9), e24678.

Yap, Pew-Thian, Fan, Yong, Chen, Yasheng, Gilmore, John H, Lin, Weili, & Shen, Dinggang. 2011b. Development trends of white matter connectivity in the first years of life. *PloS one*, **6**(9), e24678.

Yizhar, Ofer, Fenno, Lief E, Prigge, Matthias, Schneider, Franziska, Davidson,

Thomas J, O'Shea, Daniel J, Sohal, Vikaas S, Goshen, Inbal, Finkelstein, Joel, Paz, Jeanne T, *et al.* 2011. Neocortical excitation/inhibition balance in information processing and social dysfunction. *Nature*, **477**(7363), 171–178.

Yu, Yong-Chun, Bultje, Ronald S, Wang, Xiaoqun, & Shi, Song-Hai. 2009. Specific synapses develop preferentially among sister excitatory neurons in the neocortex. *Nature*, **458**(7237), 501–504.

Yu, Yong-Chun, He, Shuijin, Chen, She, Fu, Yinghui, Brown, Keith N, Yao, Xing-Hua, Ma, Jian, Gao, Kate P, Sosinsky, Gina E, & Huang, Kun. 2012. Preferential electrical coupling regulates neocortical lineage-dependent microcircuit assembly. *Nature*, **486**(7401), 113–117.

Zalesky, Andrew, Fornito, Alex, Harding, Ian H, Cocchi, Luca, Yücel, Murat, Pantelis, Christos, & Bullmore, Edward T. 2010. Whole-brain anatomical networks: does the choice of nodes matter? *Neuroimage*, **50**(3), 970–983.

Zawadzki, Krissia, Feenders, Christoph, Viana, Matheus P, Kaiser, Marcus, & Costa, Luciano da F. 2012. Morphological Homogeneity of Neurons: Searching for Outlier Neuronal Cells. *Neuroinformatics*, **10**(4), 379–389.

Zhan, Yang, Paolicelli, Rosa C, Sforazzini, Francesco, Weinhard, Laetitia, Bolasco, Giulia, Pagani, Francesca, Vyssotski, Alexei L, Bifone, Angelo, Gozzi, Alessandro, & Ragozzino, Davide. 2014. Deficient neuron-microglia signaling results in impaired functional brain connectivity and social behavior. *Nature neuroscience*.

Zhou, Yu-Dong, Lee, Sanghoon, Jin, Zhe, Wright, Moriah, Smith, Stephen EP,

& Anderson, Matthew P. 2009. Arrested maturation of excitatory synapses in autosomal dominant lateral temporal lobe epilepsy. *Nature medicine*, **15**(10), 1208–1214.

Zubler, F, & Douglas, R. 2009. A framework for modeling the growth and development of neurons and networks. *Frontiers in computational neuroscience*, **3**, 25.

Publication list

Lim, S., Han, C. E., Uhlhaas, P. J., & Kaiser, M. (2013). Preferential detachment during human brain development: age-and sex-specific structural connectivity in diffusion tensor imaging (DTI) data. *Cerebral Cortex*, doi: 10.1093/cercor/bht333 (Epub ahead of print).

Lim, S., & Kaiser, M. (2015). Developmental time windows for axon growth influence neuronal network topology. *Biological cybernetics*, 109(2), 275-286.